NUMERICAL MODELING OF TUNNEL EXCAVATION INTERACTING WITH A BUILDING

Master's Thesis

Bedirhan YETKİN

Eskişehir 2025

NUMERICAL MODELING OF TUNNEL EXCAVATION INTERACTING WITH A BUILDING

Bedirhan YETKİN

MASTER'S THESIS

Department of Civil Engineering

Programme in Geotechnical

Supervisor: Assist. Prof. Dr. Eren BALABAN

(Co-Supervisor: Prof. Dr. Emilio BİLOTTA)

Eskişehir

Eskişehir Technical University

Institute of Graduate Programs

July 2025

FINAL APPROVAL FOR THESIS

This thesis titled NUMERICAL MODELING OF TUNNEL EXCAVATION INTERACTING WITH A BUILDING has been prepared and submitted by Bedirhan YETKİN in partial fulfillment of the requirements in “Eskişehir Technical University Directive on Graduate Education and Examination” for the Degree of Master of Science in Civil Engineering Department has been examined and approved on 24/07/2025.

Committee Members	**Title, Name and Surname**	**Signature**
Member(Supervisor)	Assist. Prof. Dr. Eren BALABAN	
Member(Co-Supervisor)	Prof. Dr. Emilio BILOTTA	
Member	Prof. Dr. Murat TÜRKÖZ	
Member	Assoc. Prof. Dr. Kıvanç TAŞKIN	
Member	Assoc. Prof. Dr. Kamil Bekir AFACAN	

Prof. Dr. Harun BÖCÜK
Director of the Institute of Graduate Programs

24/07/2025

SUPERVISOR APPROVAL

Master of Science student Bedirhan YETKİN, whom I supervise, has completed this thesis titled NUMERICAL MODELING OF TUNNEL EXCAVATION INTERACTING WITH A BUILDING. According to my inspections, the work is scientifically and ethically appropriate for the student to the thesis defense exam.

Supervisor
Assist. Prof. Dr. Eren BALABAN

ABSTRACT

NUMERICAL MODELING OF TUNNEL EXCAVATION INTERACTING WITH A BUILDING

Bedirhan YETKİN

Department of Civil Engineering

Programme in Geotechnical

Eskişehir Technical University, Institute of Graduate Programs, July 2025

Supervisor: Assist. Prof. Dr. Eren BALABAN

(Co-Supervisor: Prof. Dr. Emilio BİLOTTA)

This thesis investigates the effects of tunnel excavation-induced ground movements on buildings through a numerical study of Napoli Metro Line 6. Using PLAXIS 3D finite element modeling, interactions between tunnel settlements and existing structures were analyzed. Both greenfield and soil-structure interaction scenarios were modeled to assess the influence of building stiffness and foundation properties.

The Mohr-Coulomb and Hardening Soil models, including HSsmall, simulated nonlinear soil behavior along the tunnel alignment, covering sand, pyroclastic soils, cinerite, and tuff. Model calibration was performed using results from geotechnical investigations.

Analyses focused on settlement troughs, horizontal displacements, and internal forces in building elements. Axial forces (ΔN) and vertical displacements (Δuz) were examined under interface stiffness variations (R=1 and R=0.01).

Results indicate that building stiffness significantly modifies ground deformation, reducing settlements in sagging zones while maintaining or increasing deformations in hogging zones. The study highlights the importance of soil-structure interaction and advanced numerical modeling to minimize structural risks in urban tunneling projects.

Keywords: Tunnel excavation, Soil-structure interaction, Building response, Numerical modeling, Plaxis 3d.

ÖZET

YAPI İLE ETKİLEŞİMDE OLAN TÜNEL KAZISININ SAYISAL MODELLEMESİ

Bedirhan YETKİN

İnşaat Mühendisliği Anabilim Dalı

Geoteknik Bilim Dalı

Eskişehir Teknik Üniversitesi, Lisansüstü Eğitim Enstitüsü, Temmuz 2025

Danışman: Dr. Öğr. Üyesi Eren BALABAN

İkinci Danışman: Prof. Dr. Emilio BİLOTTA

Bu tezde, Napoli Metro Hattı 6'da gerçekleştirilen tünel kazısı kaynaklı zemin hareketlerinin binalar üzerindeki etkileri sayısal bir çalışma ile incelenmiştir. PLAXIS 3D sonlu eleman modellemesi kullanılarak tünel kaynaklı oturmalar ile mevcut yapıların etkileşimi analiz edilmiştir. Hem yeşil alan (yapısız) hem de zemin-yapı etkileşimi senaryoları modellenerek, yapı rijitliği ve temel özelliklerinin deformasyon üzerindeki etkisi değerlendirilmiştir.

Mohr-Coulomb ve Hardening Soil modelleri, HSsmall modeli dahil olmak üzere, tünel güzergahındaki farklı zemin katmanlarının (kum, piroklastik zeminler, sinirit ve tüf) doğrusal olmayan davranışını simüle etmek için kullanılmıştır. Model kalibrasyonu, Napoli Metro projesi alanındaki jeoteknik inceleme sonuçları kullanılarak yapılmıştır.

Analizler, oturma çukurları, yatay yer değiştirmeler ve yapı elemanlarında oluşan iç kuvvetler üzerinde yoğunlaşmıştır. Eksenel kuvvetler (ΔN) ve düşey yer değiştirmeler (Δuz), arayüz rijitliği değişimleri (R=1 ve R=0,01) altında incelenmiştir.

Sonuçlar, yapı rijitliğinin zemin deformasyon profillerini önemli ölçüde değiştirdiğini, çökme bölgelerinde maksimum oturmaları azalttığını ve kabarma bölgelerinde deformasyonları koruduğunu veya artırdığını göstermektedir. Çalışma, zemin-yapı etkileşiminin dikkate alınmasının ve gelişmiş sayısal modellemenin, kentsel tünel projelerinde yapısal riskleri minimize etmek için önemini vurgulamaktadır.

Anahtar Sözcükler: Tünel kazısı, Zemin-yapı etkileşimi, Bina tepkisi, Sayısal modelleme, Plaxis 3d.

ACKNOWLEDGEMENTS

I would like to express my sincere gratitude to Professor Emilio Bilotta, under whose supervision I had the opportunity to conduct an internship at the University of Naples Federico II. His invaluable guidance, constructive feedback, and extensive knowledge of tunneling and geotechnical engineering greatly contributed to my technical skills and academic development.

I am also deeply thankful to my advisor, Assist. Prof. Dr. Eren Balaban, for his continuous support, encouragement, and insightful advice throughout my master’s studies. His guidance shaped the technical aspects of this thesis and inspired my dedication to engineering research.

I would like to extend my heartfelt thanks to my family for their unwavering support, patience, and encouragement throughout this process. Their support has been the foundation that enabled me to complete this thesis.

Finally, I am grateful to all my friends and colleagues who supported me academically and emotionally during my studies.

Bedirhan YETKİN

24/07/2025

STATEMENT OF COMPLIANCE WITH ETHICAL PRINCIPLES AND RULES

I hereby truthfully declare that this thesis is an original work prepared by me; that I have behaved in accordance with the scientific ethical principles and rules throughout the stages of preparation, data collection, analysis and presentation of my work; that I have cited the sources of all the data and information that could be obtained within the scope of this study, and included these sources in the references section; and that this study has been scanned for plagiarism with “scientific plagiarism detection program” used by Eskişehir Technical University, and that “it does not have any plagiarism” whatsoever. I also declare that, if a case contrary to my declaration is detected in my work at any time, I hereby express my consent to all the ethical and legal consequences that are involved.

Bedirhan YETKİN

CONTENTS

Pages

CURRICULUM VITAE

LIST OF TABLES

Pages

LIST OF FIGURES

Pages

GLOSSARY OF SYMBOLS AND ABBREVIATIONS

S: Maximum surface settlement (mm) – Maximum value of ground surface settlement caused by tunnel excavation.

I: Distance from tunnel centerline (m) – Horizontal distance from tunnel axis.

i_0: Settlement trough width parameter (m) – Parameter defining settlement trough width.

K: Dimensionless trough width parameter – Ratio of settlement trough width to tunnel depth.

VL: Volume loss percentage (%) – Percentage of soil loss volume during excavation.

ΔN: Change in axial force (kN) – Variation in axial force in columns or beams.

Δuz: Change in vertical displacement (mm) – Change in vertical ground or structure displacement.

$E_{oe}d$: Reference oedometer stiffness modulus (kPa) – Reference vertical stiffness modulus.

E_{ur}: Reference unloading–reloading stiffness modulus (kPa) – Reference stiffness modulus for unloading reloading.

G_0: Initial shear modulus at very small strains (kPa) – Shear modulus at very small deformations.

Γ: Unit weight (kN/m³) – Unit weight of soil.

σ′: Effective stress (kPa) – Effective stress in the soil.

Φ: Internal friction angle (°) – Soil's internal friction angle.

c: Cohesion (kPa) – Soil cohesion.

Ψ: Dilation angle (°) – Soil dilation angle.

ν: Poisson's ratio – Tendency of lateral expansion or contraction.

E: Young's modulus (kPa) – Elastic modulus.

q: Deviatoric stress (kPa) – Stress difference deviating from mean stress.

ε: Strain – Amount of deformation.

$\gamma_{0.7}$: Shear strain at which G reduces to 70% of G_0 – Shear strain corresponding to 70% of initial shear modulus.

P:	Face support pressure (kPa) – Support pressure at the tunnel face.
δ:	Horizontal displacement (mm) – Horizontal movement amount.
BOP:	Bottom of Pipe
CAD:	Computer Aided Design
COV:	Coefficient of Variation
CPT:	Cone Penetration Test
DOF:	Degree of Freedom
EPB:	Earth Pressure Balance
EPBM:	Earth Pressure Balance Machine
FDM:	Finite Difference Method
FEM:	Finite Element Method
GWT:	Groundwater Table
HS:	Hardening Soil Model
Hssmall:	Hardening Soil Model with Small-Strain Stiffness
LSD:	Limit State Design
MC:	Mohr-Coulomb Model
MDR:	Maximum Deflection Ratio
NATM:	New Austrian Tunnelling Method
OCR:	Overconsolidation Ratio
PLAXIS:	Plane strain and axisymmetric analysis software
SAP2000:	Structural Analysis Program 2000
SLS:	Serviceability Limit State
SPB:	Slurry Pressure Balance
SPT:	Standard Penetration Test
TBM:	Tunnel Boring Machine
ULS:	Ultimate Limit State

1. INTRODUCTION

The escalating pace of urban expansion, coupled with the diminishing availability of surface land and the ever-growing complexity of modern infrastructure requirements, has significantly amplified the demand for underground constructions. Consequently, vital facilities such as metro lines, intricate transportation tunnels, and expansive utility galleries have become indispensable, particularly within densely populated urban landscapes. However, tunnel excavations in such environments frequently occur in close proximity to existing buildings, thereby creating intricate interactions among the tunnel, the surrounding ground, and adjacent structures. These tunneling operations invariably induce ground movements, which include settlements, horizontal displacements, and internal stress redistributions. Such movements, in turn, can precipitate structural problems in neighboring buildings, manifesting as cracking, undesirable tilting, and distortion, as meticulously documented by Mair and Taylor (1997), Boscardin and Cording (1989), and Burland (1995).

A structure's inherent response to these complex ground movements is largely contingent upon several critical factors, including its foundation type, intrinsic stiffness, geometric configuration, and the precise degree of its interaction with the surrounding soil. Therefore, any robust and accurate risk assessment preceding tunneling operations must thoroughly account for both tunnel-ground and soil-structure interactions. Conventional analytical approaches frequently oversimplify this multifaceted reality by disregarding the presence of existing buildings, instead predicting settlements solely under idealized "greenfield" (building-free) conditions. Nevertheless, real-world observations consistently confirm that a building's inherent stiffness can substantially modify the ground's overall deformation profile (Potts and Addenbrooke, 1997).

This research primarily aims to numerically model and meticulously analyze the excavation of a tunnel that interacts directly with an existing structure, employing state-of-the-art advanced numerical analysis techniques. To achieve a precise and reliable simulation of both the tunnel’s behavior and the building's structural response, both PLAXIS 3D and SAP2000 software were synergistically utilized. Initially, the building was meticulously modeled in SAP2000 as a three-dimensional linear elastic frame system. Subsequently, an equivalent structural representation was carefully integrated into PLAXIS 3D, a crucial step to ensure unwavering consistency in structural behavior across both computational platforms. A rigorous comparative analysis of internal forces and displacements derived from both software packages was then conducted to thoroughly validate the accuracy and fidelity of the PLAXIS model.

Furthermore, the tunnel excavation sequence was incrementally simulated within PLAXIS, meticulously capturing the progressive advancement of the tunnel face. A particular focus was placed on understanding the intricate behavior of the soil-structure interface, specifically through the 'interface parameter' (Rinter). This parameter critically defines the shear stiffness ratio at the interface boundary between the soil and the structural lining. By systematically investigating various values for this parameter, the study comprehensively delved into how fluctuations in interface stiffness profoundly influence the internal forces and displacements observed within the building's structural elements. This meticulous methodology facilitated a thorough and nuanced evaluation of the degree of interaction between the building and the progressively advancing tunnel under diverse interface and soil conditions, with all findings rigorously assessed using both compelling graphical representations and precise numerical data.

The numerical models developed throughout this thesis draw their fundamental inspiration from the specific geometric and geotechnical characteristics observed in the Naples Metro Line 6 project. Within PLAXIS 3D, the defined excavation stages were meticulously designed to accurately replicate a Tunnel Boring Machine (TBM) excavation scenario, carefully incorporating crucial operational parameters such as face pressure and grouting pressure, which are inherent to the tunneling process. A significant and distinguishing contribution of this research lies in its detailed comparative analysis of internal forces. These forces, rigorously derived from SAP2000 at various story levels and across different beam spans, were then directly compared against their corresponding values obtained from PLAXIS 3D, thereby enabling a profound and in-depth evaluation of the overall modeling accuracy achieved.

In conclusion, this investigation presents a cohesive and robust modeling methodology that effectively bridges the gap between geotechnical and structural engineering disciplines. It powerfully demonstrates the efficacy of advanced numerical methods in comprehensively evaluating the complex and critical impact of tunnel excavations on neighboring structures, offering invaluable insights for future urban development projects.

2. THEORETICAL BACKGROUND

Tunneling operations, particularly when conducted in soft soils and within densely developed urban environments, frequently induce substantial ground movements that can genuinely jeopardize the structural integrity of nearby buildings. These consequential effects necessitate a truly comprehensive investigation from both geotechnical and structural engineering perspectives, as the intricate soil-structure interaction inevitably emerges as a critical determinant. An extensive body of experimental, analytical, and numerical research has been dedicated to thoroughly exploring the underlying mechanisms of ground deformations triggered by tunneling, developing robust methods to predict these deformations, and understanding their profound implications for adjacent structural behavior.

The specific characteristics of these ground movements are influenced by a myriad of factors, including the tunnel's diameter, the chosen excavation technique, the prevailing soil type, the excavation depth, the employed support systems, and the local groundwater conditions (Mair et al., 1993; Attewell and Woodman, 1982). Among these various deformations, surface settlement stands out as the most prominent, frequently depicted by a characteristic Gaussian distribution curve when viewed along the tunnel axis (Peck, 1969). In predictions made under "greenfield" conditions, an assumption that entirely disregards the presence of any buildings, the maximum settlement typically occurs directly above the tunnel axis, gradually diminishing as one moves laterally away from it.

However, when existing structures interact with the ground, this predictable settlement pattern can undergo a significant alteration. A building's inherent stiffness, its foundation type, and other distinguishing characteristics can profoundly influence the resulting ground deformation profile (Potts and Addenbrooke, 1997; Frischmann et al., 1994). Depending on their rigidity, buildings may either actively resist or passively conform to the underlying ground movements, which, in turn, directly affects the magnitude of induced internal forces and the potential severity of structural cracking (Burland and Wroth, 1974; Boscardin and Cording, 1989).

Approaches for accurately predicting tunnel-induced ground deformations broadly fall into three principal categories: empirical, analytical, and numerical methods.

Empirical methods rely on statistical relationships derived directly from extensive field observations to estimate both the magnitude and spread of settlement. These methods, exemplified by Peck's (1969) widely recognized Gaussian settlement model and O'Reilly and New's (1982) definition of settlement trough width, offer practical and rapid predictions. Nevertheless, their accuracy is generally limited in more complex scenarios, as they typically do not fully account for critical variables such as building stiffness, specific foundation types, or the detailed nuances of soil-structure interactions.

Analytical methods endeavor to model the complex mechanical behavior of soils by applying fundamental theories of elasticity, plasticity, and deformation mechanics to mathematically describe stress and strain evolutions during tunneling. Within this theoretical framework, concepts such as the "gap parameter," effective stress analysis, and theoretical delineations of deformation zones have been meticulously developed (Pinto and Whittle, 2014; Loganathan and Poulos, 1998). While analytical models can indeed achieve high precision under specific, well-defined assumptions, they often necessitate reliance on idealized conditions, such as perfectly homogeneous soils and simplified geometries, which may not always reflect real-world complexity.

Numerical methods have experienced a remarkable surge in prominence with continuous advancements in three-dimensional modeling capabilities. Software packages based on the Finite Element Method (FEM), such as PLAXIS 2D/3D, now enable highly detailed simulations of entire excavation sequences and intricate soil-structure interactions. Numerical models possess the distinct advantage of being able to incorporate complex geometries, various foundation systems, advanced material models, and sophisticated interface behaviors. In particular, the 'interface parameter' (Rinter) in PLAXIS 3D, which realistically represents the shear resistance at the crucial soil-structure boundary, is absolutely vital for accurately simulating authentic soil-structure interaction phenomena (Ng et al., 2015; Kasper and Meschke, 2004). By carefully calibrating this interface shear stiffness ratio, it becomes possible to achieve significantly more accurate predictions of internal force distributions within structures.

Beyond isolated structural analyses typically performed in tools like SAP2000, numerical models facilitate a truly integrated approach by seamlessly incorporating buildings into comprehensive soil-structure interaction studies. This research explicitly adopts such an integrated methodology by first modeling the structure in SAP2000 and subsequently creating an equivalent representation within PLAXIS 3D. This enables a detailed and nuanced assessment of the structural response under varying soil models and diverse interface conditions. The compelling results obtained unequivocally highlight how different modeling strategies within PLAXIS significantly influence the predicted internal forces and settlements, thus powerfully demonstrating the paramount significance of interface behavior in shaping the ultimate analysis outcomes.

Overall, while a variety of methods exist in the literature for modeling tunneling-induced ground deformations, numerical approaches, particularly those with sophisticated three-dimensional capabilities, offer superior accuracy and unparalleled reliability for complex cases involving intricate interactions with existing structures. The invaluable findings of this study will enable a realistic and holistic evaluation not only of surface ground settlements but also of critical structural parameters, such as internal forces and displacements, which are absolutely essential for comprehensively assessing building safety and performance.

2.1. A Review of Different Tunneling Methods

Tunneling stands as one of the most vital and transformative techniques in civil engineering, serving to create essential underground passages for transportation networks, critical infrastructure, and efficient water conveyance systems. As urbanization intensifies globally and available surface land becomes increasingly constrained, the inherent need for robust and sustainable underground structures grows accordingly. Consequently, the judicious selection of the most appropriate tunneling method is an absolutely fundamental decision in contemporary geotechnical and structural engineering practice (Chapman et al., 2010).

The optimal choice of tunneling method is contingent upon a multitude of factors, including the precise geological and hydrogeological conditions of the site, the tunnel's geometry and target depth, the proximity and nature of surrounding infrastructure, specific environmental considerations, and prevailing economic constraints. Conventional methods, such as the venerable New Austrian Tunneling Method (NATM) and traditional drill-and-blast techniques, continue to be widely employed across diverse soil and rock conditions. Conversely, for constructing long urban tunnels, mechanized excavation utilizing advanced Tunnel Boring Machines (TBMs) has gained considerable prominence due to their remarkable efficiency, enhanced safety protocols, and superior precision (Maidl et al., 2013; Lunardi, 2008).

Tunneling is far more than a mere excavation process; it encompasses a complex array of disciplines including meticulous ground behavior analysis, comprehensive risk assessment, sophisticated support system design, and diligent construction planning. No single method can universally address the unique requirements of every project. Successful tunnel design and construction fundamentally demand a site-specific approach, rigorously supported by empirical data from previous projects, robust numerical models that accurately account for intricate soil-structure interaction, and dynamic real-time monitoring systems throughout the construction phase (ITA Working Group, 2004).

This section undertakes a detailed examination of the primary tunneling methods commonly employed in modern engineering practice. The subject matter is systematically categorized into three main groups: conventional excavation methods, mechanized systems, and cut-and-cover techniques. Each method will be thoroughly evaluated based on its distinct construction procedures, inherent advantages and disadvantages, typical application scenarios, and its suitability for varying geotechnical conditions. By integrating critical insights gleaned from the relevant literature and drawing upon empirical comparisons, this comprehensive review aims to elucidate the multifaceted technical and economic considerations that critically inform method selection within complex engineering decision-making processes.

2.1.1. Conventional methods

Conventional tunneling methods encompass a diverse range of excavation techniques that have historically evolved for use across varying soil and rock conditions, and indeed continue to be widely employed in numerous contemporary infrastructure projects. These methods generally involve direct and intimate interaction with the ground, utilizing either mechanical or semi-mechanical equipment. Among the most common and established conventional techniques are traditional drill-and-blast excavation and the adaptable New Austrian Tunneling Method (NATM).

2.1.1.1. Drill and blast method

The Drill and Blast Method operates on the principle of systematically creating boreholes within the rock mass according to a pre-determined drilling pattern across the tunnel cross-section. These boreholes are subsequently filled with carefully selected explosives, and controlled blasting operations are then executed to loosen the rock, enabling its removal from the excavation site. This method characteristically progresses through an iterative cycle involving multiple excavation and support application phases.

For the successful implementation of this technique, the drilling pattern must first be precisely tailored based on the geological characteristics of the rock mass encountered within the planned cross-section. Prior to the detonation of explosives placed within the drilled holes, critical parameters such as hole diameter, spacing, and the charge ratio are meticulously optimized to ensure efficient fragmentation and controlled blasting (Bieniawski, 1990). Following the blast, the fragmented material is typically transported out of the tunnel by means of conveyor systems, muck wagons, or loaders. Subsequently, temporary support measures are promptly applied around the tunnel periphery. This essential support system may comprise various elements, including steel ribs, robust rock bolts, layers of shotcrete, and steel mesh.

In this method, key parameters such as the specific type of explosive employed, the blasting delay sequence, and the precise order of detonation directly and significantly influence both overall excavation efficiency and potential environmental impacts (Singh and Goel, 1999). Furthermore, the potential for blast-induced cracks to form along the tunnel perimeter and the assessment of the residual strength of the rock mass after detonation are fundamental considerations that must be rigorously accounted for during the design of the permanent support system.

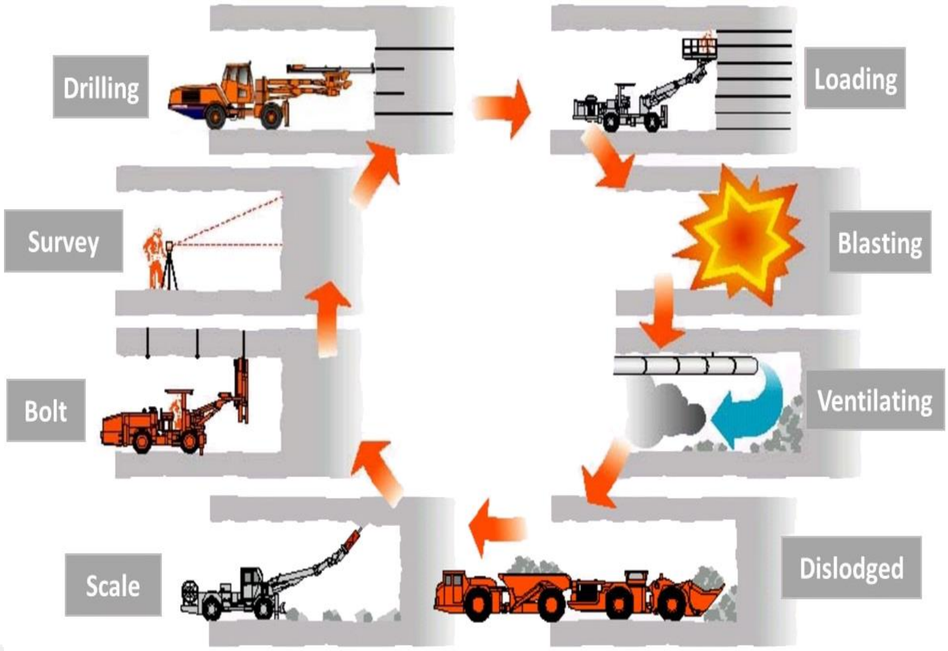

Figure 2.1. *Fundamental Stages in the Excavation Cycle of the Drill and Blast Method. (Adapted from railsystem.net)*

The Drill and Blast method operates through a meticulously controlled and cyclical excavation process. This cycle commences with an initial survey, essential for precisely establishing the dimensions of the tunnel's intended cross-section. Following this, a systematic sequence of operations unfolds: boreholes are precisely drilled into the rock, subsequently loaded with explosives, and a controlled blast is then initiated. Post-detonation, the excavation site undergoes thorough ventilation to clear fumes, and the dislodged rock material is efficiently removed. The tunnel walls are then carefully scaled to ensure cleanliness and stability, after which rock bolts are installed to provide crucial preliminary support. The cycle culminates with a repeat survey, enabling precise measurement of the newly advanced excavation face. Each of these stages is executed with rigorous precision, ensuring both the steady progression of the excavation and the ongoing structural integrity of the tunnel.

2.1.1.2. New austrian tunnelling method

The New Austrian Tunnelling Method (NATM) or its German variant Neue Österreichische Tunnelbaumethode is a new approach to excavation relying on the principle of synergistic interaction between surrounding ground or rock and support measures that are actively being introduced. Central to this approach is deliberate provision for controlled deformation of ground once excavation has occurred, and support measures afterwards inserted very carefully and deliberatively aimed at containing and consolidating these deformations. NATM was initially imagined and systematically developed by Rabcewicz in 1963 (Rabcewicz, 1964).

One of NATM's prime precepts is the requirement for contemporaneous installation of temporary support systems immediately after each incremental excavation advance. These very important support systems generally comprise the following main components:

Shotcrete: Sprayed initially as a temporary lining layer over newly excavated ground surface, it provides needed immediate stabilization and forms an initial protective shell.

Rock bolts: These are methodically engineered to augment the natural load-carrying capacity of the rock mass through effective distribution of applied loading on a larger surface contact and thereby effectively increasing ground arching effect.

Lattice girders or steel ribs: These serve as essential support elements and are provided to offer more overall strength and stiffness throughout the whole support system.

Temporary and Permanent Linings: These can be utilized as segmented precast units or cast-in-place units, and their specific choice will be based on specific project conditions and requirements. Whilst excavation work proceeds, ground deformations are carefully monitored through sophisticated geotechnical instrumentation arrays like convergence and inclinometers. With this steady stream of monitoring data coming in, support designs can actually be dynamically refined and upgraded on the very site surface itself, a capability that decidedly defines NATM as a deformation-controlled method of tunneling method (Lunardi, 2008).

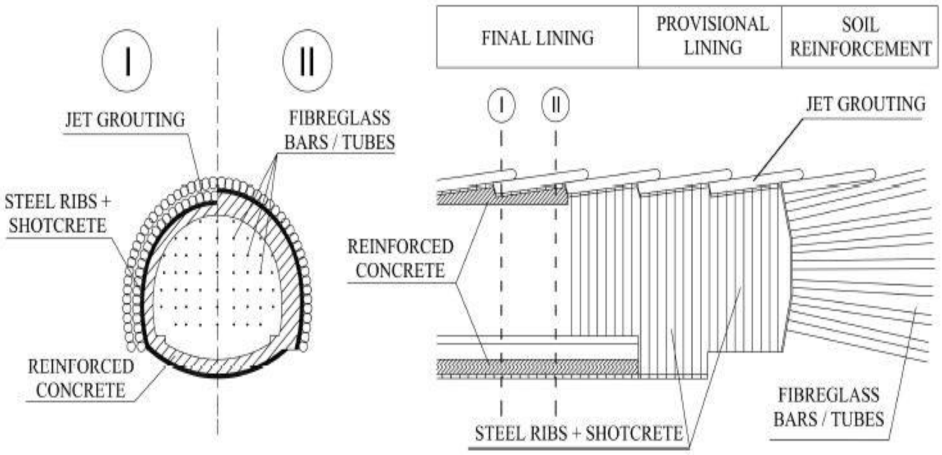

Figure 2.2. *Full-Face Excavation Application in the NATM (Ochmański et al., 2015a)*

This figure clearly shows a typical full-face excavation use case scenario as used within the context of applying the New Austrian Tunnelling Method (NATM). The figure specifically illustrates very significant ground improvement techniques, specifically through jet grouting use, among other applications utilizing robust steel support systems and the desired utilization of shotcrete. In this particular NATM practicing technique, excavation is ideally done throughout an entire cross-sectional portion of the tunnel simultaneously. For immediate face stabilization on excavated ground for purposes of obtaining face stability, temporary support is extensively ensured through an ensemble strategic utilization of steel mesh, shotcrete, and a selective utilization of a jet grout system.

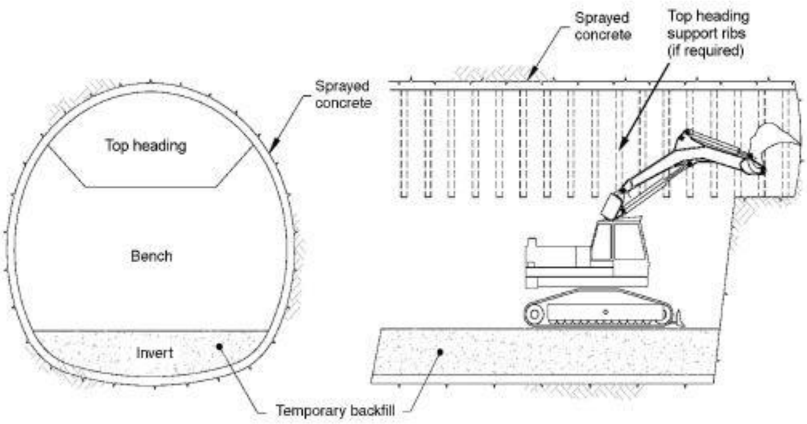

Figure 2.3. *How Partial-Face Excavation is Used in NATM. (British Tunnelling Society and Institution of Civil Engineers, 2004)*

This figure shows a type of digging called partial-face excavation, which is often used in the New Austrian Tunnelling Method (NATM). This method works in steps.

Workers dig the tunnel in parts: first the top section (called the "top heading"), and then the bottom section (called the "bench"). Each part is dug and made stable on its own. Shotcrete (sprayed concrete) is the main material used for support in this method. Sometimes, steel parts are added if extra support is needed. This method is often chosen when the ground is weak or difficult to dig, because it's very good at controlling how the ground moves during excavation.

2.1.1.3. Support and monitoring systems in conventional methods

When conventional tunneling methods are used, the design of support systems depends on several key factors. These include the type of ground, the width of the excavation, and the loads from any structures on the surface. In methods like the New Austrian Tunnelling Method (NATM), using geotechnical instruments is very important for tracking how ground deformations develop. The main monitoring systems commonly used are:

Convergence points: These measure how much the tunnel's cross-section narrows.

Piezometers: These instruments are used to measure water pressure in the ground.

Extensometers and inclinometers: These help to find out how much the ground moves at different depths.

To decide if these methods are suitable for a specific site, engineers often use ground classification systems such as RMR, Q, and GSI (Bieniawski, 1989; Barton et al., 1974).

Figure 2.4 shows a diagram of various instrumentation systems used to monitor ground and structural deformations that can happen during excavation. These systems include:

Tilt meters and crack meters: Used to watch for changes in surface tilt and crack movements.

Piezometers: Used to check the level of groundwater.

In-place inclinometers and borehole extensometers: These track horizontal and vertical movements around the excavation.

Load cells, strain gauges, and pressure cells: These systems measure the stresses on the tunnel lining.

Additionally, convergence measurements are taken using prism targets placed around the tunnel's cross-section, with help from an automatic total station device inside the tunnel. All data collected from these instruments is saved in a data logger system, which allows for continuous tracking throughout the entire excavation period.

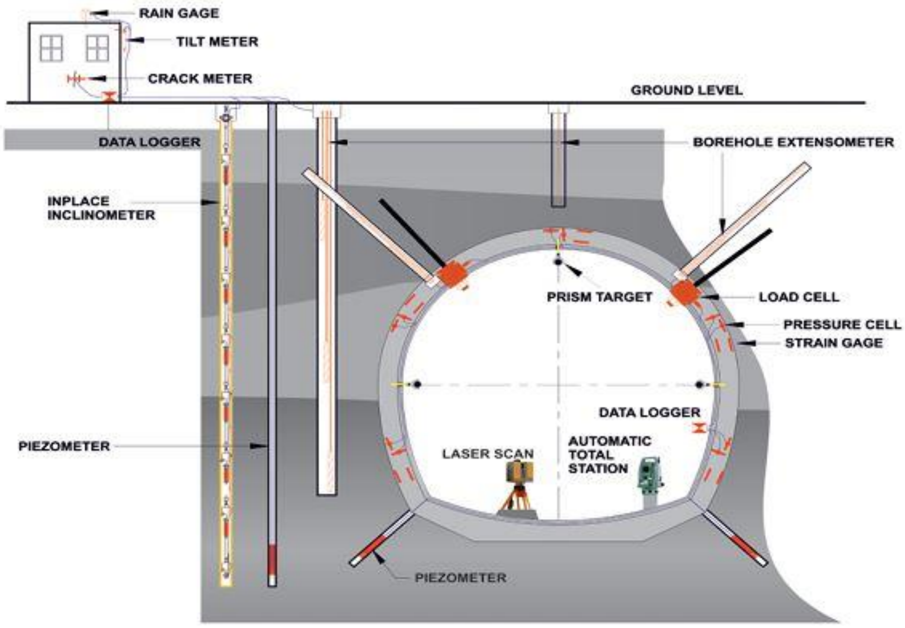

Figure 2.4. *Layout Diagram of Typical Geotechnical Monitoring Systems Used in Conventional Tunnel Excavations (Encardio-Rite Instrumentation).*

2.1.2. Mechanized methods

The mechanized tunneling methods characterize modern excavating processes through a very high level of automation and characteristic machines. During their use, tunnel excavations and support are carried out at the same time, as an integrated single process. They are especially preferred on long tunnel projects and/or challenging ground conditions. They can achieve very high precision and uninterruptible progression during their usage. General equipment used on mechanized tunneling projects are typically known as Tunnel Boring Machines (TBMs) (Maidl et al., 2013; Barla and Pelizza, 2000).

2.1.2.1. Tunnel boring machines

TBMs are complete tunnel digging machines from which excavations can be continuously carried out and controlled both in rock and ground. They include cutter head, cylindrical part (shield), segment emplacement system, and service units at the back. Excavation, support for tunnel together with final lining emplacement are continuously and at the same time carried out by these machines.

Major Structural Elements:

Cutter Head: It is that part of the cutting head which is in direct contact with ground or rock. It uses disc cutters or bucket system depending upon geologic conditions.

Shield: It is a strong steel lining which provisionally supports tunnel walls after excavation.

Segment Erector: It is utilized for positioning pre-constructed concrete segments that are used for constructing permanent lining of the tunnel.

Screw Conveyor / Slurry Circuit: This conveyor transports excavated material from the face at the front of the TBM to the back.

Trailing Backup System: It is utilized for accommodating all units for power supply, ventilation, and other logistical support functions for tunneling.

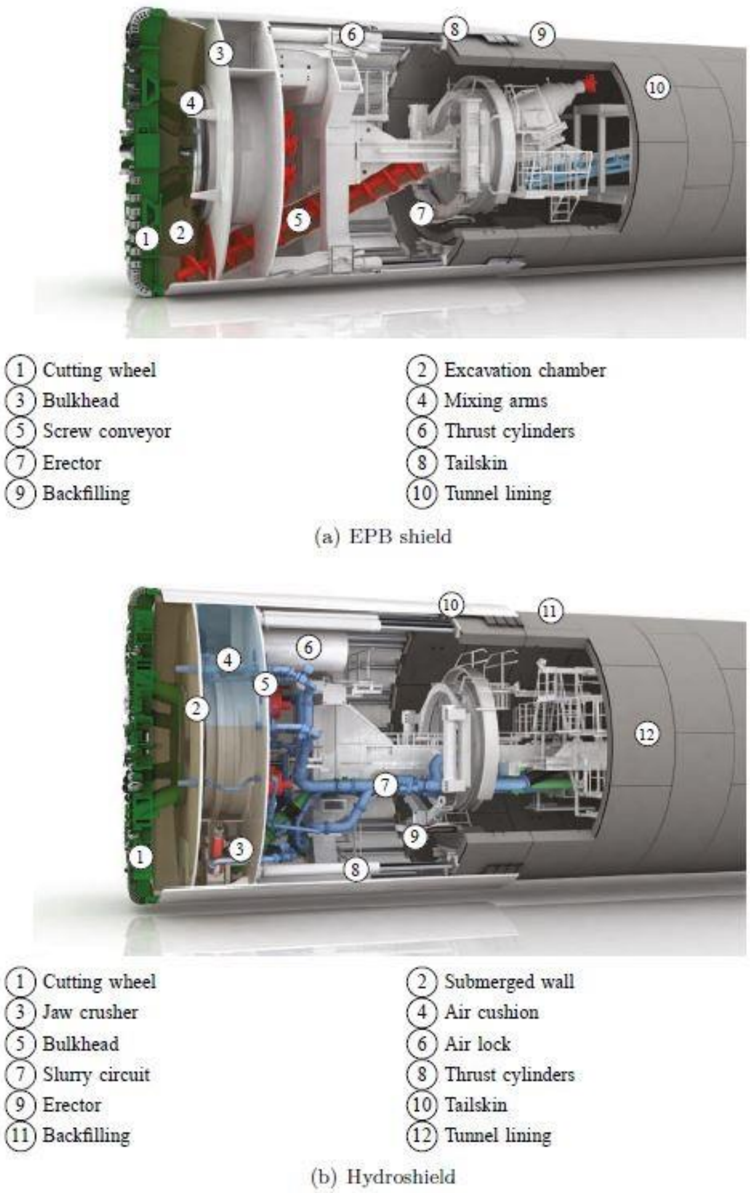

Figure 2.5. *Comparative View of EPB and SPB Type Cutterheads: Geometry and Opening Ratio (Grosso (2011); Babendererde (2015)).*

This figure shows a comparison of how Earth Pressure Balance (EPB) and Slurry Pressure Balance (SPB) type cutterheads look, specifically focusing on their shape (geometry) and how open they are (opening ratio).

2.1.2.2. Earth pressure balance (EPB) TBM

Earth Pressure Balance (EPB) machines use the excavated soil itself as an active material to balance pressure at the digging face. This method was designed to keep the excavation face stable, especially in cohesive soils (soils that stick together) that do not let much water pass through them.

Inside the TBM, the dug soil is processed into a plastic, soft state in a special chamber right behind the cutter head. This conditioned soil then applies a balancing pressure directly to the excavation face. The machine controls this pressure by adjusting the speed and turning force (torque) of a screw conveyor.

Areas where EPB TBMs are used:

Fine-grained, cohesive soils that have low water permeability.

Silty soils that are full of water.

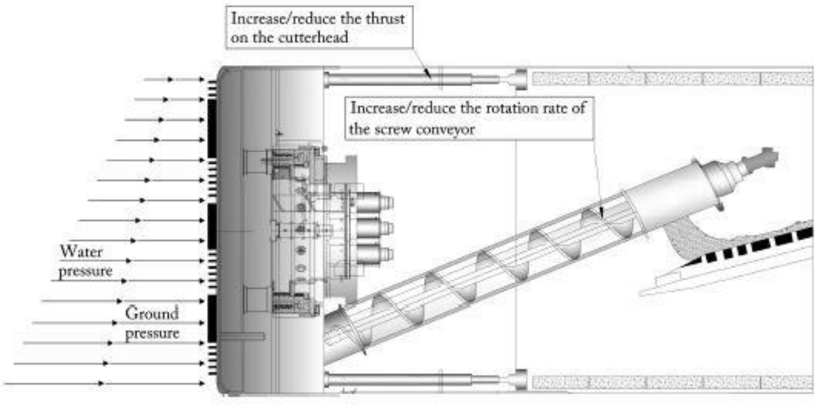

Figure 2.6. *Schematic of Excavation Pressure Control System in an EPB Shield TBM (Herrenknecht AG).*

This figure schematically shows the excavation pressure control system used in an Earth Pressure Balance (EPB) shield-type Tunnel Boring Machine (TBM). In this system, the stability of the excavation face is maintained with the help of both the cutterhead and the screw conveyor.

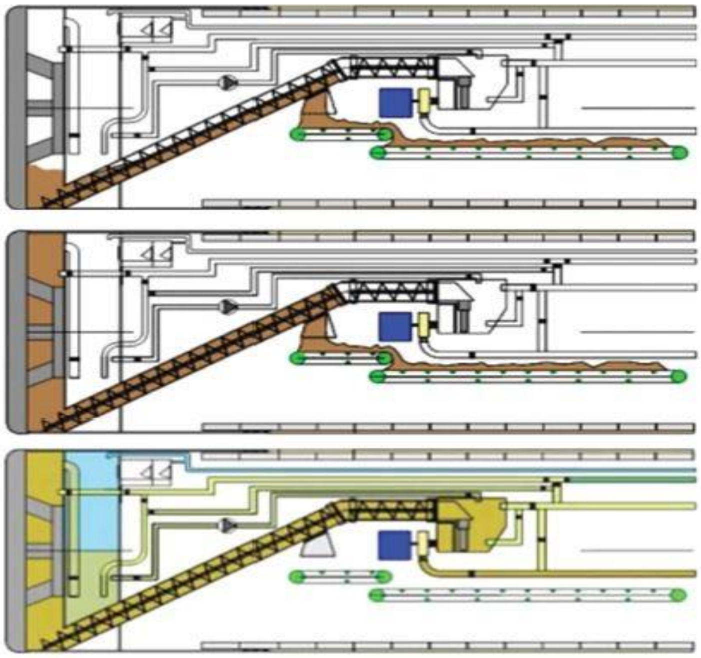

Figure 2.7. *schematic cross-sectional view of a multi-mode TBM system operating on different balancing modes (Herrenknecht AG, Multimode Shield Operation).*

The upper diagram shows Mode 1, an "open face" mode of work such that no pressure is applied on the excavation face. The second diagram from top shows Mode 2, an Earth Pressure Balance (EPB) mode. Excavated ground itself balances the face. Such excavated ground built up at the cutterhead's back is then expelled from the tunnel using a screw conveyor. The lower diagram shows Mode 3, another hydroshield system. It involves the use of a bentonite-water mixture providing fluid pressure balance at the excavation face.

Such an adaptive design allows a single TBM system to accommodate various operating modes and adapt to various geologies found during tunneling.

2.1.2.3. Slurry shield TBM

Slurry Shield machines keep the excavation face stable by using a bentonite slurry (a thick liquid mud). The liquid pressure created in the digging chamber balances the pressure from the surrounding ground and water. The dug material is moved to the back of the machine along with the slurry through a special "slurry circuit" (mud loop). The balance between the digging process and the liquid pressure is managed by a "desanding unit" (a cleaning tank) and a pressurized circulation system.

Areas where Slurry Shield TBMs are used:

Loose, cohesionless (non-sticky), water-saturated sands, silts, and gravelly soils.

Areas with high groundwater levels.

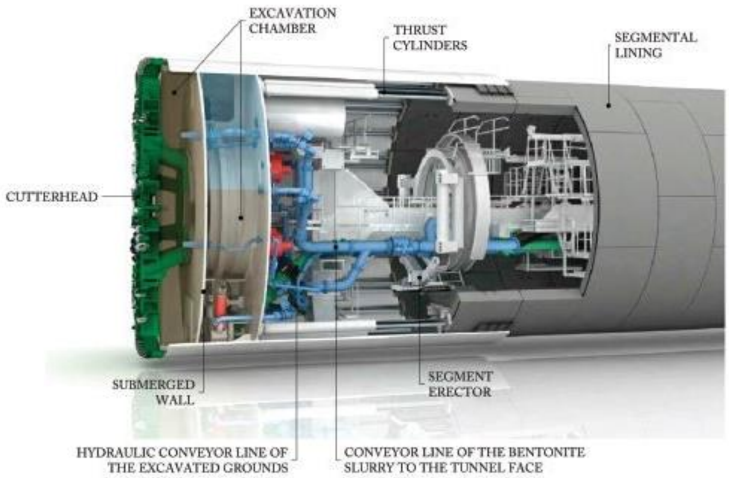

Figure 2.8. *Longitudinal Cross-Sectional View of a Slurry TBM System (Herrenknecht AG)*

This figure provides a detailed view of a Slurry Tunnel Boring Machine (TBM) system in a longitudinal cross-section. It clearly shows the bentonite circuit, the segment erection unit, and the excavation chamber.

2.1.2.4. Mix shield TBM

Mix Shield TBMs are a type of hybrid Tunnel Boring Machine designed to perform both excavation and tunnel segment installation at the same time. While the tunnel segments are being assembled at the back part of the machine, the digging process continues at the front. This design helps to make the excavation process more continuous. These machines are built with an extended shield system and telescopic cylinders.

Structural Features:

They can dig and install the lining at the same time.

They are typically used in hard rock ground conditions.

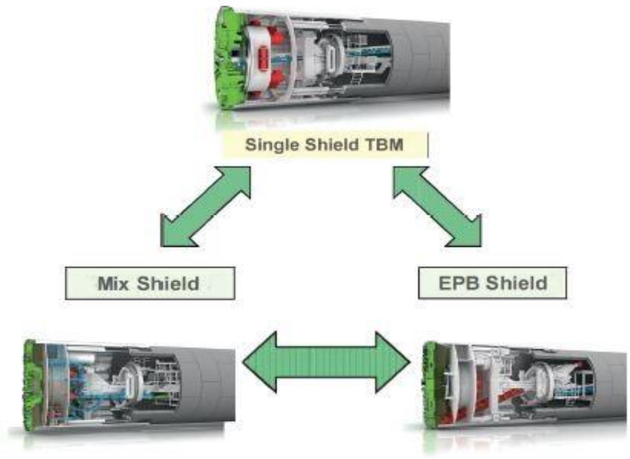

Figure 2.9. *Hybrid TBM System Showing the Principle of Switching Between EPB and Slurry Modes (Herrenknecht AG).*

This figure illustrates a hybrid Tunnel Boring Machine (TBM) system that includes two separate balancing mechanisms. These mechanisms allow the TBM to switch between Earth Pressure Balance (EPB) and Slurry operating modes.

2.1.3. Cut and cover method

Cut and Cover excavations are among those common conventional techniques used for building tunnels and sub-structures for shallow depth. For such excavations, an open trench is cut from the surface on the alignment of the future tunnel. This cut trench is supported by temporary supporting works. Permanent structural elements are then built and the surface is reclaimed.

Construction using this method typically entails two fundamental approaches:

Bottom-up Approach: With this approach, after excavation is finished fully, bottom slab, side walls and roof elements are built incrementally using cast-in-place reinforced concrete.

Top-down Approach: With the Top-down approach, preliminary work involves building walls on each side and also erecting roof slab. Then inner structure work is carried out through excavating downwards progressively from down below this completed roof (Standing and Selman, 2001; Mair et al., 1996).

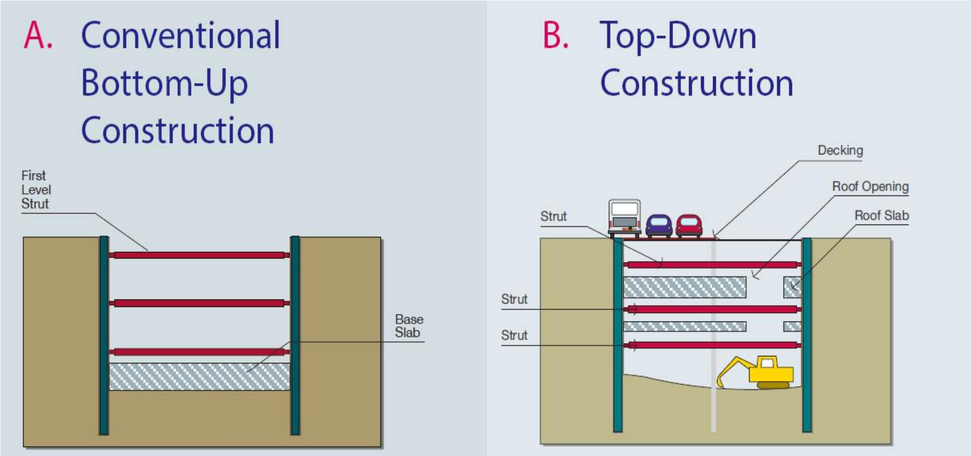

Figure 2.10. *Comparison of Two Different Construction Techniques in the Cut-and-Cover Method (British Tunnelling Society and Institution of Civil Engineers (2004))*

This figure compares two common construction techniques used in the Cut-and-Cover method. On the left, the traditional "bottom-up" method is shown. In this approach, once the digging is finished, the base slab, side walls, and roof are built using reinforced concrete, starting from the bottom.

On the right, the "top-down" (or cover-and-cut) method is illustrated. Here, the upper structural elements (like the roof slab) are put in place first. After this, digging happens downwards in stages from under these roof elements, and intermediate floor slabs are then built. This method is often preferred for urban projects, especially because it helps keep traffic flowing continuously on the surface.

For city projects, the top-down approach is frequently used. This is due to the fact that it keeps building operations and traffic moving while construction is underway. When constructing infrastructure near the surface, such as utility tunnels, underpasses, metro lines, and station structures, the Cut and Cover technique is frequently utilized.

This approach, though, may also result in a number of engineering issues. These include potential conflicts with existing subterranean lines, environmental noise and vibration, and traffic disruptions. Due to these problems, temporary road crossing systems, waterproofing barriers, and excavation support (anchored walls, diaphragm walls, and horizontal bracing) are frequently used to provide support during construction. Additionally, the relationship between the ground and the structure is continuously managed (Standing and Selman, 2001).

In terms of practical use, the digging depth for this method is usually limited to about 15–20 meters. For deeper tunnels, mechanized excavation methods based on pressure balance are recommended. These methods help maintain ground stability and reduce surface effects for deeper tunnels (Mair et al., 1996).

Figure 2.11. *A Site View of the Cut-and-Cover Method in Practice (adapted from Infrastructure Construction Archives, 2020).*

This image shows a tunnel being built using the open excavation (Cut-and-Cover) method. We can see the reinforced concrete base slab being placed on the excavation floor, and the assembly of the tunnel portal formwork has begun. During this construction process, tasks like placing segments, installing reinforcement (rebar), and pouring concrete are all done using conventional construction methods.

2.2. Ground Movements Caused by Tunnel Excavation

Ground movements that happen during tunnel excavation depend on several factors. These include the tunnel's shape and size, the type of soil, the amount of water present, the digging method used, and the support systems in place. Especially when tunnels are dug in soft ground or close to the surface, these movements can reach the surface. This can create extra stress on building foundations, potentially leading to structural damage (Attewell and Woodman, 1982; Mair and Taylor, 1997).

Ground deformations begin near the excavation face and spread upwards, appearing on the surface as a wide settlement trough (a dip in the ground). The main types of ground movements that happen because of tunnel excavation are summarized below:

Formation of a void at the excavation face: When digging is done with TBMs or traditional methods, stresses are released along the tunnel's path. This forces the ground structure to re-balance itself.

Tail void: This is the gap between the excavation surface and the tunnel lining segments. Even though this gap is filled with grout, over time, some compression and settling can still occur in this area (see Figure 2.4).

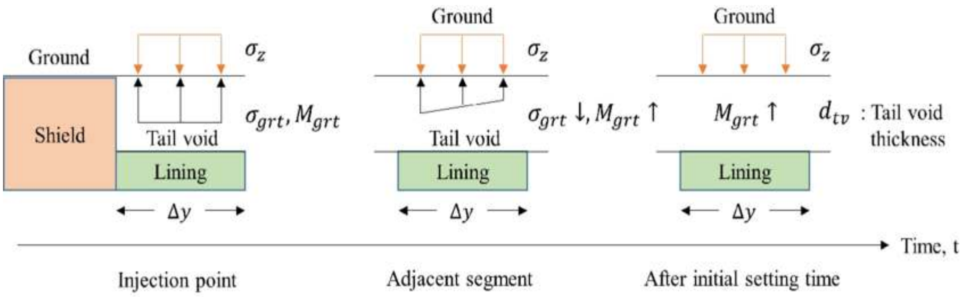

Figure 2.12. *Tail Void and the Grouting Process(Jun-Beom An et al., 2021).*

This figure illustrates the tail void, which is the space between the excavated ground and the installed tunnel segments. It also shows the process of filling this void with grout.

Settlement at the surface: Over time, delayed surface settlements may result from consolidation caused by ground deformations, particularly in cohesive soils (Mair et al., 1996).

A Gaussian (normal) distribution curve typically depicts vertical movements that take place on the surface. According to this model, which was created by Peck in 1969, the biggest settlement occurs just above the tunnel axis when viewed perpendicularly. The farther you are from the tunnel, the faster (exponentially) this amount drops (see Figure 2.13.).

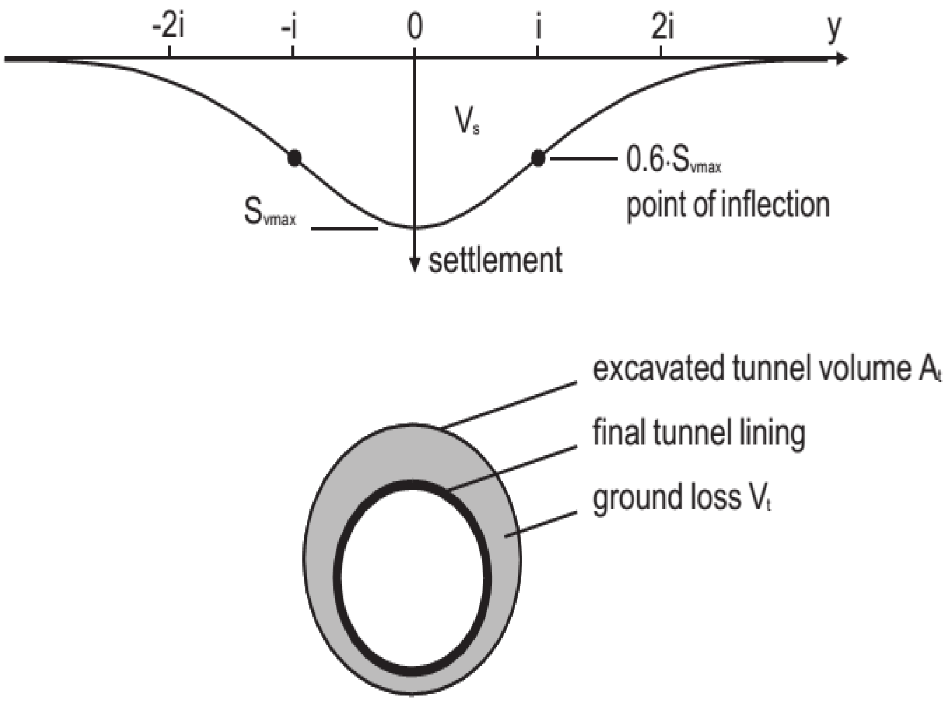

Figure 2.13. *Representation of the Surface Settlement Curve Along the Tunnel Axis Using a Gaussian Distribution (Möller (2006))*

The mathematical expression for this curve is as follows:

$$S(y) = Smax \cdot e^{(-y^2/2i^2)} \quad (2.1)$$

Where:

S(y): Represents the vertical settlement (in mm) at a distance 'y' from the tunnel's center line.

Smax: Stands for the maximum amount of settlement (in mm).

i: Denotes the width of the settlement trough (in meters).

An empirical relationship has been found between the excavation depth (Z0) and the width of the settlement curve (i) (O'Reilly and New, 1982):

$$i = k \cdot z_0 \quad (2.2)$$

Here, K is a coefficient that changes from 0.25 to 0.6, depending on the ground's specific properties. For clay soils, this value is generally around 0.5.

This settlement trough can also be seen in different layers of the ground, which vary in depth and properties. Along the settlement profile, two types of ground movement behaviors occur: sagging (where the middle part sinks down) and hogging (where the edges lift up). How these behaviors develop depends specifically on the location of nearby structures. Figure 2.14. schematically shows how these effects spread.

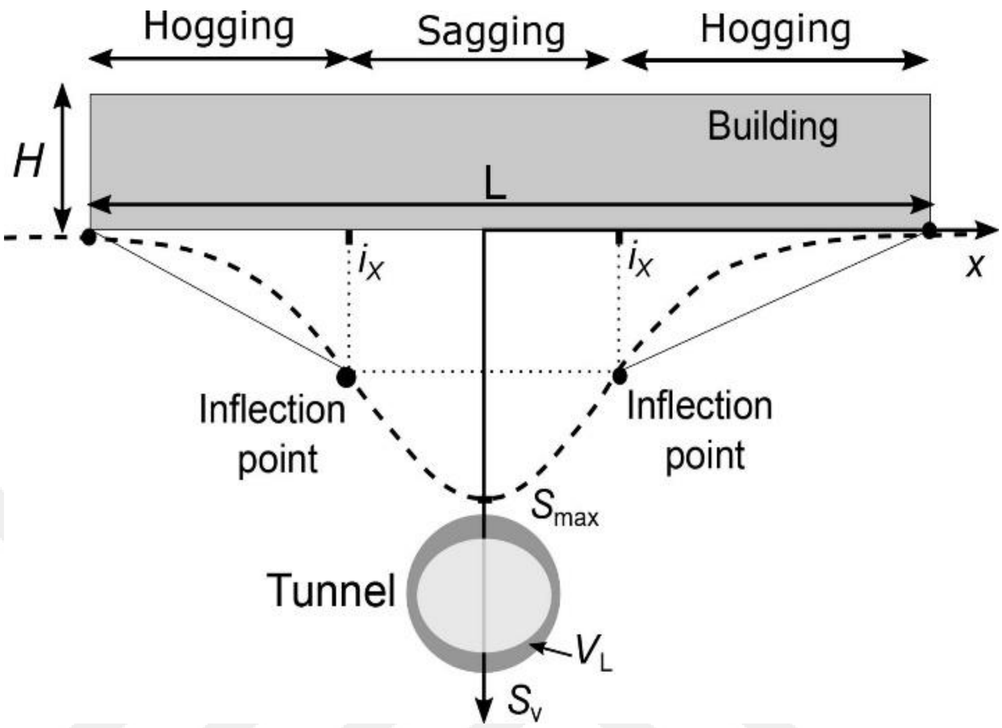

Figure 2.14. *Representation of Ground Deformation Zones (Sagging-Hogging) and Their Effects on Structures Due to Tunnel Excavation (Pinto, F., and Whittle, A. J. (2014)).*

In tunnel excavations, deformations do not only happen vertically (up and down), but also horizontally (sideways). For structures near the surface, these horizontal movements can create pulling (tensile) and pushing (compressive) stresses in the foundation, which may cause cracks. O'Reilly and New (1982) suggested the following formula, connecting horizontal movements to vertical settlements:

$$Uy = s_{(y)} \cdot \frac{y}{z_0} \tag{2.3}$$

These deformations also change in the longitudinal (along the tunnel's length) direction as the tunnel face moves forward. Attewell and Woodman (1982) stated that the settlement profile along the tunnel axis shows a Gaussian-like spread. They also noted that the maximum settlement often occurs behind the tunnel face (see Figure 2.15.). This situation becomes even clearer if support systems are not put in place quickly enough.

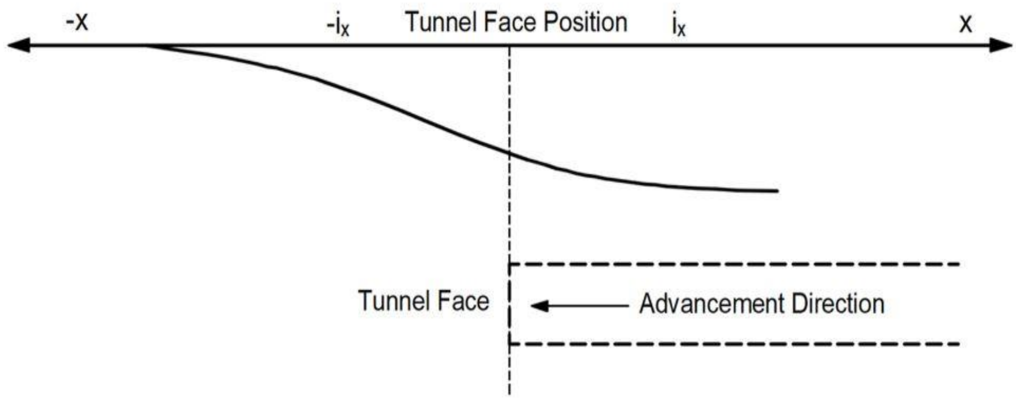

Figure 2.15. *Development of Ground Deformations as the Tunnel Excavation Progresses in the Longitudinal Direction (Moghaddasi and Noorian-Bidgoli, 2018; Zhang et al., 2017)*

The amount and spread of ground deformations also change depending on the excavation method used. Mechanized digging systems (like EPB and slurry TBMs) can control deformations by providing active pressure at the excavation face. However, in traditional methods (like NATM), this control is weaker.

2.2.1. Empirical methods

Empirical methods are models created by statistically analyzing observation data from past tunnel excavations. These models are used to predict how much the surface will settle. These methods usually work with a limited number of factors and are easy to use. The most common empirical model is the one suggested by Peck (1969), which describes surface settlements using a Gaussian (normal) distribution.

Modeling Surface Settlements with Gaussian Distribution

The settlement that happens on the surface, perpendicular to the tunnel's center line, is described by the following formula:

$$S(y) = Smax \cdot e^{(-y^2/2i^2)} \quad (2.4)$$

Where:

S(y): Represents the settlement (in mm) at a distance 'y' from the tunnel axis.

Smax: Is the maximum settlement (in mm).

i: Is the width of the settlement trough (in meters).

This distribution curve shows the symmetrical pattern of surface settlement and is presented in Figure 2.16.

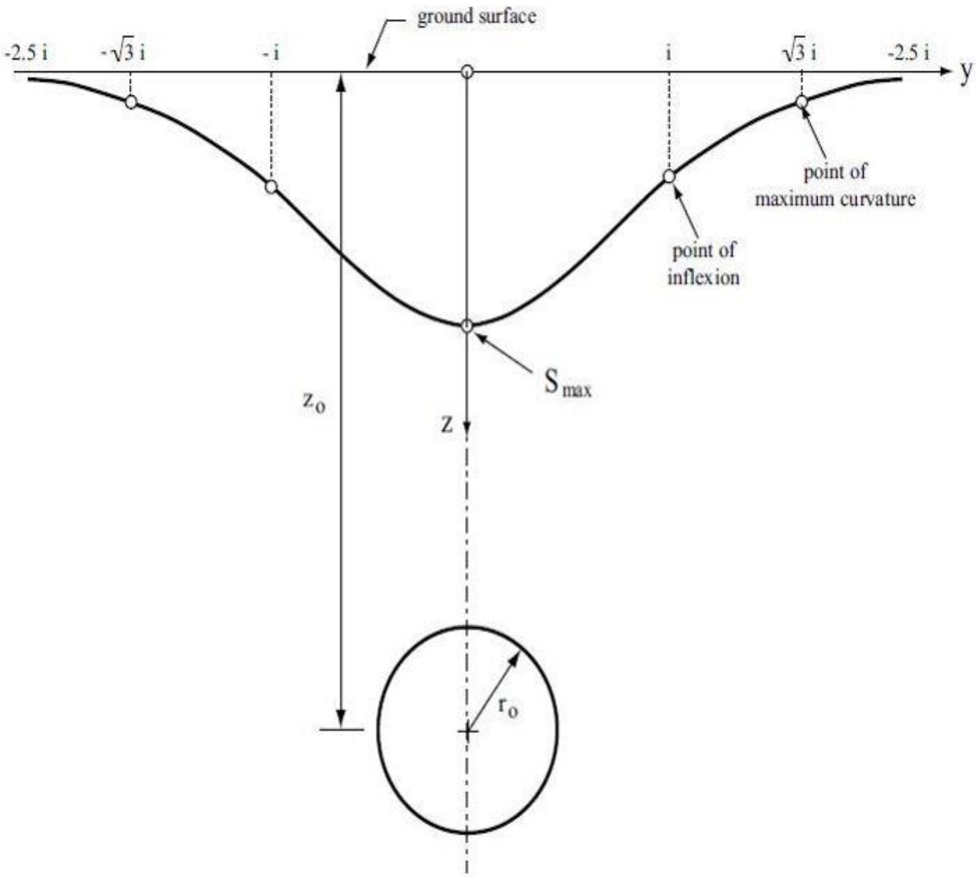

Figure 2.16. *Representation of Surface Settlement Using Gaussian Distribution (Peck, 1969).*

2.2.1.1. Determining settlement parameters

Maximum settlement is usually directly linked to ground loss. The ground loss ratio (VL) is the difference between the excavated volume and the settled volume, divided by the tunnel's volume.

$$v_L = \frac{\Delta v}{A_T} \tag{2.5}$$

The maximum settlement can be estimated as follows:

$$s_{max} = \frac{v_L}{\sqrt{2\pi i}} \tag{2.6}$$

Widely used expression by Peck (1969) and O'Reilly and New (1982) relates the width of the settlement trough (i) to the tunnel depth (Z0):

$$i = k \cdot z_0 \tag{2.7}$$

Here:

i: Is the width of the settlement trough (in meters).

z_0: Is the tunnel depth (in meters).

K: Is an empirical coefficient related to the type of ground. For sandy soils, it is generally between 0.25–0.35, and for clay soils, it is between 0.4–0.6.

Figure 2.17. presents a comparison of K values and settlement widths for different soil types.

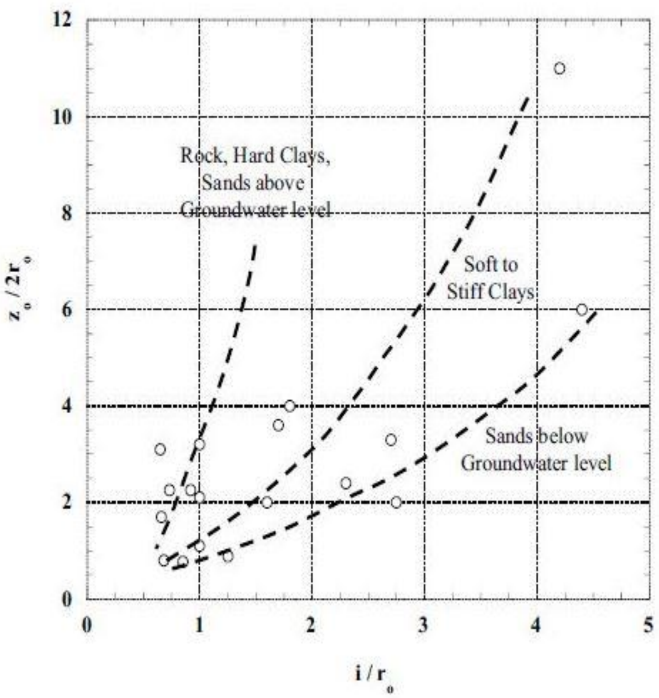

Figure 2.17. *Graphical Representation of the Relationship Between Settlement Trough Width and Soil Type (Peck, 1969)*

Additionally, the relationship between tunnel depth and the coefficient was determined using experimental data by Mair et al. (1993) and is presented in Figure 2.18.

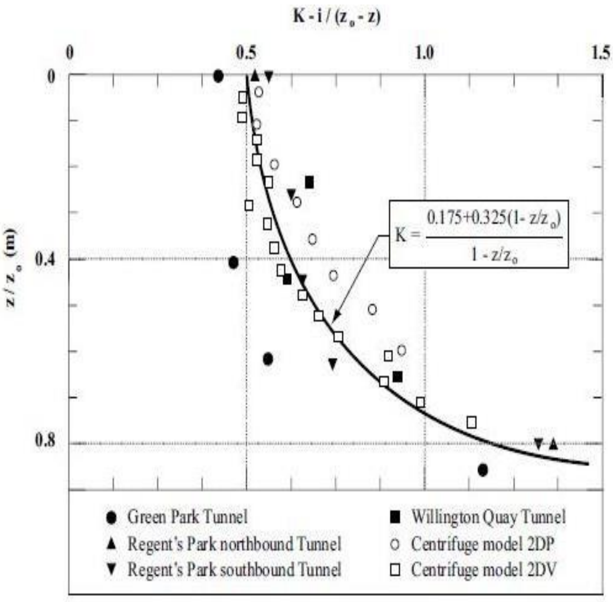

Figure 2.18. *Variation of the K-value with Tunnel Depth in Clay Soils (Mair et al., 1993).*

2.2.1.2. Estimating horizontal deformations

Horizontal deformations can also be estimated based on vertical settlement values.

$$U_x(x) = s_{\max\cdot\left(\frac{z_0}{x}\right)e}\left(-\frac{x^2}{2i^2}\right) \quad (2.8)$$

Where:

$U_x(x)$: Represents the horizontal displacement (in mm).

x: Is the distance from the tunnel axis (in meters).

z_0: Is the tunnel depth (in meters).

$Smax$: Is the maximum vertical settlement value.

The way surface settlements progress along the tunnel's length changes depending on the position of the tunnel face. This effect was shown by Attewell and Woodman (1982) in Figure 2.19.

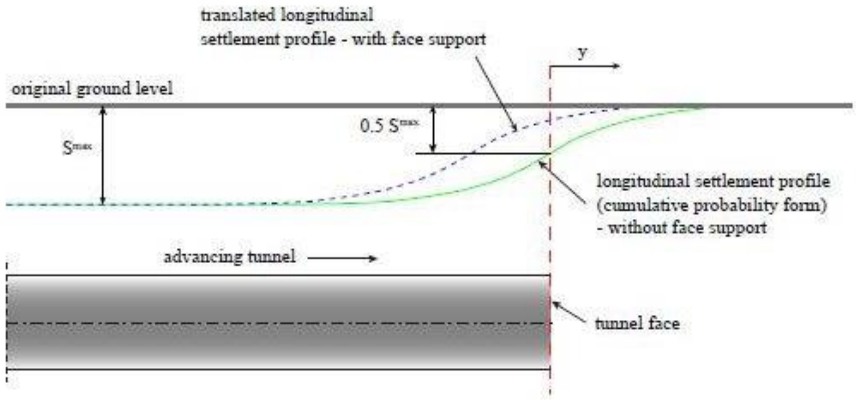

Figure 2.19. *Surface Settlement Profile According to Tunnel Face Advance (Attewell and Woodman, 1982)*

2.2.1.3. Development of settlement profile in different soil types

The coefficient (K-value), and therefore the width of the settlement spread (i), changes depending on the type of soil. For example:

Stiff clay: K = 0.4 − 0.6

Loose silt: K = 0.3 − 0.5

Sandy soil: K = 0.25 − 0.35

Additionally, how the settlement profile develops depends on the excavation stage. Field observations by Craig and Muir Wood (1978) show at which stage settlement occurs for different soil types, as presented in Table 2.1.

Type of ground	At face of shield (%)	At passage of tail of shield (%)
Sand above water table	30–50	60–80
Stiff clays	30–60	50–75
Sand below the water table	0–25	50–75
Silts and soft clays	0–25	30–50

Table2.1. *Percentage of Settlement at Tunnel Shield Face and Tail Stages According to Soil Type (Craig and Muir Wood, 1978)*

2.2.1.4. Empirical data on settlement trough width

Experimental studies have shown that the width of the settlement trough typically ranges between 30% and 60% of the tunnel's depth.

$$i = (0.3\ to\ 0.6)z_0 \qquad (2.9)$$

This relationship was statistically confirmed by O’Reilly and New (1982) and is presented in Figure 2.1.9.

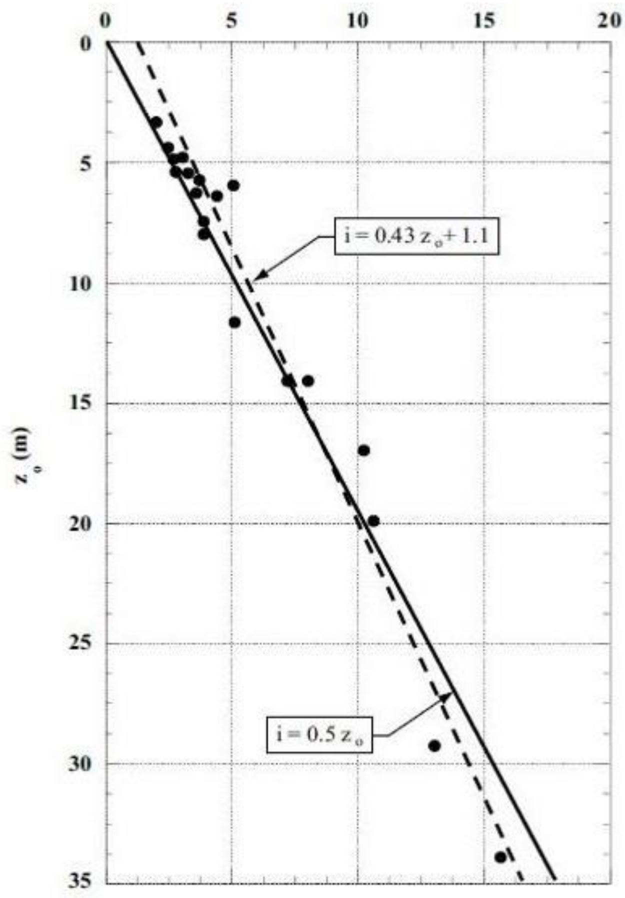

Figure 2.20. *Relationship Between Settlement Trough Width and Tunnel Depth (O'Reilly and New, 1982).*

2.2.2 Analytical methods

Analytical methods are theoretical approaches that use mathematical models to calculate ground deformations that happen during tunnel excavation. These methods are built on key assumptions, particularly from elasticity theory, porous media mechanics, and the concept of a semi-infinite medium. Under conditions where the ground is uniform (homogeneous), behaves the same in all directions (isotropic), and stretches in a straight line (linear elastic), the stresses and displacements caused by the tunnel can be solved using direct mathematical formulas.

2.2.2.1. Gap parameter and ground loss calculation

One of the most critical aspects in tunnel excavation is modeling ground loss. In this context, the "gap" parameter (often denoted as Δgap) represents the total empty space created by the excavation. This gap includes several factors: the physical void created by the cutting process, deformations caused by pressure on the tunnel face, and any tolerances that arise from the construction work itself.

$$g_P = 2\Delta + \delta \qquad (2.10)$$

Here:

Δ: Represents the overcut around the excavation.

δ: Accounts for the lining deformation and construction tolerance.

The gap parameter is a core input for models that predict surface settlement, especially in the research by Loganathan and Poulos (1998) and Lee et al. (1992).

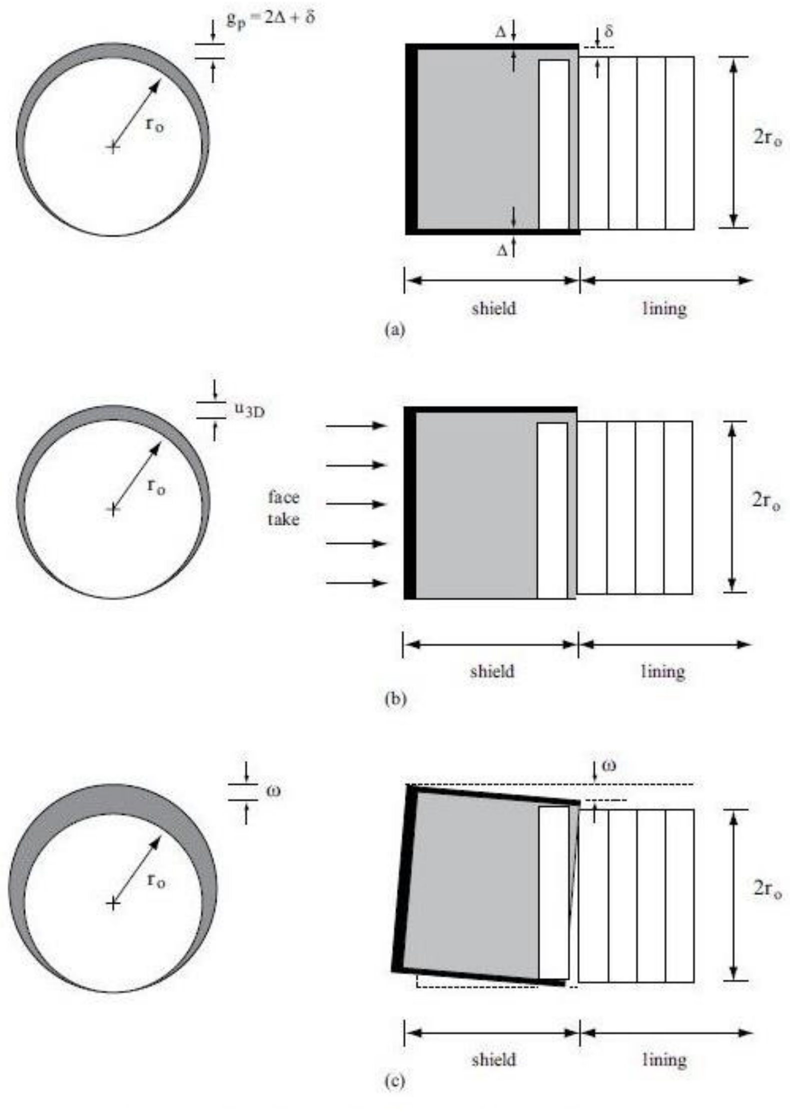

Figure 2.21. *Physical Components That Form the Gap Parameter (Lee et al., 1992).*

2.2.2.2. Elasticity-based surface settlement calculation

Models based on elasticity theory typically describe surface settlement using this formula:

$$s(y) = \frac{2g_p}{\pi} \cdot \frac{z_0}{y^2 + z_0^2} \tag{2.11}$$

Here:

S(y): The vertical settlement (in mm) on the surface at a distance 'y'.

g_p: The gap parameter (in mm).

z_0: The tunnel depth (in meters).

This formula generates a symmetrical, Gaussian-like settlement curve, with the maximum settlement occurring directly above the tunnel's center line.

2.2.2.3. Distribution of vertical deformation along depth

Below the surface, vertical displacements at various depths can be calculated using the following formula:

$$s(y) = \frac{g_p}{\pi} \cdot \frac{z}{x^2 + z^2} \tag{2.12}$$

This formula allows us to estimate how many different points above the tunnel will settle at various depths.

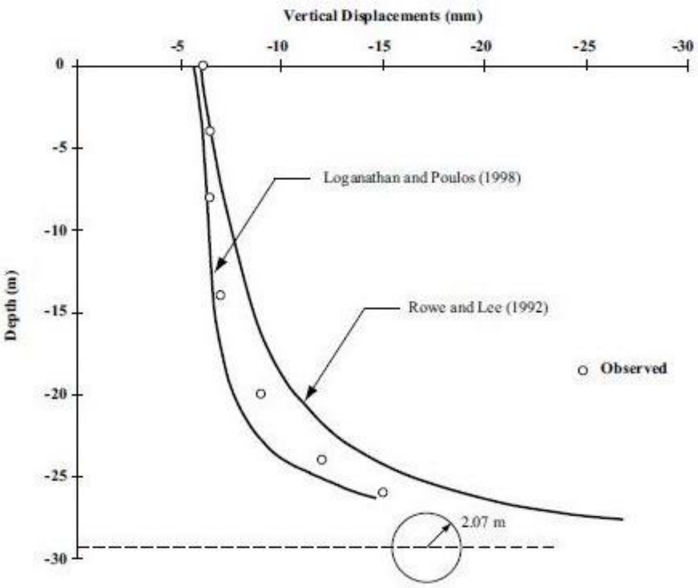

Figure 2.22. *Vertical Settlement Profile Along Depth for Green Park Tunnel (Rowe and Lee, 1992).*

2.2.2.4. Surface settlement: observation vs. prediction

The model proposed by Loganathan and Poulos (1998) has been compared with actual field observations, and it has provided very close results.

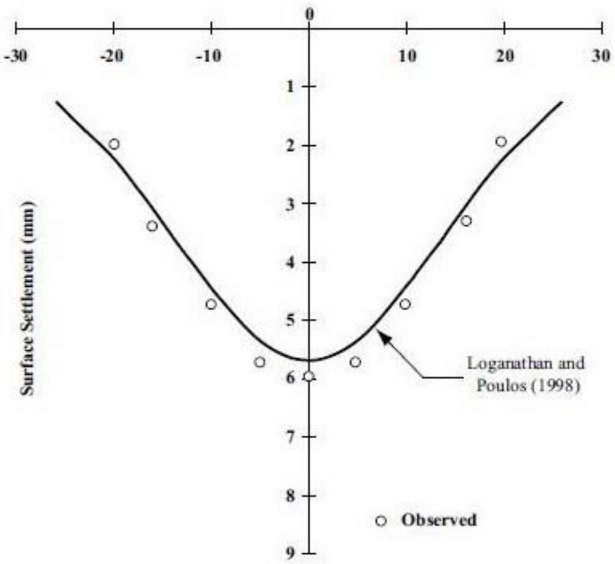

Figure 2.23. *Comparison of the Loganathan and Poulos (1998) Model with Green Park Tunnel Field Data (Loganathan and Poulos, 1998).*

2.2.2.5. Ovalization and concentric deformations

One of the most significant deformations that occurs around a tunnel is ovalization and horizontal closure. These deformations are generally described using the following parameters:

u_ϵ: Represents ovalization (surface deformation).

u_δ: Represents convergence (change in diameter).

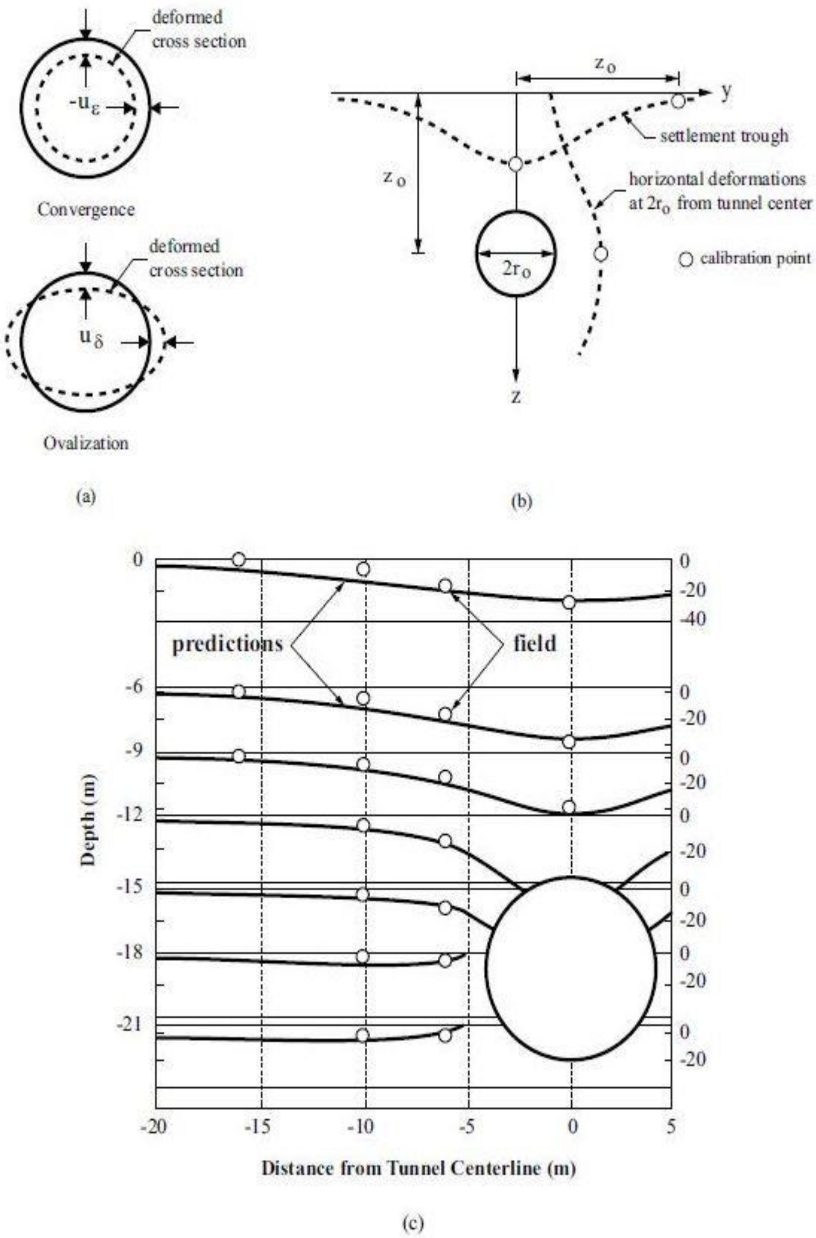

Figure 2.24. *(a) Types of Deformations Around a Tunnel (Pinto et al., 2014).*

2.2.2.6. Calibration and validation with field data

The accuracy of analytical models in real-world situations is tested through calibration studies. For example, Pinto and Whittle (2014) compared their model's predictions with observed data from the Heinenoord Tunnel and found a high level of agreement.

Figure 2.24. (c) Comparison of Analytical Model and Observational Data at Heinenoord Tunnel

2.2.3 Numerical methods

Accurately predicting ground movements caused by tunnel excavations is really important, especially in urban areas where there are existing structures. To make these predictions more precise, engineers use advanced numerical analysis methods. These methods allow them to create 3D models of complex situations, such as difficult ground conditions, multiple tunnels interacting with each other, how tunnels affect nearby buildings, and excavation processes that happen in stages.

Numerical analyses are typically done using commercial software like PLAXIS, FLAC3D, and Abaqus. These programs are based on approaches such as the Finite Element Method (FEM), Finite Difference Method (FDM), and Finite Volume Method (FVM). With this software, engineers can handle complicated shapes, varied ground structures, different digging scenarios, and detailed interactions between structures and the ground.

2.2.3.1 Ground modeling techniques

The way soil behaves is crucial for accurately predicting deformations in numerical modeling. Here are some of the most common models used for ground behavior:

Mohr-Coulomb Model: This is a simplified linear elastic-plastic model. It's often chosen for initial design phases.

Hardening Soil (HS) Model: This model considers how soil stiffness changes with stress levels and includes the effects of consolidation (when soil compacts over time).

Soft Soil Model: This one is particularly suitable for soils like organic or soft clays.

Along with elastic moduli (E_{50}^{ref}, E_{oed}^{ref},E_{ur}^{ref}), which describe how elastic the soil is, other important parameters used in these models include the internal friction angle (ϕ), cohesion (c), and dilation angle (ψ).

2.2.3.2. Phased analysis of the excavation process

Tunnel excavations are often carried out in several steps. In numerical analyses, this process is modeled using a "phased construction" approach. In each step:

1)The volume of excavated ground is removed.

2)The tunnel lining (support structure) is activated.

3)Grouting pressure (from injected material) and face pressure (from the tunnel boring machine) are applied.

4)Ground deformations are recalculated.

These step-by-step analyses provide insights into how deformations change over time and how displacement profiles develop as the excavation moves forward.

2.2.3.3. Interface modeling

To represent how the ground and the tunnel lining or structure slide against each other and stick together, interface elements are defined in numerical models. The "Rinter" coefficient is commonly used in these interfaces.

$$s(y) = \frac{2g_p}{\pi} \cdot \frac{z_0}{y^2 + z_0^2} \tag{2.13}$$

Here,$\tau_{interface}$ is the shear strength of the interface, and τ_{soil} is the shear strength of the soil. R_{inter} is generally set between 0.6 and 1.0. Lower R_{inter} values indicate a weaker connection between the soil and the lining.

2.2.3.4. Estimating deformations

In numerical analyses, we can determine surface settlements along both the tunnel's longitudinal (lengthwise) and transverse (crosswise) axes. Additionally, we can calculate the internal forces, relative displacements, and rotations that structures will experience at different construction stages in three dimensions.

Specifically, surface settlement profiles S(y) and horizontal displacement profiles Uy will change over time as the excavation progresses:

$$s_y = S_{\max} \cdot \exp\left(\frac{y^2}{-2i^2}\right)^2 \tag{2.14}$$

$$Uy = \delta(y) \cdot \frac{y}{z_0} \tag{2.15}$$

2.3. Soil-Structure Interaction Caused by Tunnel Excavation

Ground movements during tunnel excavation lead to complex deformation behaviors, not just in open "greenfield" areas, but also in environments where structures interact with the ground. When we consider the settlement and horizontal displacements in the ground alongside the stiffness, shape, and loading conditions of buildings resting on foundations, the concept of soil-structure interaction (SSI) becomes essential.

This interaction between the ground and the structure directly affects both the magnitude and distribution of deformation, which in turn determines the nature of the internal forces within the structural elements (Mair and Taylor, 1997; Potts and Addenbrooke, 1997). While settlement troughs caused by tunnels in greenfield conditions usually form symmetrical profiles (often described by a Gaussian distribution), the presence of building foundations disrupts this symmetry, causing the settlement shape to become asymmetrical. When a structure is very stiff, ground displacements beneath its foundation are restricted, and the structure passively resists the deformations from the excavation. In this situation, ground movements are partially transferred to the building, leading to increased stresses and internal deformations within the structure (Franzius et al., 2005).

There are two main approaches to evaluating soil-structure interaction: The first involves modeling the structure and the ground together in three dimensions and including them in the excavation process. The second uses equivalent beam or solid models, where the structure's effect is represented indirectly. In both approaches, it's crucial to thoroughly examine the differential settlements, rotations, and shear forces that tunnel excavation causes in building foundations (Forth et al., 2006). To do this, engineers can use both numerical modeling and field observations to figure out how the soil and structure interact.

The effects of soil-structure interaction depend on many factors, such as tunnel depth, the horizontal distance between the tunnel and the building's foundation, building height, stiffness/arching effects, foundation width, structural symmetry, and soil properties. To assess this complex interaction, many methods, both empirical and numerical analysis-based, have been developed in the literature (Mair, 2008; Frischmann et al., 1994).

2.3.1. Building deformation parameters

When evaluating how ground movements from tunnel excavation affect structures, it's really important to describe the deformation behavior quantitatively. To do this, various descriptive parameters have been developed in engineering literature. The settlement curve that a building's foundation rests on is usually examined using three main geometric characteristics: maximum settlement (Smax), angular distortion (β), and curvature (ρ). Additionally, the differential settlement (ΔS) between the building's end points is critically important for assessing damage.

These parameters are illustrated in Figure 1.18. The figure shows (a) the definition of the settlement curve, (b) the maximum vertical displacement (Smax), and (c) the rotation (θ) and angular distortion that happen in the middle of the structure.

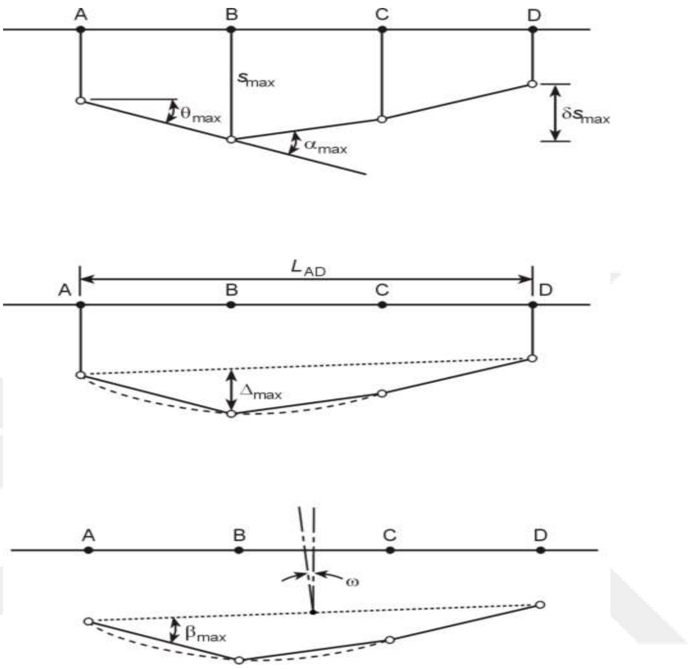

Figure 2.25. *Schematic Representation of Characteristic Deformation Parameters for the Settlement Profile Along a Building Foundation Due to Tunnel Excavation (Boscardin, M. D., and Cording, E. J. (1989)).*

(a) Shows maximum settlement (Smax), angle of rotation (θ), curvature (ρ), and

(b) differential settlement (ΔS); Illustrates maximum vertical displacement (Smax);

(c) Depicts the bending effect and rotation (θ) in the middle.

Here are the main parameters defined:

Angular distortion (β) is defined as the ratio of the settlement difference between two points on the structure to their horizontal distance:

$$\theta = \frac{\delta}{L} \tag{2.16}$$

Curvature α can be defined by the second derivative of the settlement curve; it is simply approximated as:

$$\alpha = \frac{\Delta}{L^2} \tag{2.17}$$

Maximum differential settlementδ_{max} is:

$$\delta_{\max} = \delta_{max} - s_{m_i n} \tag{2.18}$$

These parameters, especially when evaluated alongside variables like structural stiffness, foundation width, and building height, offer insights into the potential degree of structural damage. In literature, these parameters are often compared against threshold values in damage classification systems (e.g., Burland's classification) to assess structural safety.

2.3.2. Equivalent beam models for analyzing soil-structure interaction caused by tunnel excavation

When analyzing how soil and structures interact, one common way to simplify the complex shapes and features of buildings is by using equivalent beam models. These models make it easier to computationally simulate how structures react to ground displacements caused by tunnel excavations. Equivalent beam modeling allows for comparative analysis of different scenarios without needing detailed structural models.

When assessing the effects of ground deformations from tunnel excavations along a structure's foundation, the maximum angular distortion ratios are key parameters. In this context, deformations in the sagging (settlement in the middle) and hogging (uplift at the ends) zones of the foundation are defined separately. The ratio of the maximum vertical settlement difference in these areas to their corresponding horizontal distance is expressed as MDRsagging and MDRhogging, respectively. These ratios are calculated as follows:

$$MDR_{sag} = \frac{\Delta sag}{Lsag} \tag{2.19}$$

$$MDR_{sag} = \frac{\Delta sag}{Lsag} \tag{2.20}$$

Here, Δsag and Δhog represent the maximum settlement differences observed in the sagging and hogging regions, respectively. Lsag and Lhog are the horizontal distances over which these differences occur. MDR values are typically evaluated by comparing them to reference angular distortion limits to classify the risk of structural damage.

In pioneering work by Potts and Addenbrooke (1997), structures were modeled as an equivalent beam placed on a non-linear elastic-plastic soil using the 2D finite element method. This structural representation defines the structure using three main parameters: elastic modulus (E), cross-sectional area (A), and moment of inertia (I). The interface between the beam and the soil was assumed to be perfectly bonded, and the structure's weight was ignored.

To define the structural interaction in the model, two dimensionless stiffness parameters were used:

$$\rho^* = \frac{EI}{E_s(B\ /\ 2)^4} \tag{2.21}$$

$$\alpha = \frac{EA}{E_s(B\ /\ 2)} \tag{2.22}$$

Here, $E_s$represents the soil stiffness, and B represents the transverse stiffness of the structure. The results showed that as structural stiffness increased, the maximum settlement decreased. Reductions were also observed in both sagging/hogging deformations and horizontal deformation gradients.

Figure 2.26. illustrates the difference between the Gaussian-distributed settlement profile in a situation without a structure (greenfield) and the asymmetrical deformation profile under a building's foundation. The deformation differences caused by the structure's stiffness are defined in the hogging and sagging regions, and these regions were analyzed using deformation gradients and characteristic lengths.

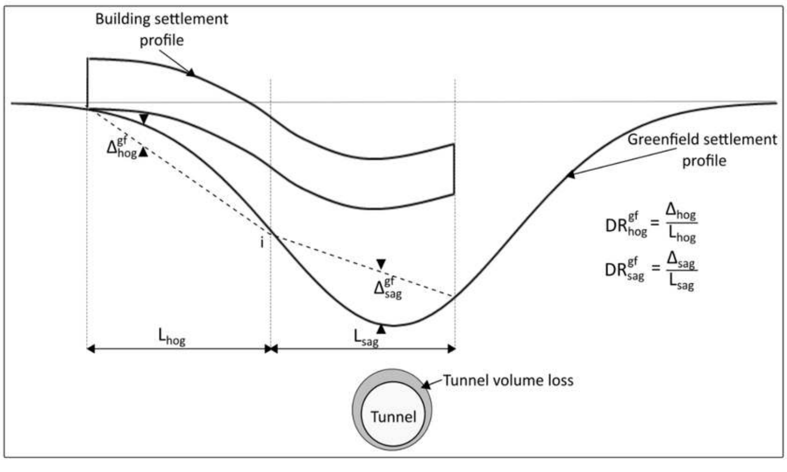

Figure 2.26. *Settlement Profiles Caused by Tunnel Excavation: Greenfield vs. Structural Influence Comparison (Mair and Taylor (1997)).*

Figure 2.27 - Figure 2.28 presents the vertical settlement profiles along the tunnel axis for different values of relative flexural stiffness ρ^*. As stiffness increases, the amplitude of surface settlement decreases, and the shape of the settlement curve changes significantly. When compared to the greenfield (no structure) condition, it's clear that the presence of a structure limits surface deformation.

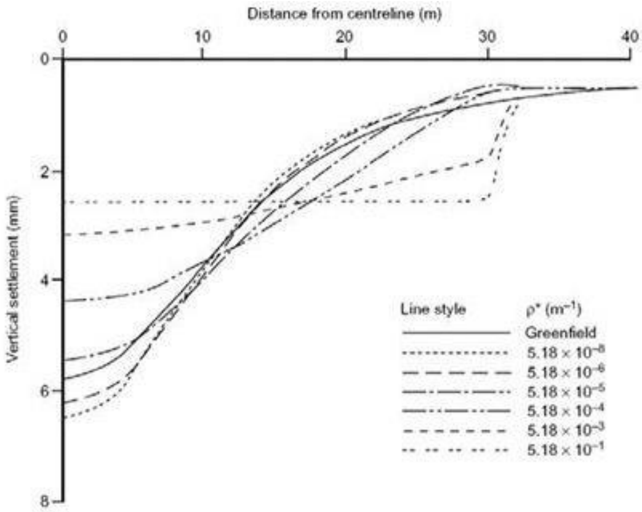

Figure 2.27. *Parametric Study of the Effect of Building Stiffness on Ground Settlements (Potts and Addenbrooke (1997)).*

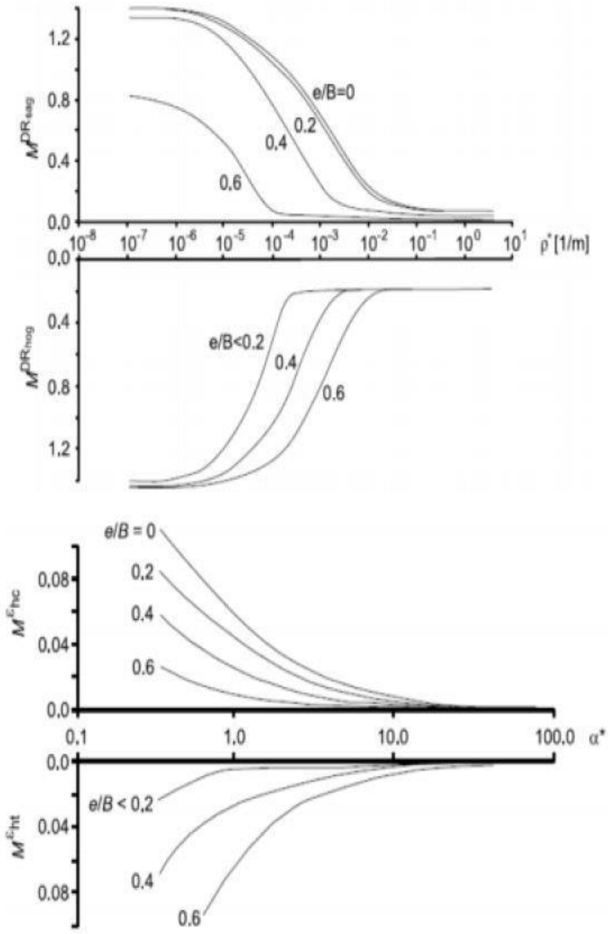

Figure 2.28. *Parametric Study of the Effect of Building Stiffness on Ground Settlements (Potts and Addenbrooke (1997)).*

2.3.3. Defining equivalent parameters for different Sstructure types

2.3.3.1. Masonry structures

Masonry structures can be treated as a single, rigid beam resting on the ground. If we consider the building's span (B), wall thickness (t), and building height (H), the equivalent parameters are calculated as follows:

The cross-sectional area (A) is:

$$A = B \cdot t \tag{2.23}$$

And the moment of inertia (I) is:

$$I = \frac{1}{12} \cdot B \cdot t^3 \tag{2.24}$$

2.3.3.2. Framed structures

For multi-story framed structures with 'm' floors, we assume there are 'm+1' floor slabs. Each slab has its own cross-sectional area $A_{slab,i}$ and moment of inertia $I_{slab,i}$. To define the structure's overall behavior, the total equivalent flexural stiffness I_{eq} is calculated by considering each slab's distance h_i from the building's overall neutral axis:

$$I_{eq} = \sum_{i=1}^{n} \left(\gamma_i \cdot I_{strain,i} \cdot A_{strain,i} \cdot h_i^2 \right) \tag{2.24}$$

Similarly, the equivalent axial stiffness area A_{eq} is:

$$A_{eq} = \sum_{i=1}^{m+1} A_{slab,i} \tag{2.25}$$

These two values ($\rho^*$and a^*) are then used in place of I and A in the calculations defined by Potts and Addenbrooke (1997) for dimensionless stiffness parameters.

2.3.3.3. Cavity masonry facades

For cavity masonry facades, the approach suggested by Pickhaver (2006) involves dividing them into vertical and horizontal strips. This allows for a hybrid model that accounts for both flexural and shear stiffness.

Figure 2.29 illustrates two different idealizations used to model the effects of tunnel excavation on a multi-story framed structure. In scheme (a), the structure is represented as rigid layers placed on the ground, while in scheme (b), the same structure is modeled as an elastic beam with equivalent stiffness properties. These representations are crucial for evaluating how parameters like building height, width, moment of inertia, and foundation depth influence the structure's behavior.

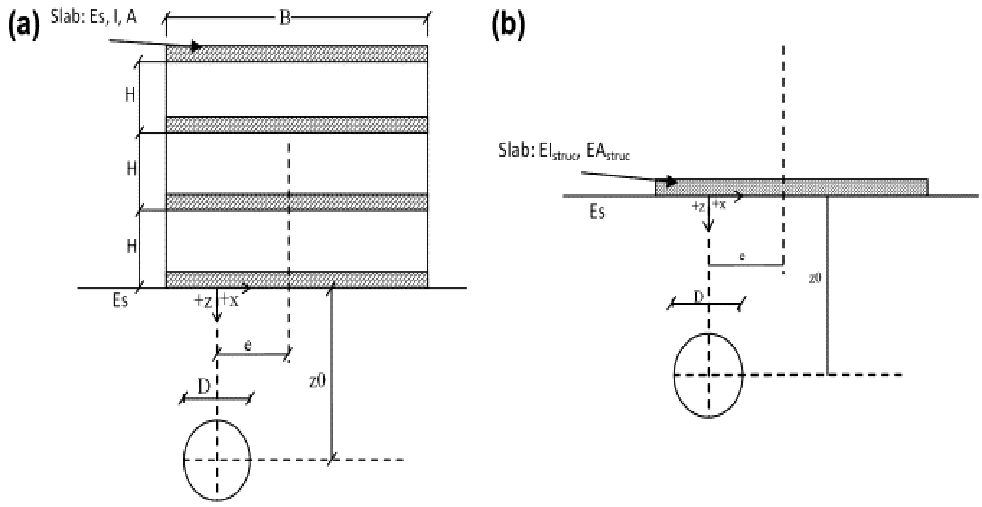

Figure 2.29. *Representation of a Framed Structure as a Rigid Block in an Equivalent Structure Model (a) and an Equivalent Elastic Beam Model (b) (Franzius et al. (2005)).*

2.3.3.4. Effect of building weight

Franzius et al. (2004) investigated the impact of building weight on ground response through experimental and numerical analyses. Their findings showed that weight significantly affects deformation in two key areas: at the tunnel level and in regions close to the foundation base. Building weight alters the stress patterns in the ground, which in turn changes how the ground reacts to excavation. In some cases, this leads to an increase in both absolute and differential settlements. However, its influence on the modification factors proposed by Potts and Addenbrooke (1997) remains limited.

2.4. Assessing Structural Damage Caused by Tunnel Excavation

Tunnel construction, particularly in urban areas, can cause significant damage to nearby structures due to ground movements. To predict and reduce this damage, various theoretical and empirical models have been developed, based on both free-field (no structure) and soil-structure interaction approaches. This study combines these two fundamental approaches to provide a comprehensive damage assessment system, enriched with calculations and supported by academic sources.

Ground deformations resulting from tunnel excavations lead to differential settlements and horizontal movements in building foundations. These deformations are generally described by three main parameters: angular distortion ($\beta=\delta v/L$), horizontal tensile strain ($\epsilon h=\delta h/L$), and deflection ratio (Δ/L).

Skempton and MacDonald (1956) found that the likelihood of damage is low when $\beta<1/300$, but significant structural damage occurs when $\beta>1/150$. Burland and Wroth

(1974) described the behavior of structures using a deep beam model and proposed various equations to determine how a structure responds to deformations.

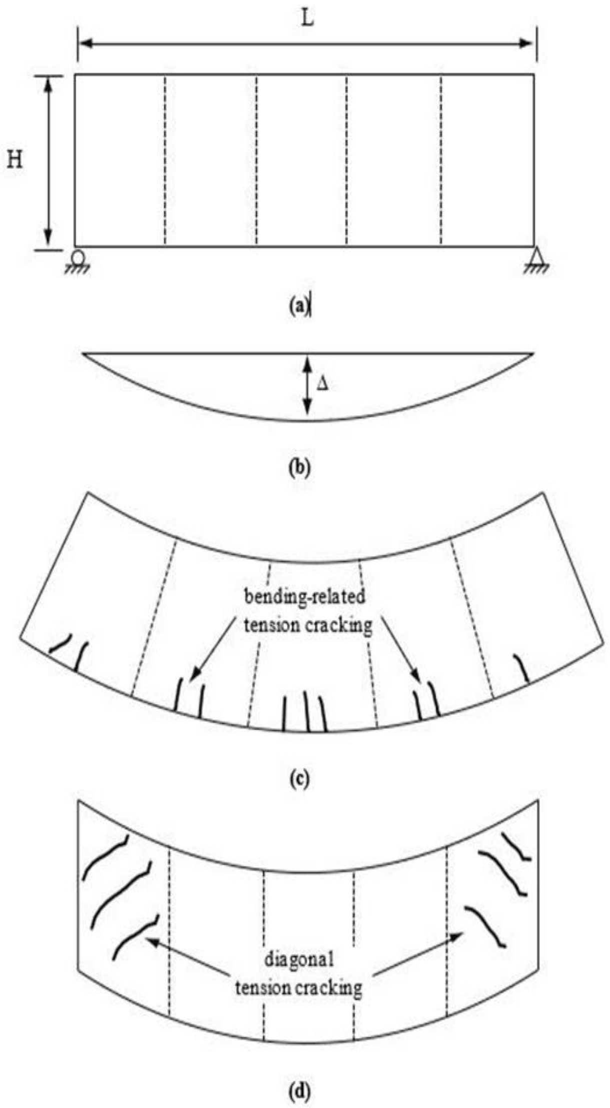

Figure 2.30. *Damage Diagram with Deep Beam Model (Burland, J. B. and Wroth, C. P. (1974). Settlement of buildings and associated damage).*

Figure 2.30. illustrates the structural model representing a Deep Beam: (a) shows the structure as a simply supported beam, (b) depicts the settlement shape (deflection), (c) indicates tensile cracks due to bending, and (d) demonstrates the formation of diagonal shear cracks. This model is used to explain how structures respond to surface deformations caused by tunnel excavations.

According to the damage classification system developed by Boscardin and Cording (1989), damage is categorized based on β (angular distortion) and ϵh (horizontal tensile strain) values as follows:

Negligible damage: $\beta<1/500$ and $\epsilon h<0.05\%$

Very slight damage: $1/500<\beta<1/300$ and $0.05\%<\epsilon h<0.075\%$

Slight damage: $1/300<\beta<1/150$ and $0.075\%<\epsilon h<0.15\%$

Moderate damage: $1/150<\beta<1/100$ and $0.15\%<\epsilon h<0.3\%$

Severe damage: $\beta>1/100$ and $\epsilon h>0.3\%$

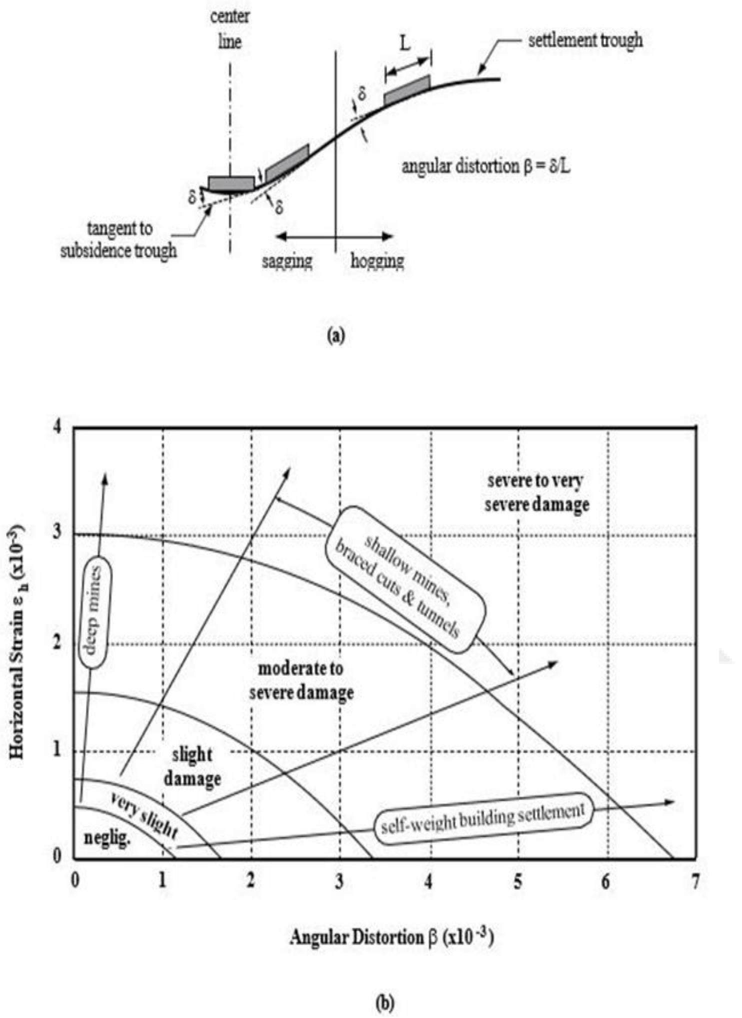

Figure 2.31. *Damage Zones Based on Angular Distortion and Strain Effects (Boscardin, M. D. and Cording, E. J. (1989)).*

Figure 2.31. displays a diagram that illustrates the damage categories based on the relationship between angular distortion (β) and horizontal tensile strain (ϵh). The classification zones in this graph help determine the impact of deformations caused by tunnel excavations on structures.

Burland (1995) also established five categories of damage, but these are based on crack width:

Category 0: Negligible

Category 1: Hairline cracks

Category 2: Cracks up to 1 mm

Category 3: Cracks up to 5 mm

Category 4–5: Cracks between 5–25 mm, along with structural deformations.

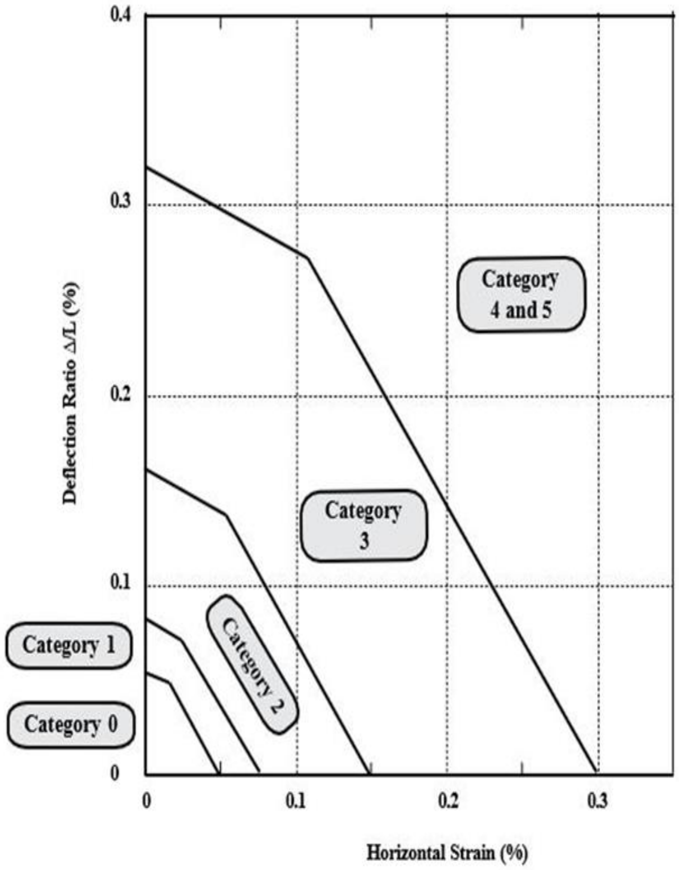

Figure 2.32. *Damage Categories Based on Deflection Ratio and Horizontal Strain (Burland, J. B. (1995)).*

Figure 2.32. shows damage categories defined by the relationship between horizontal strain (%) and deflection ratio (ΔL/L). This graph is used to evaluate the limit values for structural crack formation in hogging deformation zones.

In the Mansion House case study, conducted by Frischmann et al. (1994), the difference between the free-field settlement profile and the actual deformation highlighted the importance of structural stiffness. Damage predictions tend to be overestimated when soil-structure interaction isn't modeled.

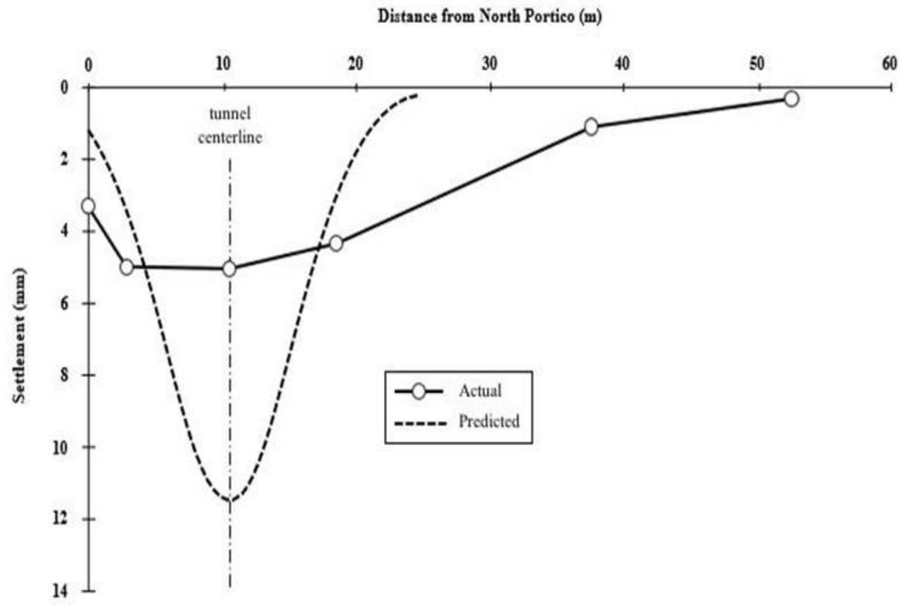

Figure 2.33. *Comparison of Predicted and Observed Settlement Profiles (Mansion House Case Study) (Frischmann, W., Potts, D. M., Addenbrooke, T. I. (1994)).*

Figure 2.33. shows the settlement profile of the Mansion House in London along the tunnel axis. It compares actual field observations with predictions made without considering structural influence. This comparison highlights the impact of accounting for soil-structure interaction on the results.

To reduce damage during tunnel excavations, you can apply these strategies:

Pressure control and grouting with the TBM (Tunnel Boring Machine).

Ground improvement techniques (like jet grouting, injection, or freezing).

Structural strengthening (such as foundation reinforcement or support systems).

Soil-structure interaction analyses using numerical models (like FEM, PLAXIS).

In conclusion, accurately assessing structural damage caused by tunnel excavations requires considering both theoretical models and empirical data together. An integrated approach that accounts for parameters like structural stiffness, soil properties, and excavation method is critical for minimizing damage risk.

2.4.1. Damage criteria

Damage criteria are threshold values used to classify the effects of ground movements from tunnel excavations on structures. These criteria are typically defined based on structural deformations (like angular distortion and horizontal tensile strain) and the size of any resulting cracks.

2.4.1.1. Fundamental deformation parameters

Ground deformations caused by tunnel excavations lead to differential settlements and horizontal movements in building foundations. These deformations are the main parameters used to assess structural damage:

Angular Distortion (â=äv/L): This is the ratio of the vertical displacement (settlement difference) between two points on a structure to the horizontal distance between those points. It causes bending deformations in structural elements.

Horizontal Tensile Strain (ϵh=äh/L): This is the ratio of the horizontal displacement between two points on a structure to the horizontal distance between them. It results in tensile or compressive stress within structural elements.

Deflection Ratio (Ä/L): This is generally defined as the ratio of the maximum deflection at the midpoint of a beam to its span.

2.4.1.2. Damage Classification Systems

Various researchers have developed different systems to classify structural damage based on the parameters mentioned above.

Skempton and MacDonald (1956): They evaluated the likelihood of damage primarily based on angular distortion.

$\beta<1/300$: Low probability of damage.

$\beta>1/150$: Significant structural damage.

Boscardin and Cording (1989): They offered a more detailed damage classification by combining angular distortion (β) and horizontal tensile strain (ϵh) (see Figure 2.32. for visual representation).

Negligible damage: $\beta<1/500$ and $\epsilon h<0.05\%$

Very slight damage: $1/500<\beta<1/300$ and $0.05\%<\epsilon h<0.075\%$

Slight damage: $1/300<\beta<1/150$ and $0.075\%<\epsilon h<0.15\%$

Moderate damage: $1/150<\beta<1/100$ and $0.15\%<\epsilon h<0.3\%$

Severe damage: $\beta>1/100$ and $\epsilon h>0.3\%$

Burland (1995): He categorized damage into five levels based on the amplitude (width) of cracks in structures (see Figure 2.32. for visual representation).

Category 0: Negligible (no cracks).

Category 1: Hairline cracks.

Category 2: Cracks up to 1 mm.

Category 3: Cracks up to 5 mm.

Category 4–5: Cracks between 5–25 mm and structural deformations.

These criteria guide engineers in evaluating the potential impacts of tunnel excavations and in taking necessary precautions.

2.4.1.3. Damage evaluation process

The structural damage evaluation process is a systematic, phased approach to analyze the potential impacts of tunnel excavations on nearby structures and to identify associated risks. This process typically consists of four main stages:

1. Preliminary Assessment

The first stage is used to conduct a general screening of structures potentially affected by tunnel excavations. At this stage, simplified criteria proposed by Rankin (1988) are often applied:

Maximum slope (è): $\theta \leq 1/500$

Maximum settlement: ≤ 10 mm

Structures that meet these thresholds are classified as "negligible risk" and don't require further analysis. This preliminary screening is usually performed by drawing settlement contours along the tunnel's alignment.

2. Second-Stage Assessment

Structures identified as risky during the preliminary assessment undergo a more detailed examination in this stage. Here, the structure is modeled as a simple beam under "greenfield" (no existing structure) conditions, assuming its foundations move along with the ground. When the structure lies within the settlement trough, it can be subjected to two different deformation zones:

Sagging zone: Settlement occurs in the middle part of the structure, leading to horizontal compressive strain.

Hogging zone: Settlement occurs at the ends of the structure, resulting in horizontal tensile strain, which increases the risk of cracking.

At this stage, the structure's behavior along the free-field curve and the points of maximum settlement/slope are analyzed.

3. Second-Stage Assessment with Relative Stiffness

The simple beam model often provides conservative results because it ignores a structure's stiffness. To overcome this, an approach developed by Potts and Addenbrooke (1997) considers the structure's stiffness using two ratios:

Axial stiffness ratio:

$$K = \frac{E_b I_b}{E_s L^3} \tag{2.26}$$

Flexural stiffness ratio:

$$\rho^* = \frac{E_b I}{E_s L_s^3} \tag{2.27}$$

Analyses using these parameters show how structural stiffness affects surface settlements. As stiffness increases, the structure deviates from the "greenfield" curve, and deformation is reduced.

4. Detailed Evaluation

If the second-stage assessment classifies a structure as Category 3 (slight damage) or higher according to the Boscardin and Cording (1989) classification, a detailed evaluation is necessary. This analysis is specific to the structure and considers the following factors:

1. **Material parameters:** Structural material properties like wall type and elastic modulus.
2. **Past settlements and cracks:** The structure's previous deformation history.
3. **Foundation system:** Types of foundations such as raft foundations or pile foundations.

Superstructure stiffness distribution: Differences in stiffness across various parts of the structure.

This detailed evaluation typically uses advanced numerical modeling techniques, such as 2D or 3D finite element analyses (FEM). For deformation assessment, Burland's (1995) classification diagrams are referenced based on the Δ/L and ϵh parameters.

This phased process is critical for accurately assessing structural damage caused by tunnel excavations and for developing appropriate engineering solutions.

3. CASE STUDY DESCRIPTION

This section introduces the Napoli Metro Line 6 project, which forms the basis for the 3D finite element analyses performed to assess the impact of tunnel excavation on structures. We'll detail the selection process for the model parameters, considering the soil profile and excavation method.

3.1 Napoli Metro Line 6: A 3 km Tunnel in a Densely Urban Area

The Napoli Metro Line 6 is a significant infrastructure project designed to integrate with the existing rail transport system and enhance it with new transfer points. This line is part of a 90 km railway network and consists of four distinct sub-sections. For this study, we've focused on the Mergellina–Municipio section, as it's considered the most critical in terms of its interaction with existing structures.

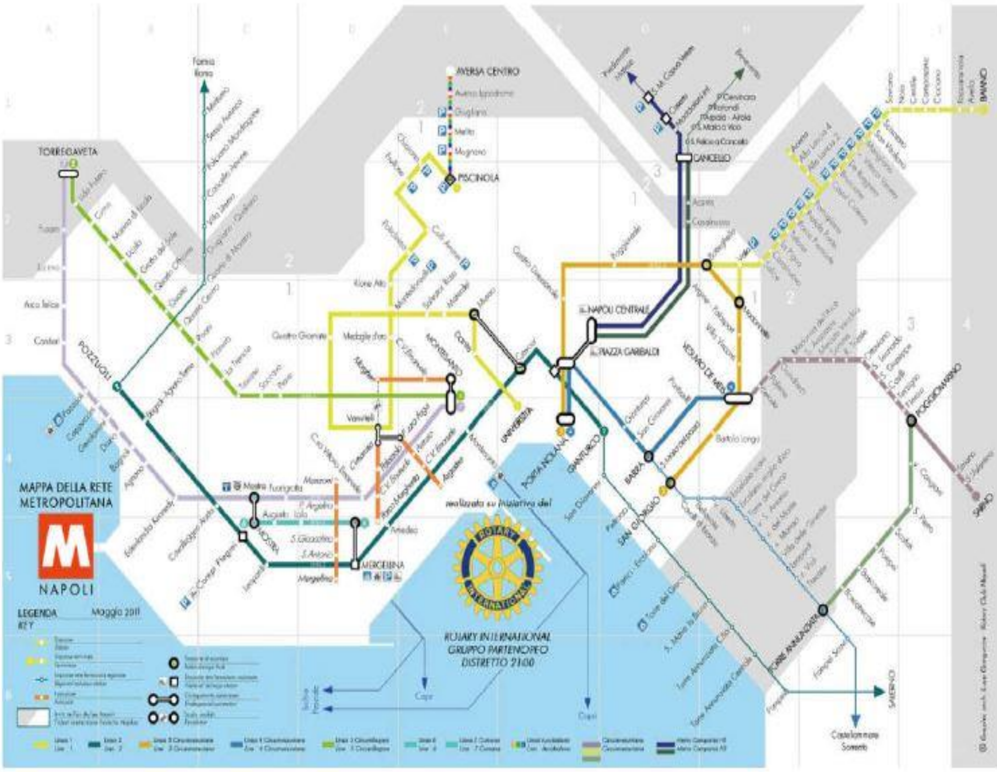

Figure 3.1. *Schematic representation of the Naples Metro transportation network (Celentano, 2015).*

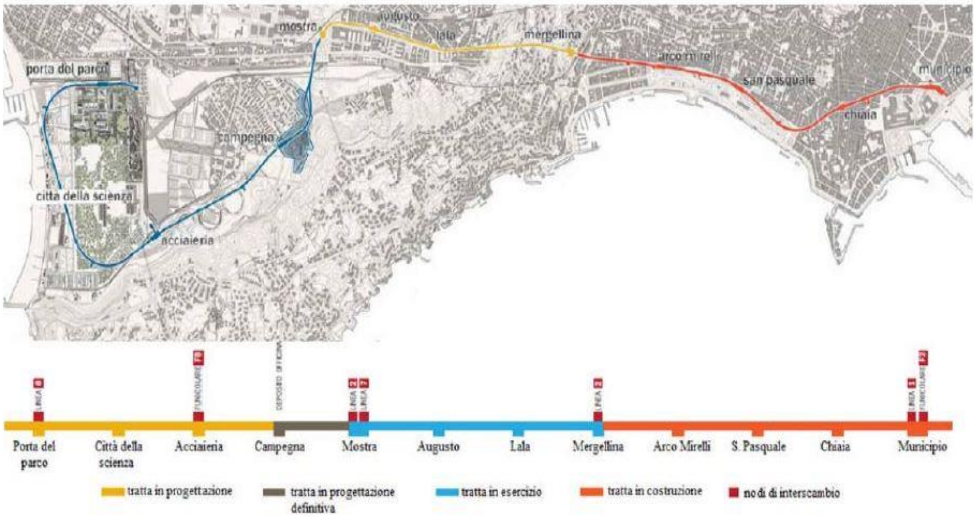

Figure 3.2. *Divided plan of Line 6 (Celentano, 2015)*

3.1.1. Definition and technical specifications of line 6

The tunnel section between the Mergellina and Lala stations was excavated using an Earth Pressure Balance (EPB) type TBM, specifically the TB816H/GS model. This TBM has a diameter of 8135 mm. The tunnel lining, made of reinforced concrete segments, has an inner diameter of 3625 mm and an outer diameter of 3925 mm. Each segment is 300 mm thick, and the ring width is 1.7 m.

Along with the EPB method, ground conditioning was carried out using mixtures containing water, foam, bentonite suspension, or polymers. During tunneling, the annular gap behind the TBM was filled with grout to minimize surface deformations.

3.2. Ground Conditions

Along the tunnel's path, various soil layers were identified, including loose pyroclastic soils, volcanic tuff, pumice, and fill layers. Notably, between Via Piedigrotta and Piazza dei Martiri, the ground shows both high permeability and critical characteristics regarding soil-water interaction. The base tuff level was observed to rise up to -6 meters below sea level at times along the soil profile.

The groundwater level is approximately 1–1.5 meters below the ground surface. Consequently, a significant portion of the tunnel lies beneath the water table.

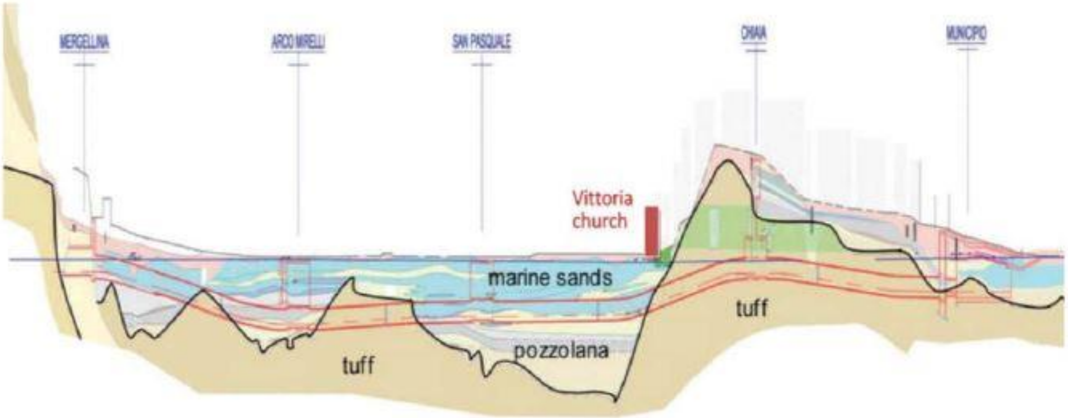

Figure 3.3. *Typical soil profile along the tunnel alignment (Celentano, 2015).*

3.3. Geotechnical Investigation Studies

Within the scope of the project, four separate geotechnical investigations were carried out in 1990, 1998, 2005, and 2008. These campaigns involved SPT (Standard Penetration Test), CPT (Cone Penetration Test), Lefranc tests, core drillings, and laboratory tests.

1990 Geotechnical Investigations: Undisturbed samples were taken from loose soils to determine their permeability and strength values.

1998-2000 Geotechnical Investigations: Soil layers were detailed through 24 boreholes, 60 SPTs, and 6 CPT profiles.

2005 and 2008 Geotechnical Investigations: Intensive drilling and CPT studies were concentrated around the Arco Mirelli and San Pasquale stations. Additionally, cross-hole tests were integrated into these campaigns.

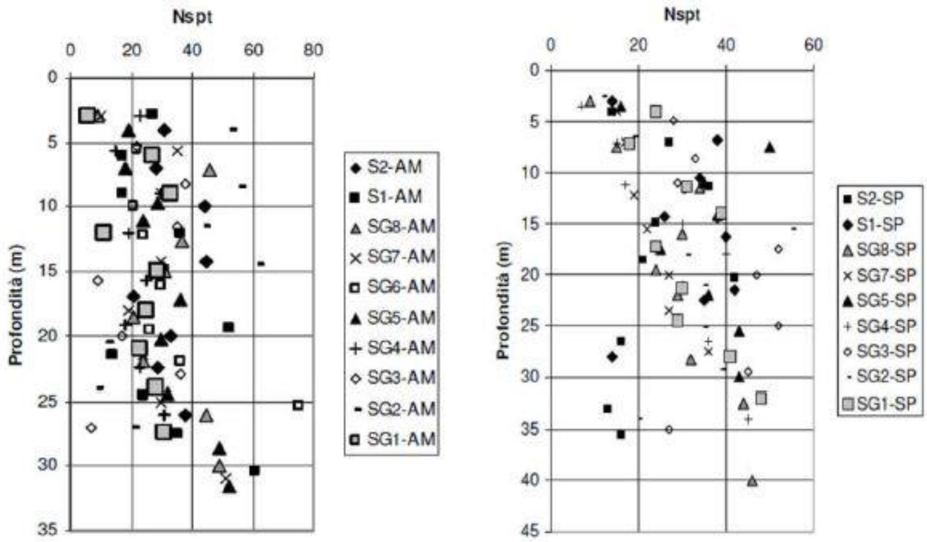

Figure 3.4. *SPT profiles around Arco Mirelli and San Pasquale (Celentano, 2015).*

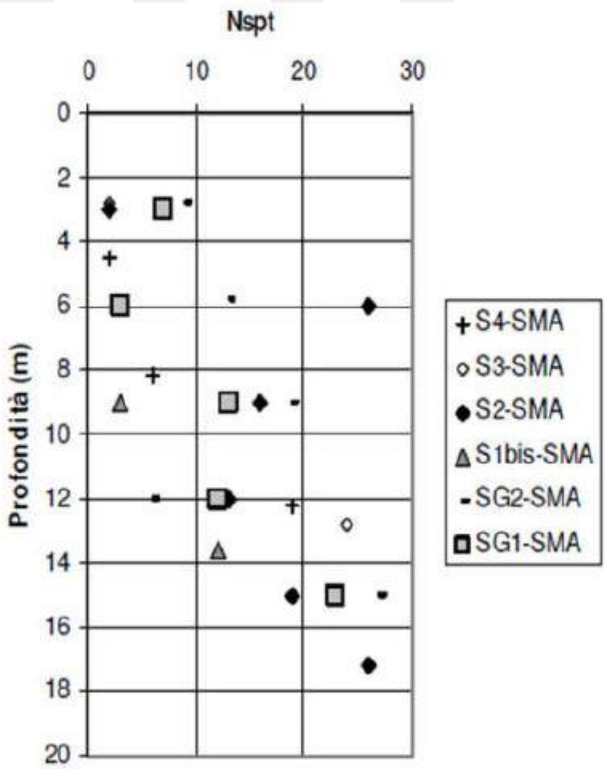

Figure 3.5. *SPT Data Collected Around Chiaia Station (Celentano, 2015).*

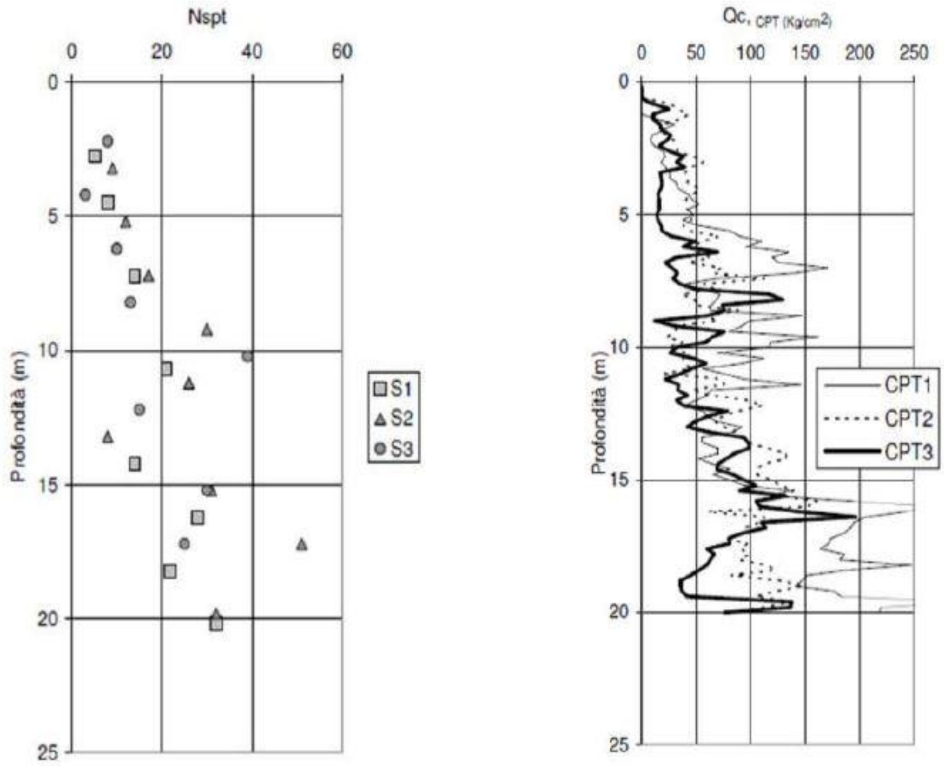

Figure 3.6. *CPT and SPT data between Mostra and Campegna (Celentano, 2015).*

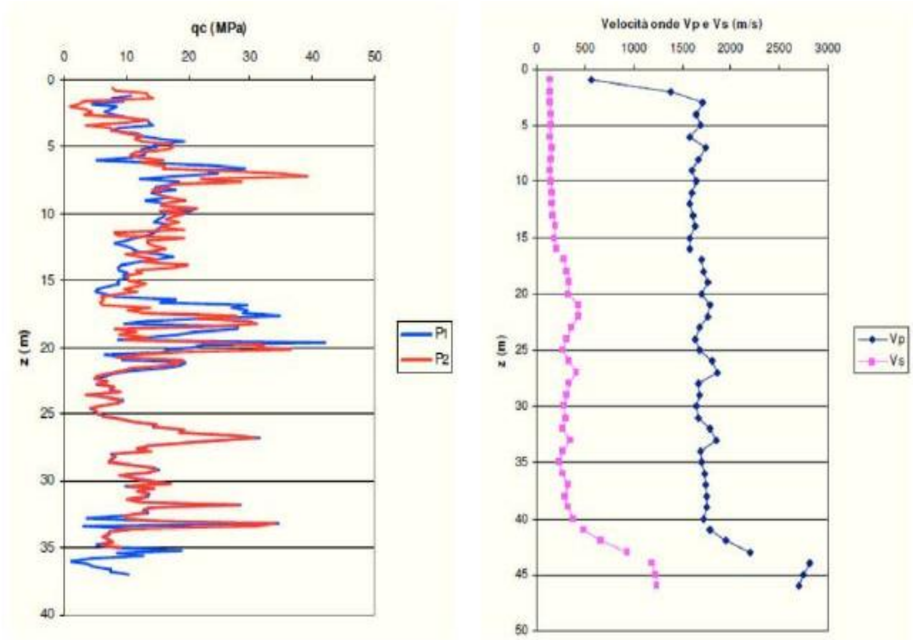

Figure 3.7. *CPT and Cross-hole Test Profilea) CPT (Cone Penetration Test) profiles conducted in the San Pasquale station area. b) Cross-hole test results obtained in the San Pasquale station area (Celentano, 2015).*

3.4. Geological and Geotechnical Classification

This section provides the physical and mechanical properties of the main soil types identified at the project site. These parameters were primarily determined through laboratory tests and then cross-referenced with data from CPT (Cone Penetration Test), SPT (Standard Penetration Test), and cross-hole tests (Bitetti et al., 2012; De Vivo, 2013).

3.4.1. Sand

Sand layers are found both above and, notably, below the groundwater level. For these soils, drained triaxial and penetration tests indicated a peak friction angle of approximately 37°. The sand layers exhibit high permeability in terms of local ground conditions, with an average elastic modulus of 5000 kPa and a Poisson's ratio of 0.3.

3.4.2. Pyroclastic soils

Pyroclastic soils are present in both saturated and unsaturated zones. Drained triaxial tests on these soils showed a peak friction angle of around 43°, although CPT and SPT results yielded values in the 36°–40° range. These highly dense soils have an average elastic modulus of 4000 kPa.

3.4.3. Cinerite (Volcanic Ash)

Layers of volcanic ash form thin transition zones between the sand and pyroclastic layers. Their mechanical properties are similar to those of pyroclastic soils. The average elastic modulus was estimated at 5000 kPa, and the internal friction angle at approximately 37°.

3.4.4. Tuff

Naples Yellow Tuff constitutes the foundational soil for most of the line and is predominantly located below the groundwater level. During the 1998–2000 geotechnical campaign, undisturbed samples from these soils were subjected to laboratory tests to determine unit weight and void ratio values. For strength parameters, values proposed by Evangelista and Pellegrino (1990) were adopted. The tuff's cohesion value was assumed to be 500 kPa, and its internal friction angle was 27°.

Soil Type	γ[kN]	γsat[kN]	K[cm/s]	c[kPa]	$\emptyset^0$	E'[kPa]	Rc[MPa]
Sand	16	18	$10^{-4} - 10^{-5}$	0	37	5000	-
Pyroclastic	14	16	$10^{-4} - 10^{-5}$	0	36	4000	0.3
Cinerit	14	16	$10^{-4} - 10^{-5}$	0	37	5000	0.3
Tuff	14	16	500	500	27	1000	-

Table 3.1. *Average physical and mechanical parameters for the main soil types identified along the Naples Metro Line 6 alignment.(Adapted from Bitetti et al., 2012; De Vivo, 2013; Evangelista and Pellegrino, 1990)*

3.5. Material Modeling Assumptions and Parameter Calibration

Accurately modeling soil behavior is critical for numerical analyses of geotechnical problems, especially those involving pronounced soil-structure interaction, like tunnel excavations. Considering the limitations of simpler constitutive models, such as the conventional elastic-perfectly plastic Mohr-Coulomb model, this thesis opted for advanced elastoplastic models available in PLAXIS software (PLAXIS, 2023): the Hardening Soil (HS) model and its version enhanced for small-strain behavior, the Hardening Soil with Small-Strain (HSsmall) model. These models are capable of representing the complex stress-strain relationships of soils, their dependence on stress history, and stiffness degradation more realistically.

3.5.1. The hardening soil and hardening soil small-strain (HSsmall) models

3.5.1.1. General structure of the hardening soil (HS) model

The Hardening Soil model is a sophisticated constitutive model developed based on plasticity theory. It can describe time-independent plastic deformation behavior under both deviatoric and isotropic loading conditions. Unlike many other elastoplastic models, the yield surface in the Hardening Soil model isn't fixed; it expands as the soil is subjected to loading, driven by both shear hardening and compression hardening mechanisms. This feature allows the model to realistically reflect how the soil's stiffness and strength properties change based on its loading history (PLAXIS, 2023).

The model's characteristic parameters are derived from experimental data that reflect soil behavior under various loading conditions:

E_{50}^{ref}: This is the secant elastic modulus from drained triaxial tests at a reference stress p_{ref}.

E_{oed}^{ref}: This is the tangent modulus from oedometer (consolidation) loading at a reference stress p_{ref}.

E_{ur}^{ref}: This is the elastic modulus for unloading and reloading cycles at a reference stress p_{ref}.

m: This is an exponent parameter that expresses the stiffness's dependency on the stress level.$E \sim \sigma^m$

R_f: This is the failure ratio, defined as the ratio of the peak deviatoric stress q_f to the asymptotic deviatoric stressq_a . $R_f = q_f \,/\, q_a$

p_{ref}: This is the reference stress, typically taken as 100 kPa, indicating that the parameters are calibrated relative to this reference pressure.

c,φ,ψ: These are cohesion, internal friction angle, and dilation angle, respectively. These parameters are common to the Mohr-Coulomb failure criterion and define the soil's ultimate strength.

The Hardening Soil model accurately describes how soil stiffness changes with stress levels, especially at small strains. While the classic Mohr-Coulomb model cannot represent this behavior with a constant elastic modulus (E) value, in the HS model, for example, the oedometer modulus is expressed with the following stress dependency:

$$E_{oed} = E_{oed}^{ref}\left(\frac{\sigma}{p_{ref}}\right)^{m} \tag{3.1}$$

The selection of m=1 in this context realistically represents the logarithmic compression behavior, especially in soft clays (PLAXIS, 2023).

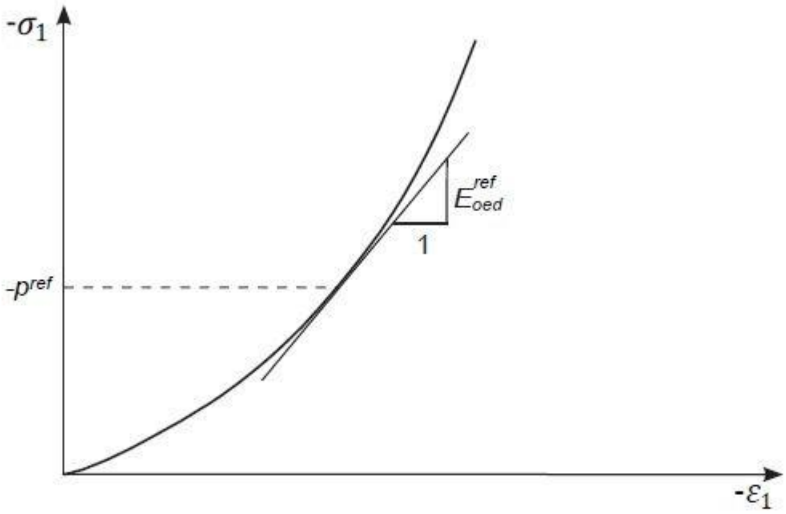

Figure 3.8. *Definition of* E_{oed}^{ref} *and* E_{ur}^{ref} *test (Adapted from PLAXIS, 2023).*

Hyperbolic stress-strain approach

The Hardening Soil (HS) model effectively simulates the stiffness degradation and plastic deformations that soils exhibit during loading. It does this by using the following hyperbolic stress-strain relationship:

$$\varepsilon_1 = \frac{1}{E_i} \cdot \frac{q}{1 - \frac{q}{q_a}} \tag{3.2}$$

Here, E_i represents the initial stiffness, which is related to E_{50} as follows:

$$E_i = \frac{2E_{50}}{2 - R_f} \tag{3.3}$$

The model also controls reaching the yield criterion through the concept of plastic shear strain (ε_1^p):

$$\varepsilon_1^p \approx \frac{1}{2}\left(\frac{q}{E_i(1 - q/q_a)} - \frac{q}{E_{ur}}\right) \tag{3.4}$$

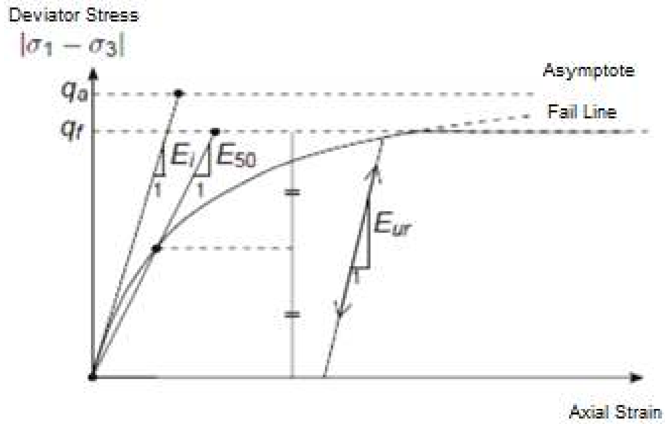

Figure 3.9. *Curve showing the hyperbolic relationship between deviatoric stress and axial strain in a drained triaxial test. (Adapted from PLAXIS 2D/3D Material Models Manual, 2023).*

The curve defines the initial stiffness E_i, secant stiffness (E_{50}), unloading-reloading modulus (E_{ur}), asymptotic deviatoric stress (q_a), and the failure point (q_f).

Unloading and reloading stiffness

During unloading and reloading phases, elastic deformations are defined, and the elastic modulus is formulated as follows, depending on the stress level:

$$E_{ur} = E_{ur}^{ref}\left(\frac{c\cos(\varphi) - \sigma_3'\sin(\varphi)}{c\cos(\varphi) - p_{ref}\sin(\varphi)}\right)^m \tag{3.5}$$

These expressions demonstrate that the HS model is sensitive to stiffness changes under different stress paths and accounts for the soil's loading history to some extent.

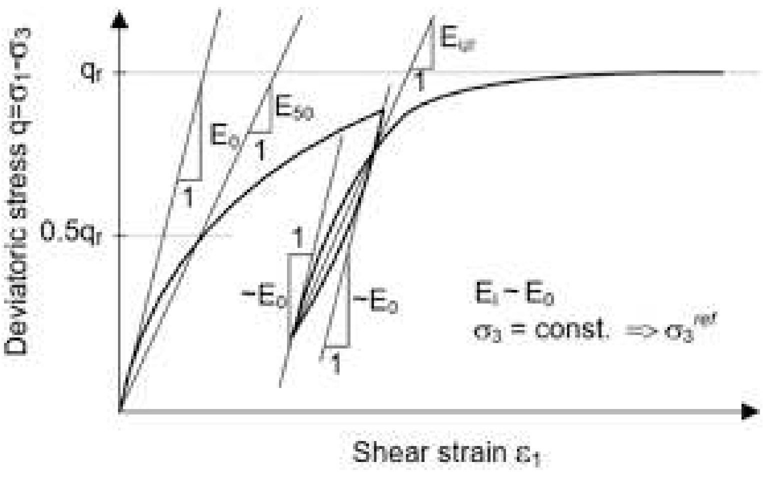

Figure 3.10. *Observed elastic stiffnesses during unloading and reloading in drained triaxial tests (Adapted from PLAXIS 2D/3D Material Models Manual, 2023).*

The curve compares the initial stiffness (E_i), secant stiffness (E_{50}), and unloading-reloading modulus (E_{ur}), illustrating stiffness degradation and recovery. This relationship represents the elastic behavior during stress-strain cycles.

Expanding yield surface and cap curve

The Hardening Soil model incorporates a hexagonal "shear yield surface" constrained by the Mohr-Coulomb failure plane, along with an elliptical "cap yield surface" that accounts for isotropic compression. The size of this cap surface is controlled by the isotropic preconsolidation stress (P_P) and is defined by the following equation:

$$f_c = \frac{\widetilde{q^2}}{M^2} + (p')^2 - p_p^2 = 0 \tag{3.6}$$

This approach allows for the independent modeling of parameters for both shear and isotropic loading, providing a more comprehensive understanding of the soil's volumetric and deviatoric behaviors.

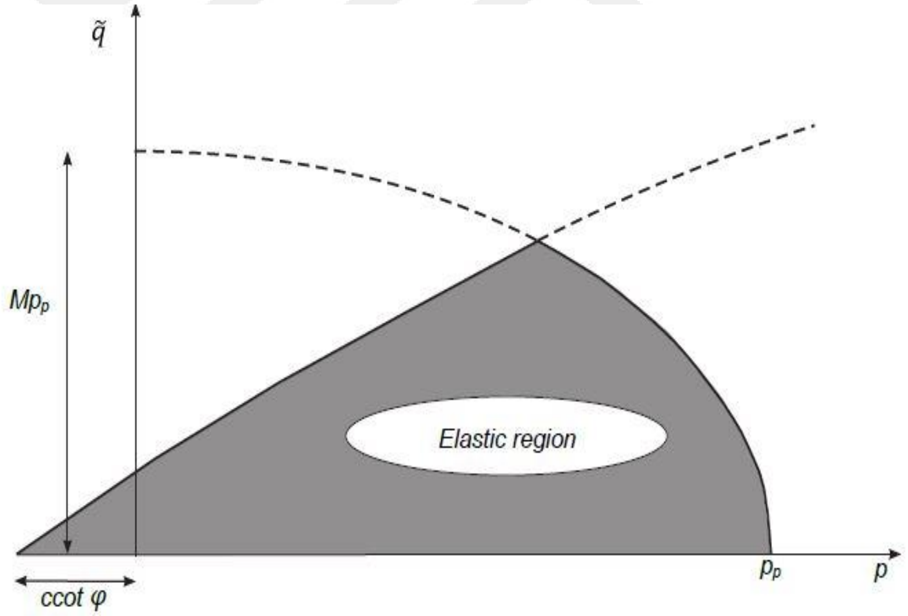

Figure 3.11. *Expanding Yield Surfaces Delimiting the Elastic Region in the Hardening Soil Model. (Adapted from PLAXIS 3D Material Models Manual, 2023).*

This figure illustrates the straight lines corresponding to shear hardening and the elliptical surfaces corresponding to compression (cap) hardening in the p−q plane. The elastic region is located centrally, with the cap boundary defined by the preconsolidation stress (P_P). This structure allows for the modeling of both deviatoric and isotropic hardening.

3.5.1.2. The hardening soil small-strain (HSsmall) model

The Hardening Soil with Small-Strain Stiffness (HSsmall) model, an extension of the Hardening Soil model, offers a more accurate representation of soil stiffness, especially at very small strain (γ) levels. Real soil behavior differs significantly at small strain levels; soil stiffness decreases non-linearly as strain increases, often exhibiting a logarithmic pattern. While the traditional Hardening Soil model defines unloading and reloading processes as elastic, the elastic range observed in real soils corresponds to a very narrow deformation range. Therefore, for analyses involving sensitive ground movements like tunnel excavation, the HSsmall model is crucial for accurately modeling high stiffness under small stresses (PLAXIS, 2023).

Stiffness degradation at small strains

Two additional parameters are included in the HSsmall model to define stiffness degradation at small strains:

G_0: This is the initial (very small strain) shear modulus.

$\gamma_{0.7}$: This is the shear strain at which the stiffness reduces to 70% of G_0.

In this model, the shear modulus (G_s) is expressed by the following formula, depending on the stress level:

$$G_s = \frac{G_0}{1 + 0.385 \cdot \frac{\gamma}{\gamma_{0.7}}} \tag{3.7}$$

And the tangent shear modulus (G_t), which is the derivative of this curve, is given as:

$$G_t = \frac{G_0}{\left(1 + 0.385 \cdot \frac{\gamma}{\gamma_{0.7}}\right)^2} \tag{3.8}$$

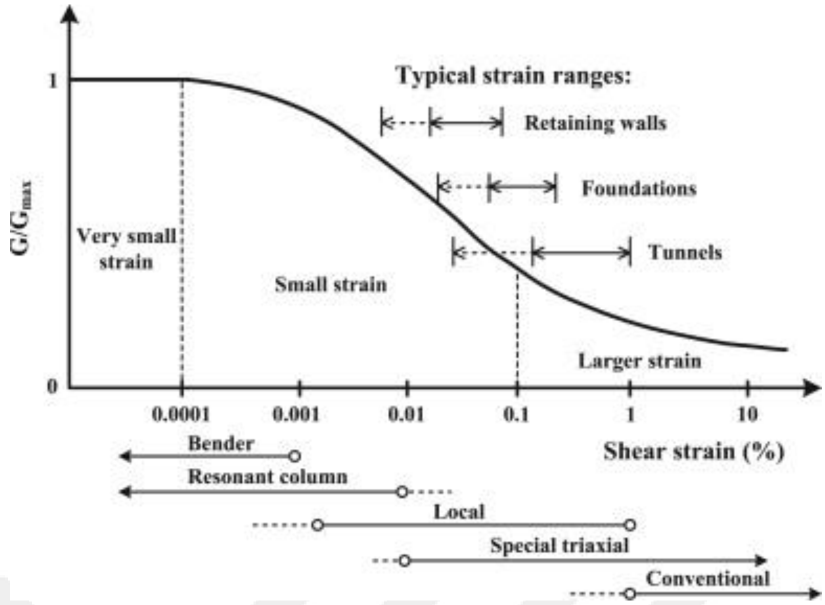

Figure 3.12. *Reduction in soil stiffness against different strain levels (Adapted from PLAXIS 3D Material Models Manual, 2023).*

The curve shows that the $G \, / \, G_{max}$ ratio decreases, reflecting the stiffness's sensitivity to the strain level. It also indicates the characteristic strain ranges for various structure types, such as tunnels, foundations, and retaining walls. This approach, facilitated by the Hardening Soil Small-Strain model, enables more accurate analyses at small strain levels.

Limiting stiffness degradation

To prevent an unlimited drop in stiffness at very small strains, stiffness is limited and cannot fall below a certain minimum value. This minimum stiffness is capped by the reloading stiffness (G_{ur}) obtained from classical laboratory tests:

$$G_t \geq G_{ur} = \frac{E_{ur}}{2(1 + \nu_{ur})} \tag{3.9}$$

The critical strain ($\gamma_{cut-off}$) corresponding to this threshold value is calculated using the following formula:

$$\gamma_{cut-off} = \frac{1}{0.385}\left(\frac{G_0}{G_{ur}} - 1\right)\gamma_{0.7} \tag{3.10}$$

Stress dependency and parameter definition

The HSsmall model also accounts for the stress-dependent variation of the initial shear stiffness (G_0). This dependency is expressed by the formula below:

$$G_0 = G_0^{ref}\left(\frac{c\cos(\varphi) - \sigma'_3\sin(\varphi)}{c\cos(\varphi) + p_{ref}\sin(\varphi)}\right)^m \quad (3.11)$$

According to this expression, the initial shear stiffness can depend not only on the stress level but also on the void ratio (e). In practice, the empirical formula proposed by Hardin and Black (1969), based on the initial void ratio, can also be used:

$$G_0 = 33 \cdot \frac{(2.97 - e)^2}{1 + e} \quad [MPa] \quad (3.12)$$

Application areas of the HSsmall model

The HSsmall model is particularly favored for sensitive geotechnical engineering problems where soil-structure interaction and small strains are crucial. These applications include the analysis of tunnel excavations, deep excavations, and foundation systems. The model can also exhibit hysteretic behavior under loading history and cyclic loading. However, phenomena like permanent deformation or pore water pressure accumulation are not directly considered by this model; more advanced models might be necessary for such effects.

3.5.1.3. Limitations of the mohr-coulomb model and justification for model choice

While the Mohr-Coulomb model effectively represents the failure criterion of soils in a simplified manner, it falls short in reflecting actual soil behavior. The main limitations of the Mohr-Coulomb model include:

Stress-Level Dependent Stiffness Variation: In real soils, stiffness changes significantly based on the applied stress level and stress history. In contrast, the Mohr-Coulomb model uses constant values for the elastic modulus (E) and Poisson's ratio (ν).

Loading-Unloading Cycles: The changes in soil behavior (hysteretic behavior) and permanent deformations observed during loading and unloading cycles cannot be accurately represented by the Mohr-Coulomb model.

Small Strain Behavior: The Mohr-Coulomb model cannot effectively simulate the high stiffness exhibited by soils at very small strain levels, nor the subsequent stiffness degradation.

Cap Effect (Cap Hardening): The "cap hardening" behavior, which is observed particularly under isotropic compression and is related to volumetric deformations, cannot be expressed with the Mohr-Coulomb model.

For these reasons, especially in displacement analyses related to tunnel excavation and for the accurate assessment of damage to surrounding structures and precise prediction of ground movements, choosing the Hardening Soil and HSsmall models is essential for obtaining realistic and reliable numerical analysis results. These models address the complex behaviors of soils more comprehensively, providing more accurate predictions for engineering design and evaluation processes.

3.5.2. Parameter calibration

For numerical analyses to produce reliable results, it's crucial to define the material models with accurate parameters. This is especially true for advanced soil models like Hardening Soil (HS) and Hardening Soil Small-Strain (HSsmall), where parameters must be meticulously calibrated using experimental data from both field and laboratory tests. This calibration process ensures the model accurately represents soil behavior across both small and large strains.

In this section, we'll technically detail the methods used to determine the parameters for these models and the experimental data they rely on. We'll also explain how the deformation parameters for the soil models used in this thesis were determined, based on values presented by De Vivo (2013) and results from previous research campaigns including CPT, SPT, triaxial, oedometer, and cross-hole tests. The fundamental physical and strength parameters of the soils (unit weight, internal friction angle, cohesion, Poisson's ratio) were presented in Section 3.4. This section focuses on detailing the methods for determining deformation moduli and the specific parameters utilized in the models.

3.5.2.1. HS model parameter calibration

Table 3.1 summarizes the essential parameters that need to be calibrated for the Hardening Soil (HS) model and the methods used to determine them.

Parameter	Description	Source Method
E_{50}^{ref}	Secant elastic modulus from drained triaxial test	Triaxial test (CD/UU)
E_{oed}^{ref}	Modulus under oedometer loading	Oedometer test
E_{ur}^{ref}	Elastic modulus for unloading/reloading coefficient	Triaxial+unloading
m	Stress-level dependent stiffnesss variation coefficient	Triaxial test/SPT-CPT
ψ	Dilation angle	Empirical

Table 3.2. *Hardening Soil Model Parameters and Calibration Methods*

Example Calibration Approach:

The E_{50}^{ref} is determined from the slope taken at the 50% deviatoric stress point of the hyperbolic stress-strain curve, which is obtained from drained triaxial test data.

The E_{ur}^{ref} is calculated from the elastic linear segment obtained during the unloading phase after loading (see Figure 3.11.).

The m value typically ranges from 0.5 to 1.0 in literature (Janbu, 1963). It can be assumed as 0.5 for sands and 1.0 for clays.

3.5.2.2. HSsmall model parameter calibration

The HSsmall model includes two additional critical parameters beyond those in the HS model. These parameters are specifically designed to model the stiffness degradation behavior of soil at small strains. These extra parameters are presented in Table 3.2.

Parameter	Description	Calibration Method
G_0^{ref}	Very small-strain stiffness (initial shear modulus)	Bender element / Literature correlation
$\gamma_{0.7}$	Shear strain value at which stiffness reduces to 70%	Correlation / Estimated value

Table 3.3. *Additional Parameters and Calibration Methods for the Hardening Soil Small-Strain Model*

Correlations:

For G_0^{ref}, the relationship proposed by Hardin and Black (1969) is often used:

$$G_0^{ref} = 33 \cdot \frac{(2.97 - e)^2}{1 + e} \quad [MPa] \tag{3.13}$$

For γ0.7, typical values can be found in the literature, often categorized by soil type.

Soil Type	$\gamma_{0.7}$(Approx)
Sand	$10^{-4} - 10^{-3}$
Silt	$5x10^{-5}$
Clay	$10^{-5} - 10^{-4}$

Table 3.4. *Typical γ0.7 Values by Soil Type (PLAXIS, 2023)*

Calibration Steps:

The G_0^{ref} value is obtained through literature correlations or specialized laboratory tests, such as bender element tests.

ã0.7 is usually estimated from typical values found in literature, based on the soil type or plasticity index.

Validation for these parameters is performed by generating stiffness degradation curves within PLAXIS (see Figure 3.14.).

3.5.2.3. Parameter adjustment method (recommendation)

In the HSsmall model, the assumption that $E_{ur}^{ref} = 3. E_{50}^{ref}$ is generally considered valid.

If the soil is highly compressible, such as soft clay, $E_{50}^{ref} = 1.25 . E_{oed}^{ref}$ and m=1 can also be utilized.

The assumption of $K_0 = 1 - sin(\varphi)$ is suitable for the initial horizontal-stress ratio.

Sensitivity analysis for G_0 and $\gamma_{0.7}$ values can be performed using the Parameter Reduction option in PLAXIS.

3.5.2.4. Soil model parameters used in the thesis

The deformation parameters of the soil models used in this thesis are based on the values presented by De Vivo (2013) and the results of various tests (such as CPT, SPT, triaxial, oedometer, and cross-hole tests) conducted in different areas during previous research campaigns. The basic physical and strength parameters of the soils are presented in Section 3.4. This section explains the methods used to determine the deformation moduli and details the parameters applied in the models.

Sand

The sand layer was represented using the Hardening Soil Small-Strain (HSsmall) model. The parameters used in the calibration process are given below:

$E_{50} = 40MPa$

$E_{oed} = 40MPa$

$E_{ur} = 85MPa$

$\mathrm{G}_0 = 88MPa$

$\gamma_{0.7} = 0.00013$

$\mathrm{p_{ref}} = 115kPa, m = 0.5, R_f = 0.9$

The E_{50} value was determined based on the deformation modulus obtained from the CPT tests. The E_{oed} value obtained from the oedometer tests was assumed to be equal to the E_{50} value derived from the CPT results. The reloading stiffness E_{ur} was calculated as approximately 2.2 times the value obtained from the CPT. The initial shear modulus G_0 was derived from cross-hole tests. The γ0.7 value, which represents the stiffness degradation at small strain levels, was estimated based on an experimental curve obtained from sands with similar gradation.

Cinerite

The cinerite layer was also defined using the Hardening Soil Small-Strain (HSsmall) model. The parameters used are given below:

$E_{50} = 47MPa$

$E_{oed} = 47MPa$

$E_{ur} = 100MPa$

$\mathrm{G}_0 = 182MPa$

$\gamma_{0.7} = 0.00019$

$\mathrm{p_{ref}} = 170kPa, m = 0.5, R_f = 0.9$

The deformation modulus obtained from the CPT tests was again defined as E_{50} and assumed to be equal to the oedometer value. The reloading stiffness Eur was taken as approximately 2.2 times this value. The initial shear modulus G_0 was directly obtained from cross-hole tests. The γ0.7 value was estimated using experimental curves derived from soils with similar grain size distributions.

Neapolitan Yellow Tuff

Considering its high strength and deformation properties, the Neapolitan yellow tuff formation was represented using the Hardening Soil (HS) model. The parameters for this model are given below:

$E_{50} = 70MPa$

$E_{oed} = 70MPa$

$E_{ur} = 200MPa$

$\mathrm{c} = 500MPa$

$\varphi = 27^0$

$m = 0.5$

$Rf = 0.9$

These values were obtained from laboratory tests and the results of previous geotechnical studies. In addition, based on field observations and experimental analyses, a distinct layer exhibiting higher stiffness values was identified in some areas of the tuff layer close to the surface. This layer was defined separately using the Hardening Soil (HS) model, and the parameters given below were used.

$E_{50} = 70MPa$

$E_{oed} = 70MPa$

$E_{ur} = 200MPa$

4. NUMERICAL MODELING IN THE PLAXIS 3D ENVIRONMENT

This section provides a detailed explanation of the numerical modeling process carried out using PLAXIS 3D software for the tunnel excavation along the route determined within the scope of the Naples Metro Line 6 project. This modeling study aims to comprehensively evaluate both the potential impacts of the tunnel excavation on surrounding structures and the ground deformations. The numerical modeling process addresses in detail many parameters, including the definition of boundary conditions, the stratigraphic arrangement of soil layers, excavation stages, lining systems, and the modeling of structural elements.

In addition, this section systematically presents key steps such as the methods used to create the finite element mesh, the type of analysis (e.g., staged construction analysis), the determination of initial stress conditions, and the definition of loading scenarios. The main objective of the modeling is to perform a three-dimensional analysis of the effects of the constructed tunnel on the behavior of nearby structures under different ground conditions and to reliably evaluate the tunnel-structure interaction based on the data obtained from these analyses. In this context, general information about the features and operation of the PLAXIS 3D software selected as the modeling tool will first be provided.

4.1. Overview of PLAXIS Software

4.1.1. Historical development and application area

PLAXIS is a numerical analysis software widely used in geotechnical engineering applications, based on the finite element method (FEM). It was first developed in 1987 at Delft University of Technology to model the behavior of low-permeability soils under seismic effects (Brinkgreve et al., 2004). The name of the software is derived from the concepts of “Plane strain and axial symmetry.” Initially, it only provided solutions for two-dimensional plane strain problems, but today it has evolved into an advanced tool capable of modeling complex geotechnical engineering problems in both 2D and 3D environments.

PLAXIS can be applied to a wide variety of engineering problems, including soil-structure interaction, tunnel construction, deep excavations, dam safety, foundation design, ground improvement techniques, dynamic analyses, and seepage analyses. It is especially a powerful analysis tool for evaluating settlements and structural deformations caused by ground movements during tunnel excavations (Schweiger, 2002).

4.1.2. Finite element approach and element types

PLAXIS 3D uses 10-node tetrahedral elements for three-dimensional modeling. These elements have three degrees of freedom at each node (displacements in the x, y, and z directions), allowing a more accurate representation of the deformation field. The 10-node elements are particularly preferred because of their ability to reduce numerical locking issues encountered in modeling incompressible soils (e.g., soft clay) (Sloan and Randolph, 1982; Vermeer and Brinkgreve, 1994).

Stress and strain calculations are performed at the Gauss points within each element. The number and location of Gauss points directly affect the solution accuracy. As mesh refinement increases, accuracy improves; however, computation time and memory consumption also increase.

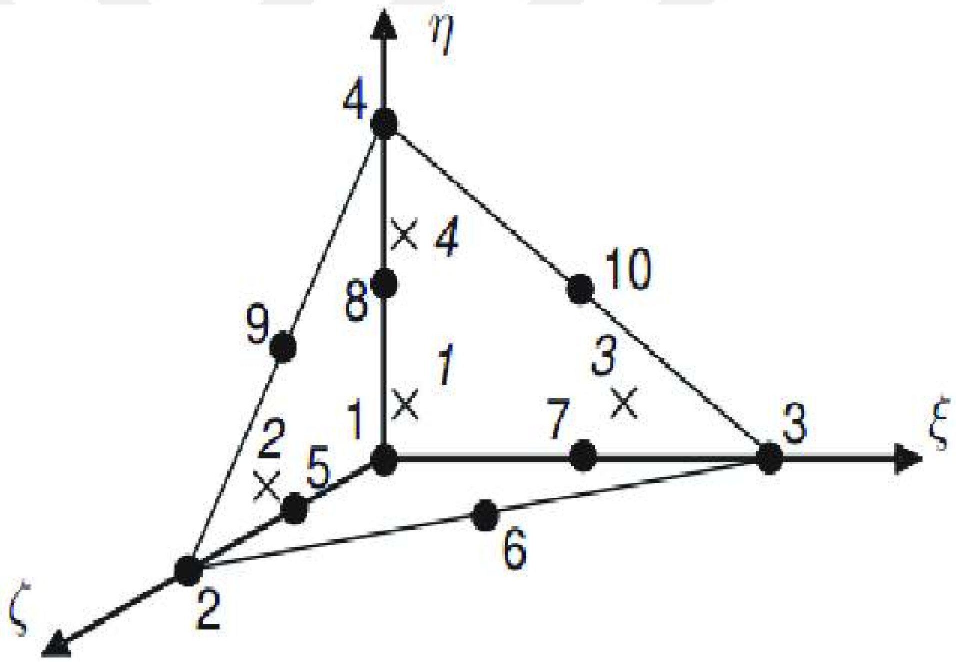

Figure 4.1. *A 10-node tetrahedral element (Brinkgreve et al., 2015).*

4.1.3. Material models and customizability

One of the strongest features of PLAXIS is its extensive library of material models. These models include:

Mohr-Coulomb: Represents simple elastic-perfectly plastic behavior.

Hardening Soil (HS) and Hardening Soil with Small-Strain (HSsmall): Reflect realistic hardening behavior, stiffness degradation, and small-strain effects.

Soft Soil and Soft Soil Creep: Suitable for modeling the time-dependent deformation of soft, consolidated soils.

Modified Cam-Clay: A model based on critical state theory, preferred for partially saturated, consolidated soils.

Hoek-Brown: Suitable for rock masses.

UBC3D-PLM: Developed for behavior under seismic loading conditions.

Thanks to the User Defined Soil Model (UDSM) framework, it is also possible to integrate different models into the system by adding user-defined models.

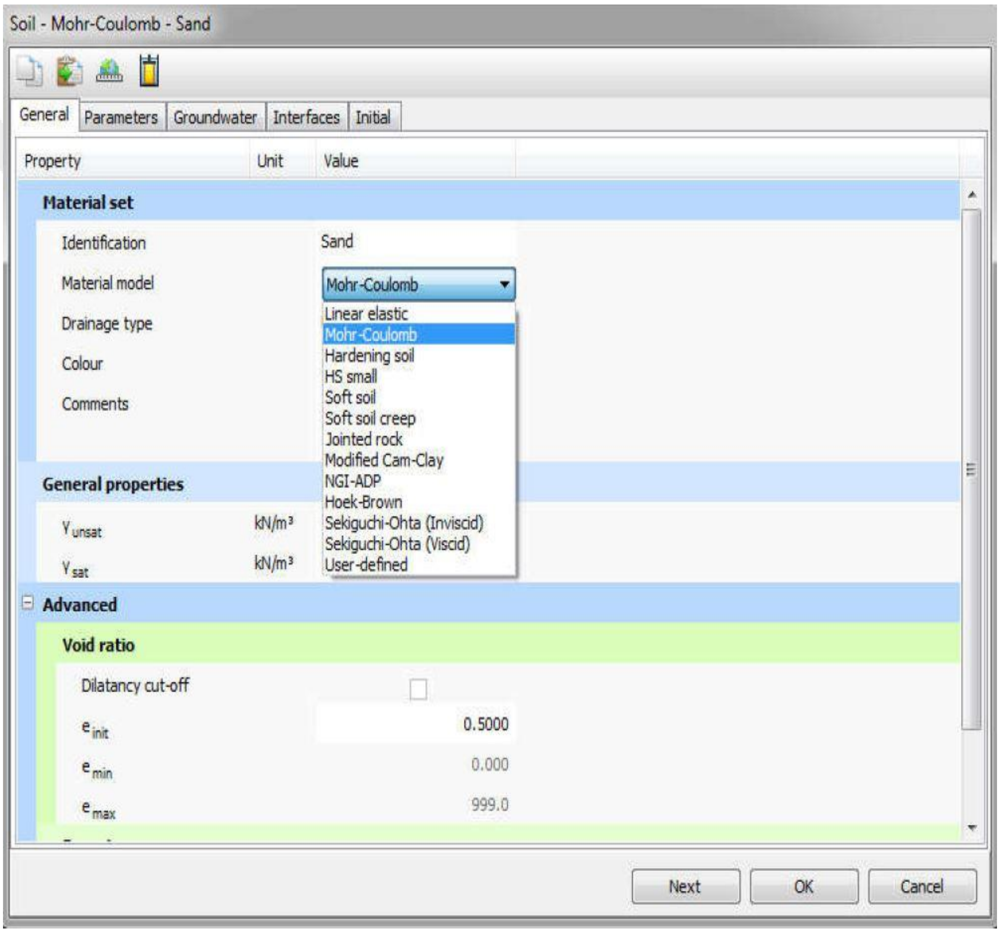

Figure 4.2. *PLAXIS material model library (Plaxis3D).*

4.1.4. Software workflow and modular structure

PLAXIS 3D software consists of two main modules: Input and Output.

- The Input module enables geometric modeling, material definitions, boundary condition assignments, mesh generation, and the definition of analysis stages.

- The Output module allows the evaluation and visualization of analysis results. In this module, stress distribution, displacements, settlements, and plastic zones can be analyzed in detail.

In PLAXIS, compressive stresses are considered negative and tensile stresses positive. Additionally, the simulation direction used in the finite element solution is consistent with these sign conventions.

4.1.5. Model scaling and mesh definition

During the modeling process, the dimensions of the analysis area must be carefully determined to ensure that the effects of the tunnel excavation do not reach the model boundaries. In PLAXIS, the mesh density can be controlled using the “coarseness factor,” and local refinement can be applied in zones with high deformation to increase calculation accuracy (Brinkgreve et al., 2010).

4.1.6. Hydraulic definitions and water conditions

To analyze the effects of water within the soil, PLAXIS 3D can model steady-state or transient flow conditions. The groundwater level can be defined as a fixed level, or more complex seepage analyses can be performed using the PlaxFlow module. In these analyses, water pressure, flow, and drainage conditions are directly defined within the model. In this study, the analysis was performed assuming a constant groundwater level within the soil.

4.2. Geometric Model and Boundary Conditions

In the analyses conducted within the scope of this thesis, an appropriate geometric model was created to accurately represent the behavior of the tunnel and the surrounding soil. The model dimensions were determined to ensure that the effects of tunnel excavation and construction on the soil would not be influenced by the boundary conditions.

4.2.1. Geometric model dimensions

The axial dimensions of the model created in PLAXIS 3D were defined as follows:

- **Y direction (Parallel to Tunnel Axis):** The model was designed to have a length of approximately 140 meters in the direction parallel to the tunnel axis.

This length allows the full development of tunnel advancement and soil-structure interaction without reaching the model boundaries.

- **X direction (Perpendicular to Tunnel Axis):** Perpendicular to the tunnel axis, the model was designed with a width of approximately 90 meters. This width was kept sufficiently large to ensure that the stress and deformation distributions around the tunnel would not be affected by the lateral model boundaries. If a symmetric model is used, half of this width (45 meters) can be modeled.
- **Z direction (Depth):** A model with a depth of approximately 40 meters from the ground surface was created. This depth was considered sufficient to accurately reflect the behavior of the soil layers below the tunnel and potential deformation mechanisms.

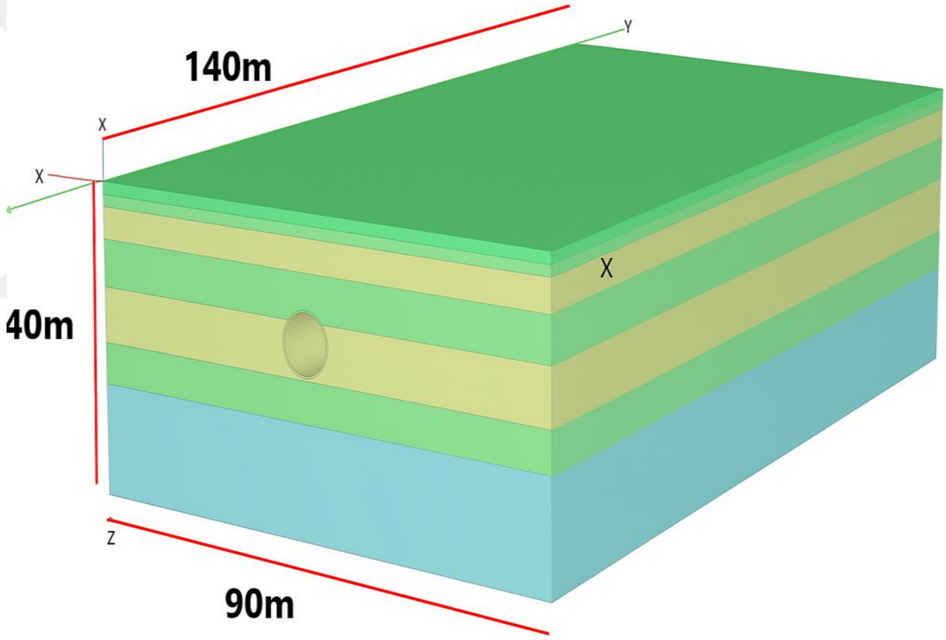

Figure 4.3. *General dimensions of the three-dimensional soil model created for the numerical analysis (Prepared within the scope of this study).*

4.2.2. Soil stratigraphy and material assignments

The soil environment was modeled as a multi-layered system to reflect the site conditions. The definition of soil layers and the assignment of materials were carried out in PLAXIS using the Borehole feature. The following layers were defined at the specified depths from the ground surface:

Made Ground: The upper fill or artificial soil layer extending from the ground surface (0 m) to a depth of -1.5 m.

Cinerite (Layer 1): The first cinerite layer extending from a depth of -1.5 m to -2.9 m.

Sand (Layer 1): The first sand layer extending from a depth of -2.9 m to -7.0 m.

Cinerite (Layer 2): The second cinerite layer extending from a depth of -7.0 m to -12.9 m.

Sand (Layer 2): The second sand layer extending from a depth of -12.9 m to -20.20 m.

Cinerite (Layer 3): The third cinerite layer extending from a depth of -20.20 m to -25.40 m.

Tuff: The tuff layer extending from a depth of -25.40 m to -40.0 m.

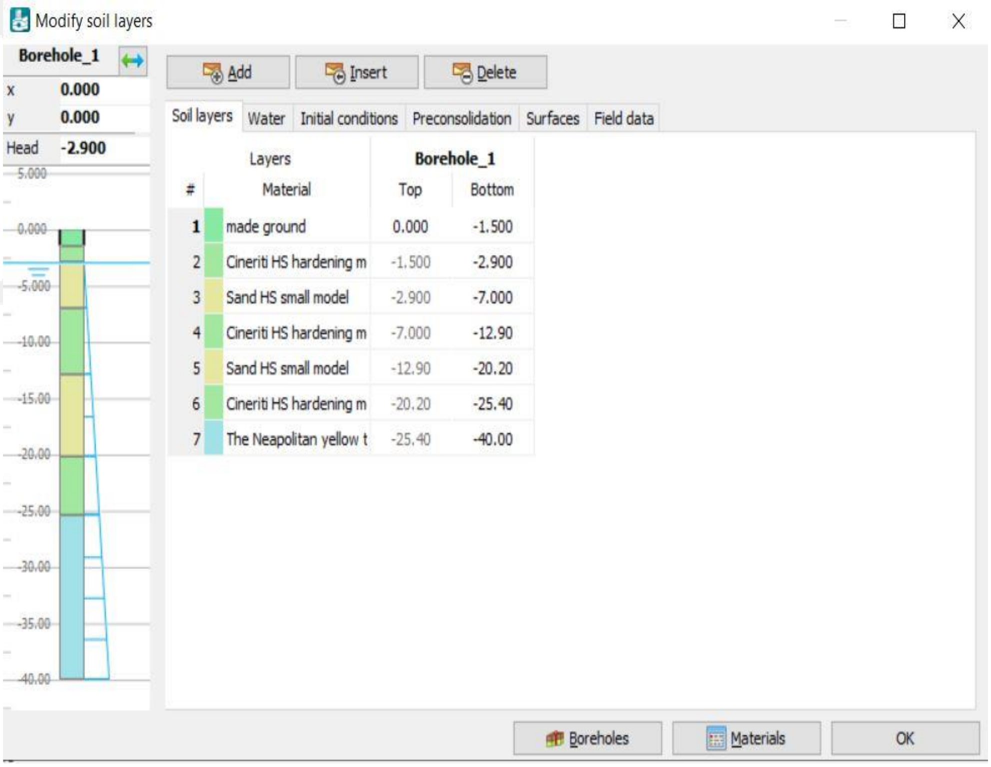

Figure 4.4. *Stratigraphic arrangement and depth intervals of the soil layers defined in the PLAXIS 3D environment (Prepared within the scope of this study).*

The geotechnical parameters determined for each soil layer (unit weight, cohesion, internal friction angle, modulus of elasticity, Poisson’s ratio, etc.) are detailed in the section titled “3.5.2.4 Soil Model Parameters Used in the Thesis.” These material datasets were created in PLAXIS and assigned to the corresponding soil layers.

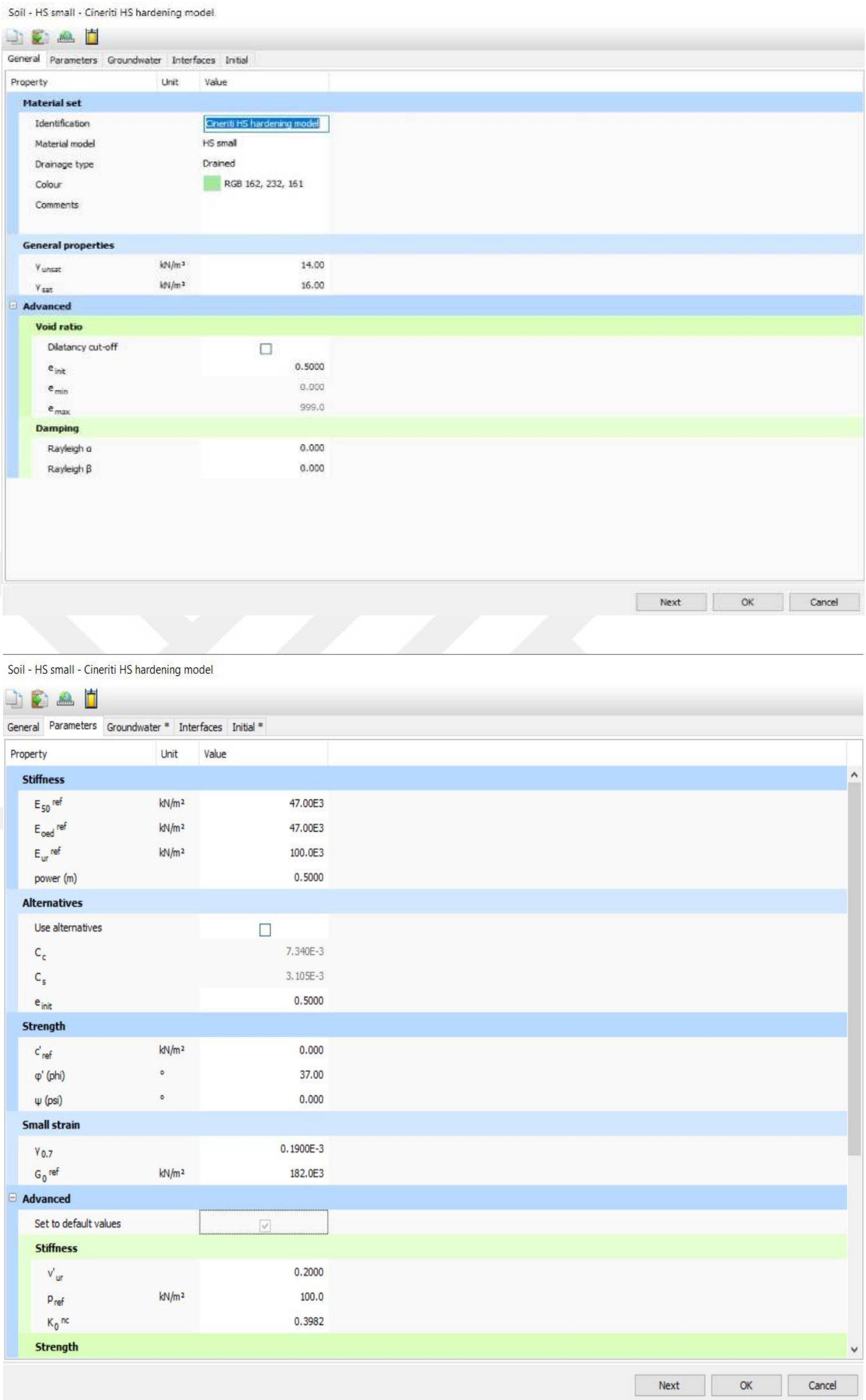

Figure 4.5. *Example of "Cinerite HS Hardening Model" soil definition in the PLAXIS 3D environment (Created within the scope of this study).*

4.2.3. Hydrological conditions

In this study, the groundwater level was assumed to be constant. The groundwater table was defined at a depth of -2.9 meters. This assumption is based on the expectation that there would be no significant change in the water level during and after construction.

4.3. Modeling of the Tunnel and Lining Elements

This section explains how the TBM tunnel excavated within the scope of the Naples Metro Line 6 was geometrically and mechanically defined in the PLAXIS 3D environment, and details the methods used to model the tunnel excavation and lining. The modeling process includes the removal of the excavation volume, the staged activation of the lining and shield elements, application of face convergence, pressure loads, and jack forces.

4.3.1. Tunnel geometry and TBM specifications

The modeled tunnel has a circular cross-section with an inner diameter of 7.250 meters and an outer diameter of 7.850 meters. The tunnel invert is located approximately 20.0 meters below the ground surface, while the tunnel crown is at about 12.15 meters depth. The TBM shield has an excavation head with a diameter of 8.15 meters, and the shield diameter itself is 8.13 meters. This diameter difference (0.02 meters) creates a shrinkage effect behind the excavation, resulting in a gap for grouting.

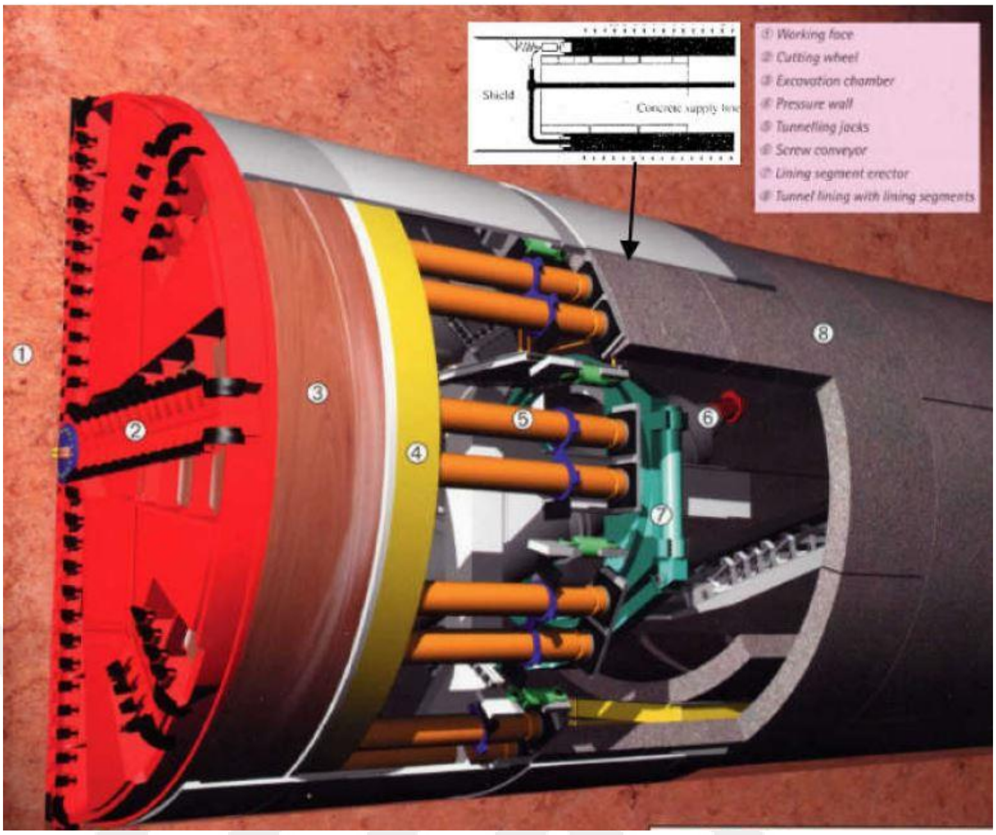

Figure 4.6 *illustrates the general structure of the TBM (Tunnel Boring Machine) and its components involved in the excavation process. The rotating cutter head (1) located at the front excavates the tunnel face by loosening the soil. The excavated material is directed to the excavation chamber (3) behind the cutter head, where it is transported backward using the screw conveyor (6). The injection chamber (4) is supplied with grout to fill the gap created behind the excavation, while the tunnel segments are installed using the segment erector robot (7). The TBM's thrust system consists of multiple hydraulic jacks (5) that push against the tunnel lining. The protective steel shield, which extends throughout the entire TBM structure, stabilizes both the machine and the excavation face. This image is presented to illustrate the general structure of the TBM geometry used in the modeling.(herrenknecht.de)*

In the PLAXIS 3D environment, the TBM shield was modeled as a Plate element. The elastic properties of the shield were defined as detailed in Table 4.1 (presented in this section). These properties represent the rigidity of the TBM shield and the forces it transfers to the ground.

Property	Value
Thickness (d)	0.35m
Material Weight (γ)	120kN/m^3
Material Behaviour	Linear, isotropic
Young's Modulus(E1)	2.30x10^8kN/m^2
Poisson's Ratio ($\nu 12$)	0.00
Shear Modulus (G12)	11.5x10^8kN/m^2

Table 4.1. *Defined material properties for the TBM shield (EPBM Plate) (Prepared within the scope of this study).*

4.3.2. Tunnel lining elements and material definitions

The tunnel lining consists of reinforced concrete rings, each 1.70 meters long, installed simultaneously with the excavation progress. These rings are arranged in the model to form a continuous cylindrical lining.

In this study, the lining rings were defined as "Soil" (solid element) in the PLAXIS 3D environment instead of as "Plate" elements. This approach provides a more detailed representation of the three-dimensional volumetric behavior of the lining, especially in analyses focusing on detailed soil-lining interaction.

The material model defined for the lining segments assumes linear elastic behavior and non-porous (undrained) properties. This allows the stress-strain relationship of the reinforced concrete lining to be represented within the framework of elasticity theory. The defined thickness of the lining ring is 0.30 meters, the unit weight is 25 kN/m^3, the modulus of elasticity is 3.83×10^7 kN/m^2, and the Poisson's ratio is 0.20. These properties are detailed in Table 4.2.

This modeling approach enables a more accurate evaluation of the contact stresses developed between the lining and the surrounding soil. The lining elements were activated in each analysis phase together with the corresponding excavation segment, allowing the staged construction process to be realistically represented in PLAXIS 3D.

Property	Value
Material Model	Linear elastic
Material Weight (γ)	25kN/m^3
Drainage Type	Impermeable
Young's Modulus(E)	3.83x10^7kN/m^2
Poisson's Ratio (ν)	0.20

Table 4.2. *Defined concrete material properties for the tunnel lining (Concrete Rck 45 MPa) (Created within the scope of this study).*

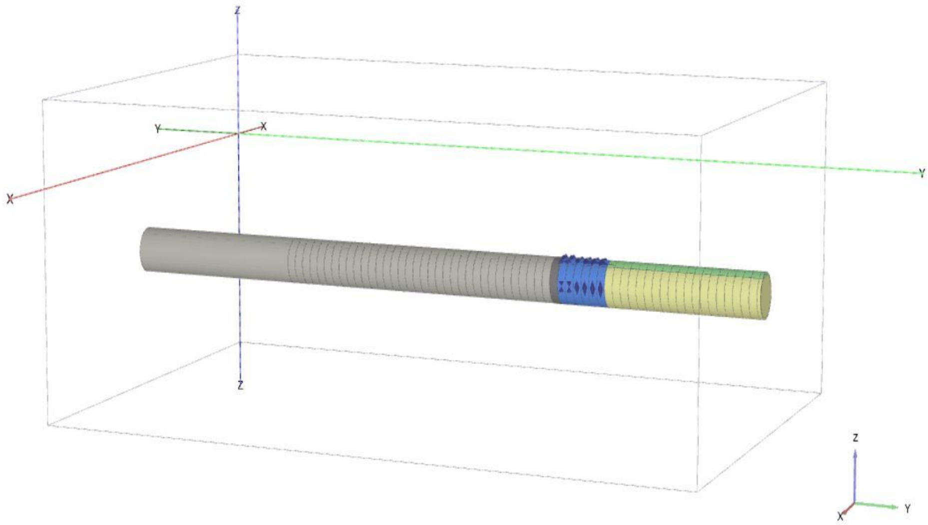

Figure 4.7. *Excavation stages of the tunnel in the PLAXIS 3D model(Created within the scope of this study).*

In the model, the section shown in gray represents the previously excavated tunnel segment supported with the reinforced concrete lining. This section corresponds to the area where segments have been installed after excavation and is modeled using structural elements. The blue section indicates the excavation zone where the TBM shield is currently active. This part was modeled to simulate the TBM's advancement phases and apply the associated face loads (e.g., face pressure and grout pressure). The section shown in yellow represents the soil block that has not yet been excavated. As excavation progresses, this volume is deactivated, and its place is taken by the TBM and lining elements.

4.3.3. Definition of excavation loads and interactions

During the tunnel excavation process, the interactions between the TBM and the soil were modeled through various load applications. These loads were modeled based on field measurements obtained in the initial section of the Naples Metro Line 6 project (Bitetti et al., 2012) and are summarized in Table 4.3 (presented in this section).

Parameter	Value
Grout Pressure (Tail Grouting Pressure)	180 kPa (at crown), increase: 20 kPa/m
Face Pressure	230 kPa (at crown), increase: 18 kPa/m
Jack Load	634.5 kN
Contraction (Average Shrinkage)	0.21% (distributed axially)

Table 4.3. *Key loads and face contraction values applied during the TBM and tunnel excavation process (Adapted within the scope of this study).*

4.3.4. Jack loads

The jack loads (634.5 kN) are not defined as a direct force but rather as a normal stress applied to the rear surface of the tunnel lining during the Sequencing step. This is done by selecting the surface in the Plane Rear tab, activating the appropriate Surface Load, and entering the σn,ref value.

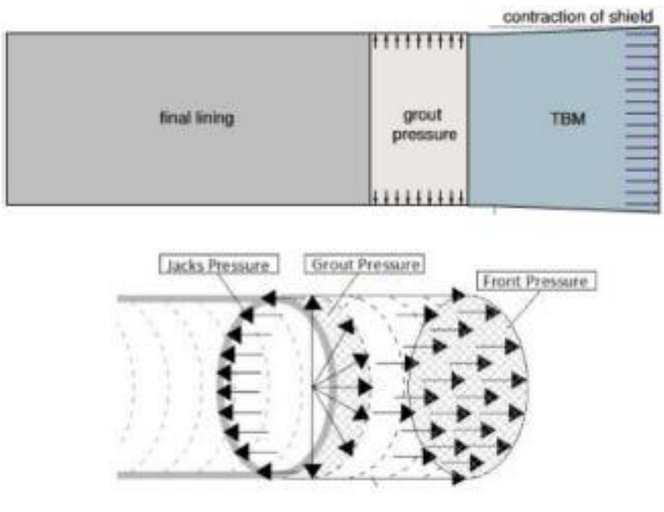

Figure 4.8. *Main loading components defined during the TBM excavation process (Adapted from Bitetti et al., 2012).*

3.3.5. Excavation process and definition of stages

In the model, a 100-meter section of the tunnel was excavated progressively in 50 stages. Each stage represents an advancement corresponding to a 1.7-meter lining ring.

This process was defined using PLAXIS's Staged Construction feature in the following sequence:

1. **Initial Phase:** The initial stress state in the soil model was established using the K0 procedure. In this phase, the tunnel elements are not yet active.

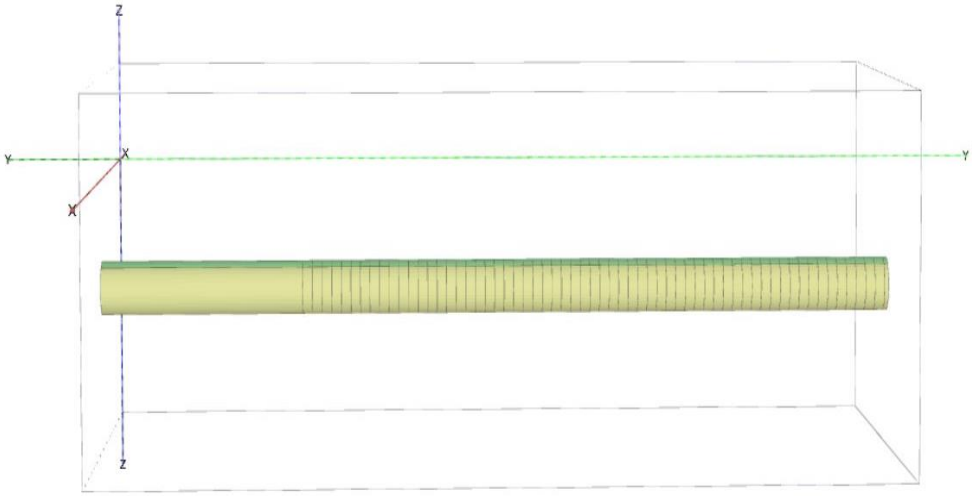

Figure 4.9. *Initial stress state (Initial Phase) (PLAXIS 3D model created within the scope of this study).*

In this initial stage, the tunnel structure has not yet been included in the model. The soil mass was brought to equilibrium under its own weight using the K_0 procedure, resulting in the initial lithostatic stresses. This stress state represents the natural soil conditions prior to excavation.

2. **Phase 1 (Initial TBM Position and Contraction):** The initial position of the TBM was defined as 35.6 meters ahead of the starting reference point. In this phase, a contraction value of 0.21% was applied to the first segments in relation to the TBM's advancement.

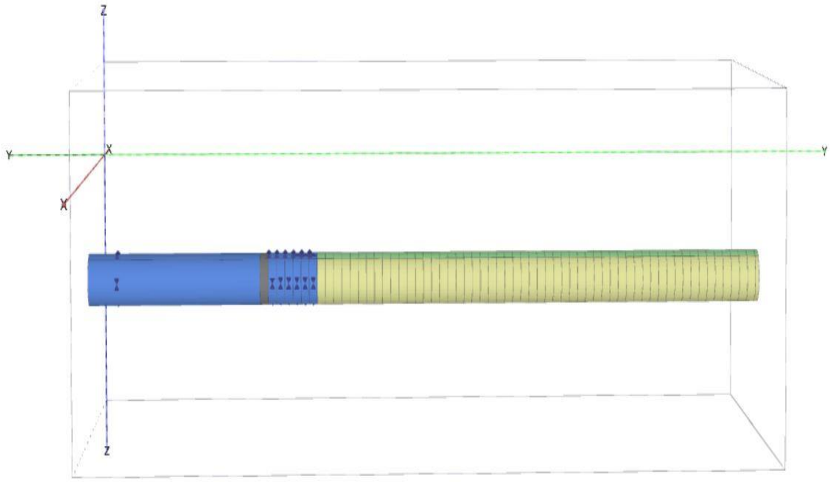

Figure 4.10. *Initial TBM position and conical contraction effect (Phase 1)) (PLAXIS 3D model created within the scope of this study).*

In the first phase, it was assumed that the TBM had advanced 35.6 meters from the excavation starting point. The TBM shield was activated in this phase, and a maximum axial contraction of 0.21% was defined. This contraction simulates the gaps left between the tunnel shield and the soil, as well as the need for grouting.

3. **Phases 2 and Subsequent Phases (Repeating Excavation Cycle):** Each phase simulates an advancement of 1.7 meters of the tunnel and includes the following steps:

Excavation Volume Deactivation: The soil volume of the corresponding tunnel segment is deactivated to simulate the excavation process.

TBM Shield Activation: The TBM shield, which supports the soil during tunnel excavation, is activated for the corresponding segment.

Lining Ring Activation: The reinforced concrete lining ring installed behind the TBM is activated to provide permanent tunnel support.

Application of Contraction, Grout Pressure, Face Pressure, and Jack Load: In each phase, surface contraction resulting from the conical shape of the TBM, tail grout pressure, face support pressure, and jack forces pushing the tunnel are applied to the relevant segment. The contraction values (0.00000 → 0.00042 → ... → 0.00210) are adjusted based on the specific part of the TBM corresponding to each phase.

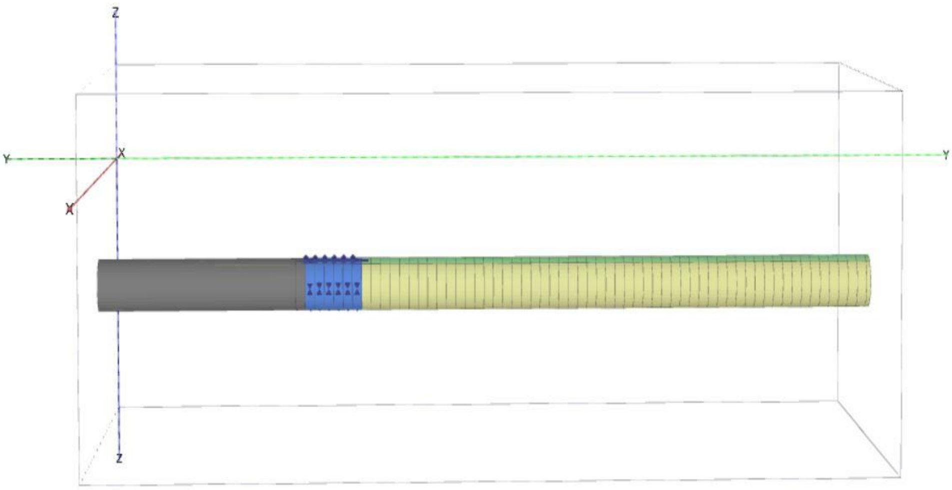

Figure 4.11. *Installation of the first lining segment and application of loads (Phase 2) (PLAXIS 3D model created within the scope of this study).*

In the second phase, the first tunnel segment was installed behind the TBM shield. This segment was defined as a soil element with linear elastic concrete properties. In this phase, the grout pressure, face pressure, and jack forces were also activated.

5. STRUCTURAL VALIDATION

In this thesis study, the structural element modeling capabilities of the PLAXIS 3D software were evaluated to verify whether it accurately reflects the load-bearing system behavior of the reinforced concrete structure under consideration. Among finite element method-based software commonly used in structural analyses, PLAXIS 3D's ability to integrate geotechnical and structural components is of critical importance. In this context, the modeling and accuracy of structural elements were assessed in light of the methodological framework and results provided by similar studies in the literature (e.g., Gragnano et al., 2014). This section details the definition of the load-bearing system of our building model, the structural elements used, and the modeling approach for the infill walls.

5.1. Definition of the Structural System

The building considered in this study has a three-dimensional reinforced concrete load-bearing system. The structure consists of columns and shear walls that carry vertical loads, and beams and slabs that transfer horizontal loads. The modeling of the structural system was carried out using structural analysis software; beam and column elements were represented with beam elements, while slabs were represented with plate elements. The building's foundation was modeled as a 1.00 meter thick raft foundation.

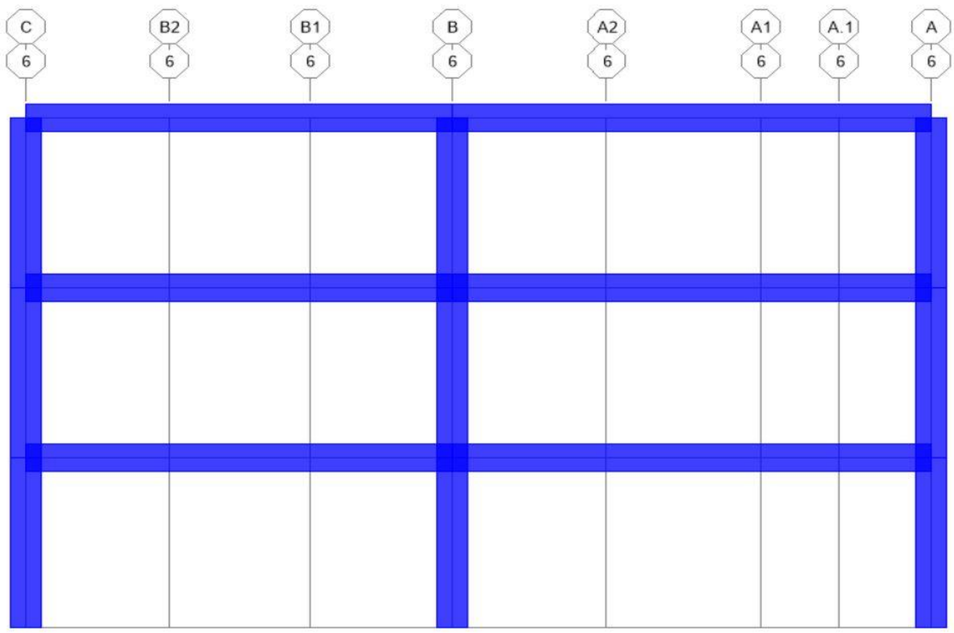

Figure 5.1. *Front view of the building from the YZ plane (Axis 6) (SAP2000 Building Model, prepared within the scope of this thesis study.).*

This image shows the front view of the building model along Axis 6 when viewed from the YZ plane. In the three-story building model, columns were defined as vertical load-bearing elements and beams as horizontal load-bearing elements on each floor. In the image, all beam and column elements are represented in blue. The reinforced concrete elements forming the building's load-bearing system were modeled using beam-type finite elements in the PLAXIS 3D environment.

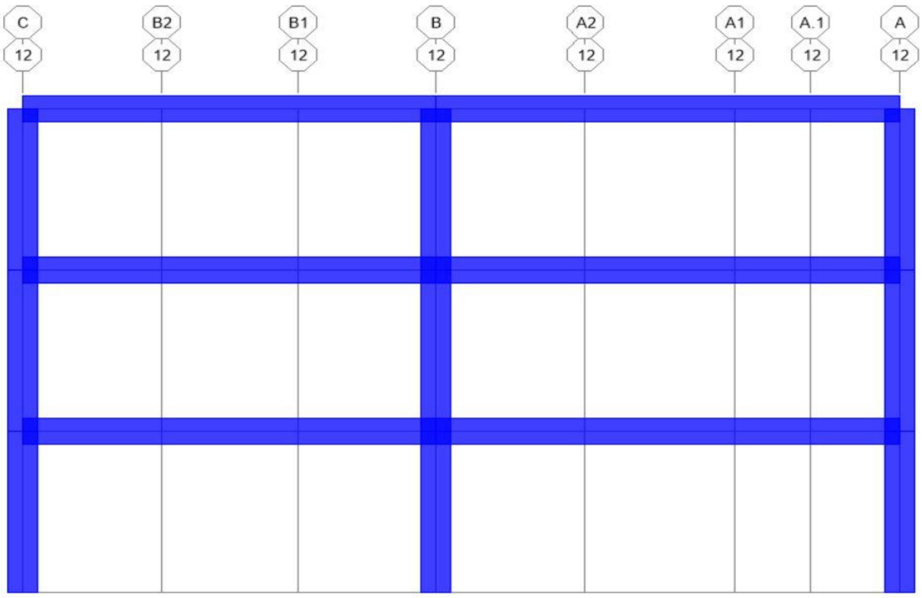

Figure 5.2. *Rear view of the building from the YZ plane (Axis 12) (SAP2000 Building Model, prepared within the scope of this thesis study.).*

This image shows the view of the building model obtained when looking from the opposite direction, i.e., along the C axis. It can be seen that the columns and beams form a regular grid system both vertically and horizontally. The model is not symmetrical, and different dimensions were used in some column spans.

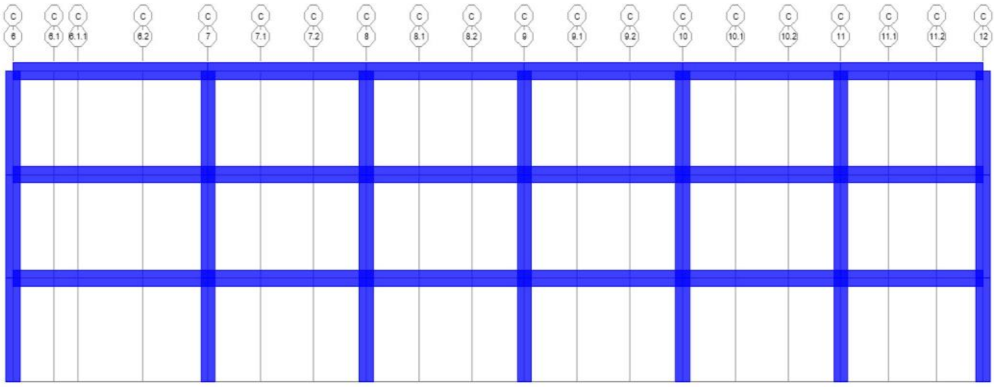

Figure 5.3. *Rear view of the building from the XZ plane (Axis C)(SAP2000 Building Model, prepared within the scope of this thesis study.).*

This figure shows the view of the building along the C axis in the XZ plane. The entire load-bearing system across the three stories is visible in the image, with shear walls installed on the ground floor to increase horizontal load-carrying capacity shown in pink. The shear walls were defined only between axes 6 and 12, aiming to locally increase horizontal stiffness.

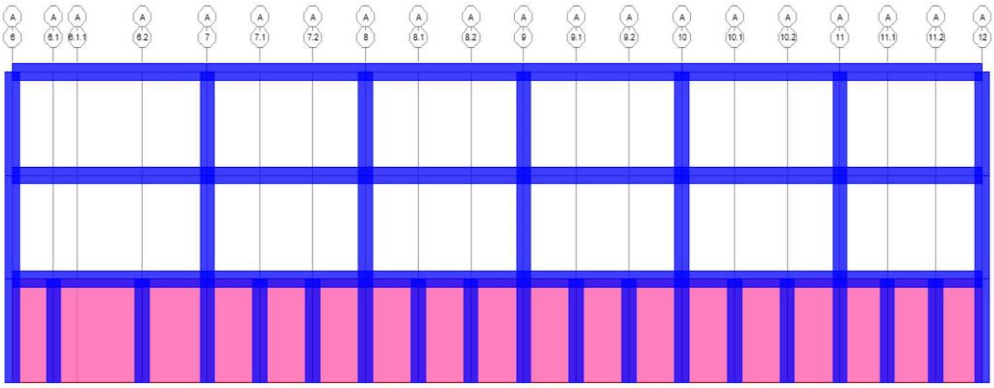

Figure 5.4. *Display of shear walls along Axis 6 in the YZ plane(SAP2000 Model Image, prepared within the scope of this thesis study.).*

In this view, only the shear walls defined along Axis 6 at the ground floor level are highlighted. The transparent pink areas represent the shear walls, which are located exclusively on the ground floor and between specific axes. These high-stiffness elements were modeled to increase the building's horizontal load-carrying capacity.

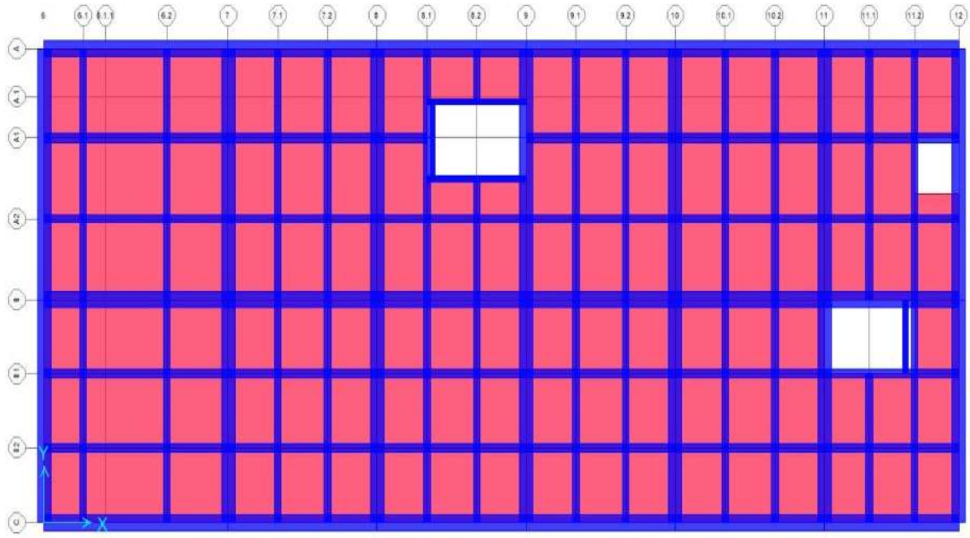

Figure 5.5. *First floor plan view of the structure in the XY plane(SAP2000 Floor Plan Image, prepared within the scope of this thesis study.).*

In the first floor of the building, the slab system and beam layout are shown. The pink areas represent the slabs, while the blue lines represent the beams. The slabs were modeled as 0.20-meter-thick flat slabs and defined using plate-type elements in the PLAXIS 3D environment.

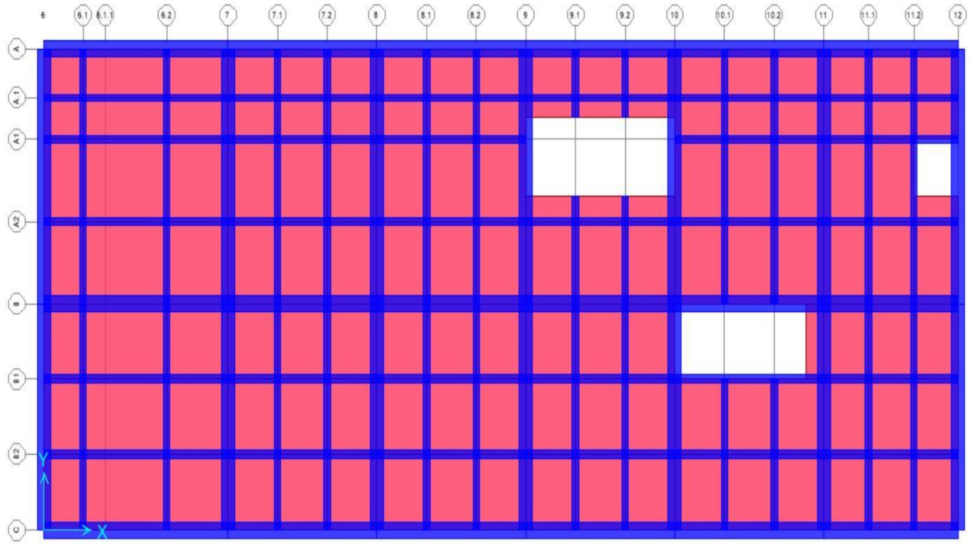

Figure 5.6. *Second floor plan view of the structure in the XY plane(SAP2000 Floor Plan Image, prepared within the scope of this thesis study.).*

In the plan view of the second floor, the beam and slab system is shown aligned with the vertical elements of the lower floor. The presence of openings in certain areas is notable. These types of openings were considered among the parameters affecting the structural stiffness.

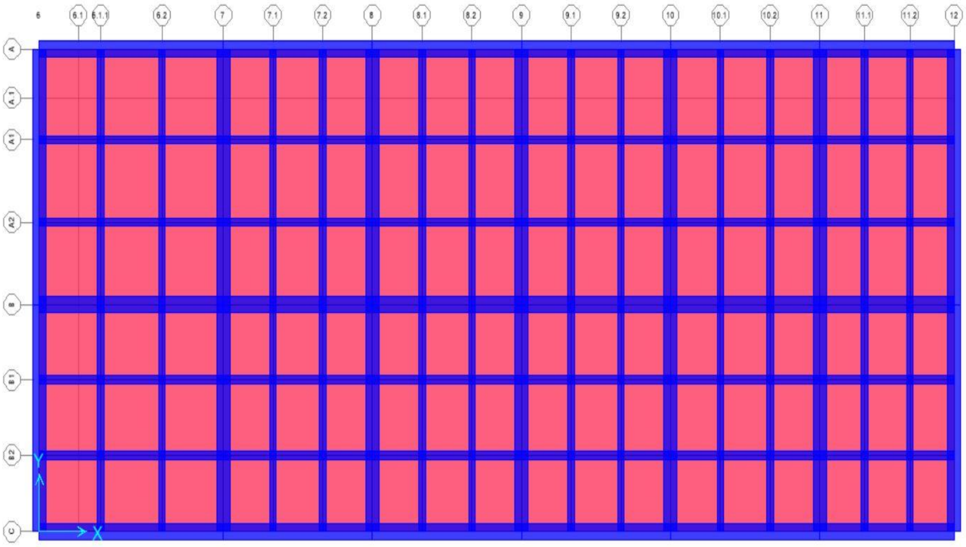

Figure 5.7. *Third floor plan view of the structure in the XY plane(SAP2000 Floor Plan Image, prepared within the scope of this thesis study.).*

In the third-floor plan, it can be seen that the slab areas are completely enclosed, with no slab openings present. This increases the stiffness contribution of the upper floor and plays an important role in limiting horizontal displacements.

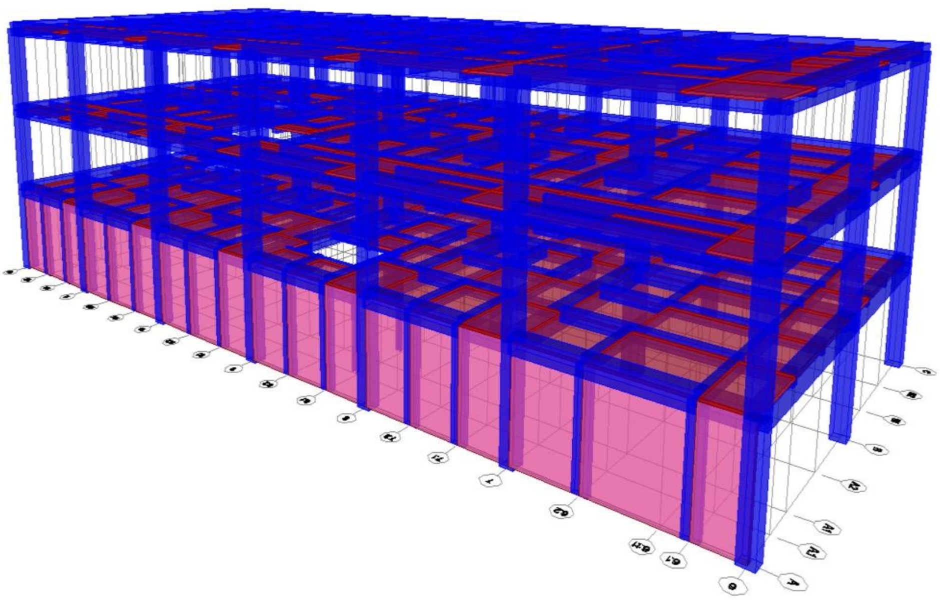

Figure 5.8. *Three-dimensional model of the building's load-bearing system(Modeled by the author in the SAP2000 environment.)*

This figure presents the three-dimensional view of the three-story reinforced concrete building's load-bearing system modeled in the SAP2000 software environment.

The blue elements represent the beam and column system of the structure, while the pink (pink-toned) areas indicate the shear walls.

5.1.1. Beam and Column Elements

The beams and columns with different cross-sections used in the structure directly affect the dimensioning and load-bearing capacity of the structural system.

Beam Sections:

B40/60: 40 cm wide, 60 cm high.

B50/60: 50 cm wide, 60 cm high.

B80/80: 80 cm × 80 cm square cross-section, used especially in large-span areas.

Column Sections:

C100/100: 1 m × 1 m.

C80/80: 80 cm × 80 cm.

C80/30: 80 cm × 30 cm.

The story height was kept constant throughout the structure at 5.00 meters. Additionally, on the first floor of the building, a 0.30-meter-thick shear wall located between axes A6 and A12 was included to effectively resist horizontal loads. This shear wall increases the building's horizontal stiffness and allows for a more rational evaluation of the contribution of infill walls.

Principle of Definition in PLAXIS 3D:

When defining beams and columns as beam elements, separate material datasets are created for each section type (B40/60, B50/60, B80/80, C100/100, C80/80, C80/30). The relevant cross-sectional areas, moments of inertia, and the elastic properties of the concrete (Young's Modulus, Poisson's Ratio) are entered into these datasets. The shear wall is usually modeled either as a large vertical plate element or, if available and suitable in PLAXIS 3D, using dedicated wall elements.

5.1.2. Slab system

A 0.20-meter-thick flat slab system was applied on all floors. This system transfers loads directly to the columns in areas without beams, increasing the structural stiffness, and it was appropriately represented using plate elements in the modeling.

Principle of Definition in PLAXIS 3D:

Slabs are defined using plate elements with a thickness of 0.20 meters. The elastic properties of the concrete (Young's Modulus, Poisson's Ratio) are assigned to these plate elements. Plate elements can model both in-plane and out-of-plane stiffness, enabling them to accurately represent the behavior of the slab system.

5.1.3. Modeling of infill walls

Instead of directly defining infill walls as volume elements in the structural model, they were integrated into the model using equivalent diagonal struts. These elements were defined as beam or node-to-node anchor elements that can only carry axial forces and have zero tensile capacity. This approach enables a simpler and more effective assessment of the contribution of infill walls to the structural stiffness and is a widely used method in the literature (Mainstone, 1971; Panagiotakos and Fardis, 1996).

The axial stiffness (k) of the equivalent diagonal elements was calculated as follows:

$$k = E_w \cdot b_w \cdot t_w \tag{5.1}$$

where Ew is the Young's modulus of the infill material, bwb_wbw is the width of the strut, and t_w is the thickness of the panel. According to the empirical expression proposed by Mainstone (1971), the strut width (b_w) is defined as:

$$b_w = \beta \cdot d_w \cdot \left(\frac{h_w}{d_w}\right)^n \tag{5.2}$$

The width was determined using Excel-based calculations depending on the panel geometry (d_w: diagonal length; h_w : panel height) and the moments of inertia of the columns in the structure. Since the presence of openings (doors, windows, etc.) reduces the stiffness of the infill walls, a reduced Young's modulus value (Ew=0.5 GPa) was used in the calculations.

An elastoplastic model was adopted for the infill elements. While the tensile strength was taken as zero, the compressive strength (F_{max}) was defined as:

$$F_{max} = \tau_{cr} \cdot A_w \tag{5.3}$$

Where τ_{cr}=0.2MPa and A_w is the cross-sectional area of the panel.

Sample stiffness values calculated for the panels between axes A6–B6 and C6–C12 are presented in the following tables:

Angle(°)	λh	bw (m)	Kw (kN/m)	EA (kN)
22.00	0.2490	2.172	271500	3665250
24.17	0.2536	1.943	242875	2965504

Table 5.1. *Calculated Values Between Axes A6–B6*

Panel	lw (m)	λh	bw (m)	Kw (kN/m)	EA (kN)
C6–C7	12.17	0.2583	1.923	240375	2668163
C7–C8	10.30	0.2671	1.605	200625	1805625
C8–C9	10.30	0.2671	1.605	200625	1805625
C9–C10	10.30	0.2671	1.605	200625	1805625
C10–C11	10.30	0.2671	1.605	200625	1805625
C11–C12	9.52	0.2708	1.476	184500	1494450

Table 5.2. *Panel Data Between Axes C6–C12*

5.1.3.1. Principle of integration into the finite element model in PLAXIS 3D

The calculated stiffness values were applied in the nonlinear analysis software PLAXIS 3D as follows:

Diagonal Elements: The equivalent diagonals representing the infill walls were modeled as node-to-node anchor elements in PLAXIS 3D (as also indicated in the study by Gragnano et al., 2014). For these elements, the calculated axial stiffness (EA) and compressive strength (Fmax) for each panel were assigned.

Tensile Strength: The tensile strength was defined as zero in the material model of the node-to-node anchor elements. This reflects the assumption that the infill walls do not have tensile load-carrying capacity.

Geometric Definitions: The angle of each panel was measured and verified on the structural model, and the geometric position of the node-to-node anchor elements was adjusted accordingly.

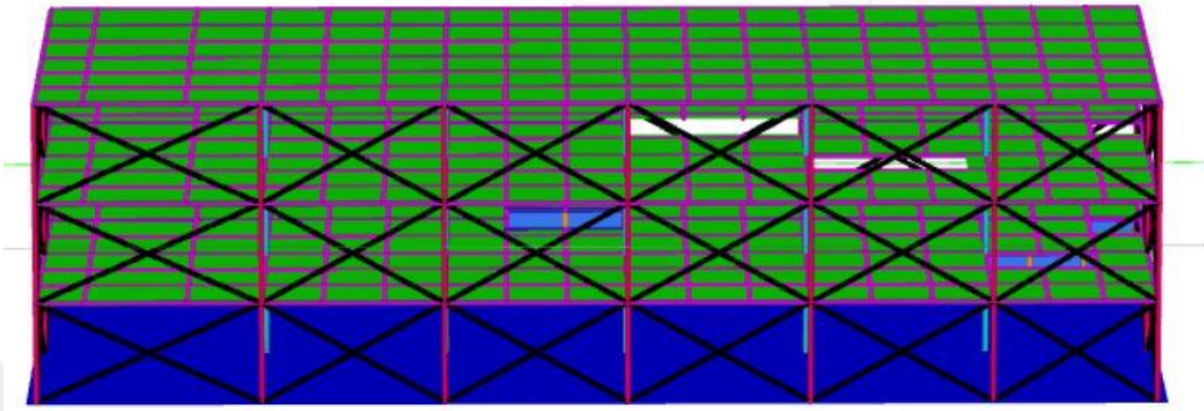

Figure 5.9. *Finite element model of the structure in the Y-Z plane in the PLAXIS 3D environment(PLAXIS 3D model – prepared within the scope of this thesis.).*

In the model, the slabs and beams are defined in green, the shear walls in blue, and the diagonals in black. The truss-like arrangement of the diagonal reinforcements can be seen. The structure extends along 12 axes and consists of three stories vertically. The beam and column systems were modeled with beam elements, while the slabs were modeled with plate elements.

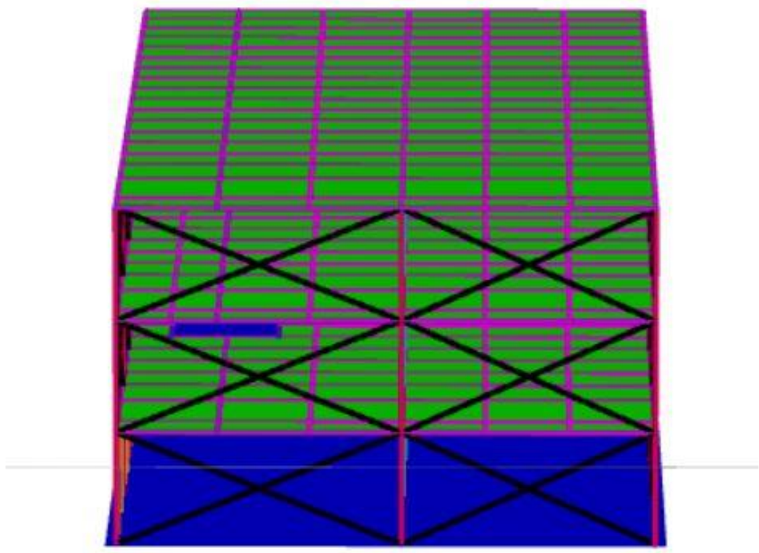

Figure 5.10. *Front view of the structure – PLAXIS 3D structural model(PLAXIS 3D model – prepared within the scope of this thesis.).*

The front facade shows the column and beam system along with the shear wall systems, differentiated by color.

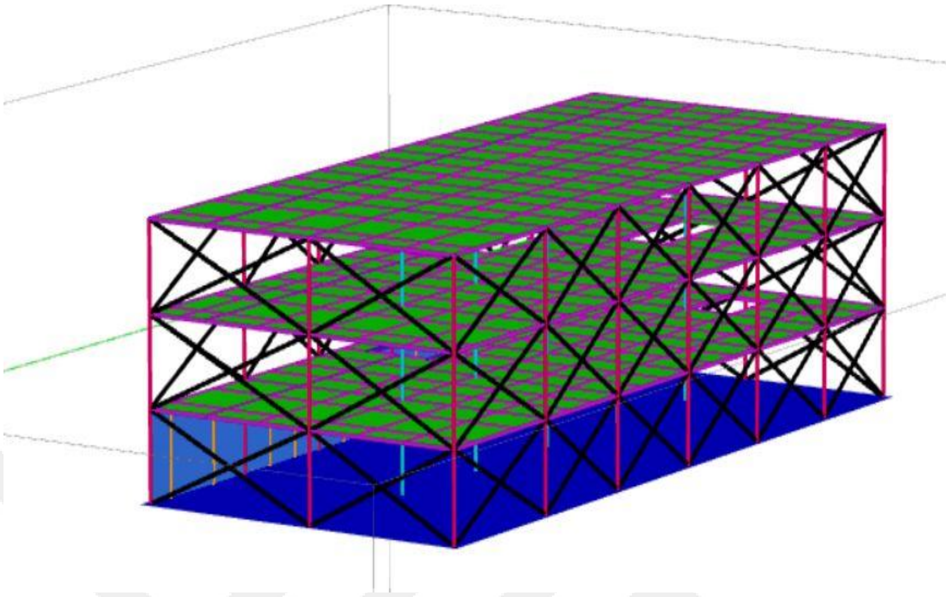

Figure 5.11. *View of the model in the PLAXIS 3D environment(PLAXIS 3D analysis scene modeled within the scope of this study.).*

The three-dimensional geometry of the structure is shown, including the entire load-bearing system, slabs, and diagonals.

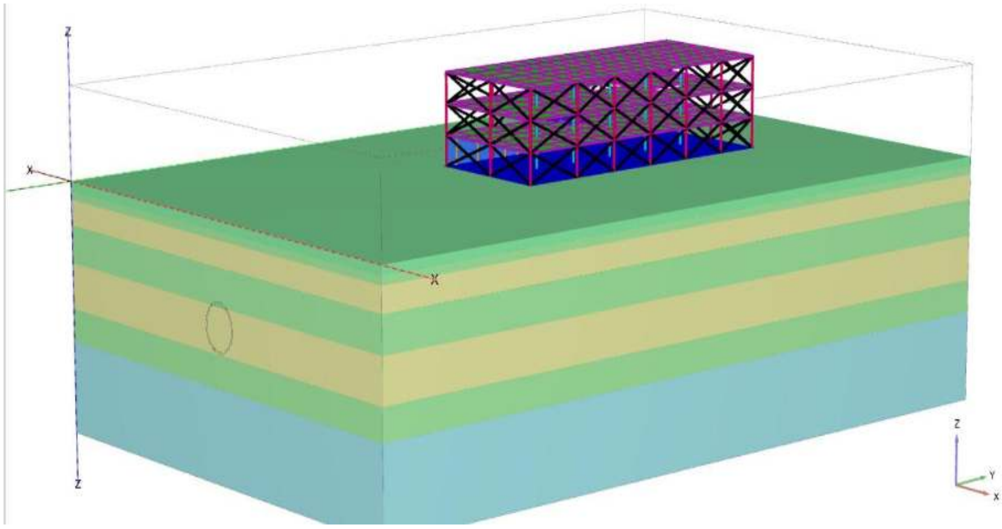

Figure 5.12. *Combined modeling of the structure and soil system – full PLAXIS 3D view(PLAXIS 3D analysis scene modeled within the scope of this study.).*

The building model was modeled together with the soil layers in a 3D environment, and an interaction analysis was performed. The soil layers are color coded, with the structure positioned on top.

6. STRUCTURAL VALIDATION AND COMPRASION: SAP2000 AND PLAXIS 3D MODELS

This section presents a comparison between the conventional structural analysis model of the building created in SAP2000 and the structure-soil interaction model developed in the PLAXIS 3D environment. In this comparison, internal force distributions (shear forces, moments) and vertical displacements in selected structural elements were evaluated alongside the results obtained from different analysis environments.

The study is based on the methodological approach proposed by Gragnano et al. (2014) in the literature, which compares the performance of structural components modeled in PLAXIS 3D and SAP2000. Within this framework, analyses were carried out on primary beams selected from the structure (e.g., the B80/80 section beam between axes A6-B6), revealing differences in behavior between the geotechnically integrated and purely structural models.

Three different models were evaluated in this comparison:

1. **PLAXIS 3D – Cross-Branched Model Only**

   The model in the PLAXIS 3D environment where the infill walls are represented by equivalent diagonal struts.

2. **PLAXIS 3D – Cross-Branched Model with Basement**

   An extended version of the above model that also includes a one-story-deep basement modeled below the structure.

3. **SAP2000 – Reference Structural Model**

   A conventional analysis model created in SAP2000 containing only the structural system components.

The purpose of these comparisons is to evaluate the reliability and accuracy of PLAXIS 3D's capabilities not only for geotechnical but also for structural analysis, relative to SAP2000, a widely used structural analysis program. In particular, this section investigates in detail how PLAXIS 3D's advantage of three-dimensional modeling and ability to account for soil-structure interaction results in behavioral differences in the structure.

In the first step, a B80/80 section beam element located between axes A6-B6 on the first floor was selected, and the shear force, moment, and vertical displacement values for this beam were analyzed. The obtained data were compared and evaluated between the SAP2000 and PLAXIS 3D models.

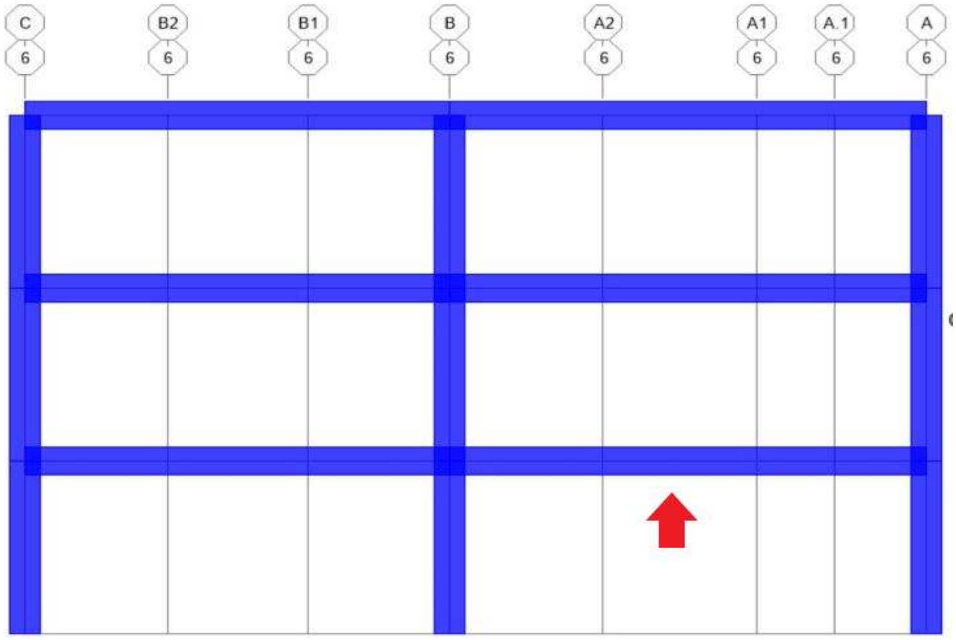

Figure 6.1. *Location of the selected beam in the structural model*

The position of the B80/80 section beam selected for analysis, located between axes A6–B6 on the first floor, is indicated with a red arrow in the structural model. The internal force and displacement results obtained along this beam are presented in the following graphs.

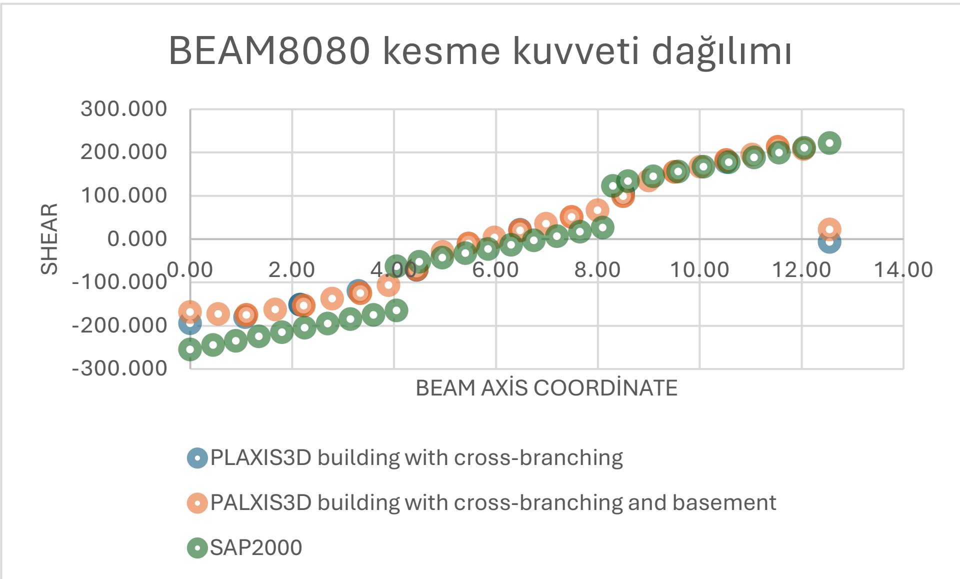

Figure 6.2. *Shear force distribution along the A6–B6 beam – First floor*

This graph shows the distribution of shear force obtained along the A6–B6 beam. The building modeled in the PLAXIS 3D environment was analyzed in two different scenarios: one with only diagonal reinforcement and another including both diagonal reinforcement and a basement. SAP2000 results were included for comparison purposes.

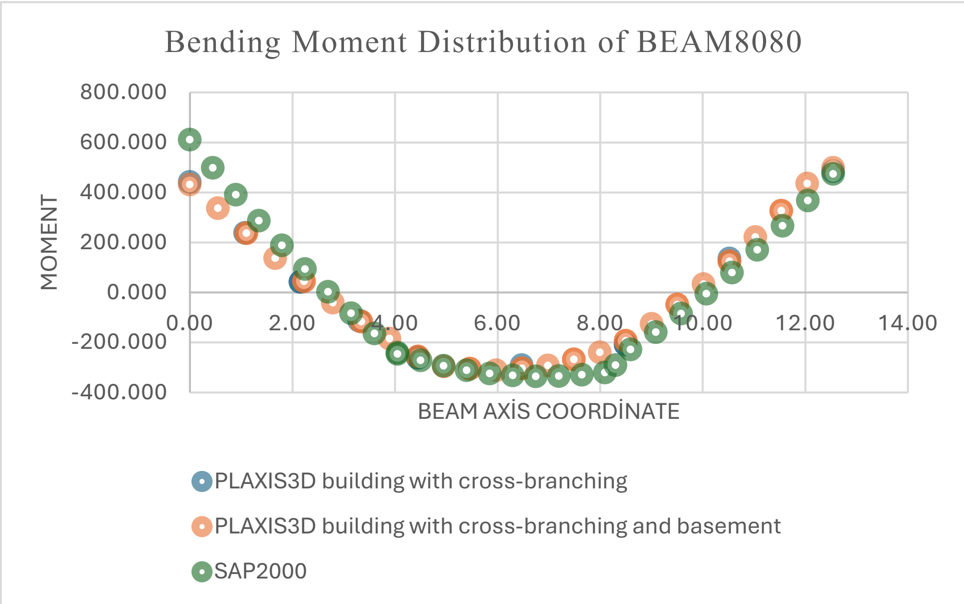

Figure 6.3. *Bending moment distribution along the A6–B6 beam – First floor*

The bending moment distribution shows that maximum moment values occur at the mid-span of the beam, with the moments decreasing toward the beam ends. The similarity of the distribution curves between PLAXIS 3D and SAP2000 confirms the adequacy of PLAXIS 3D in terms of structural analysis.

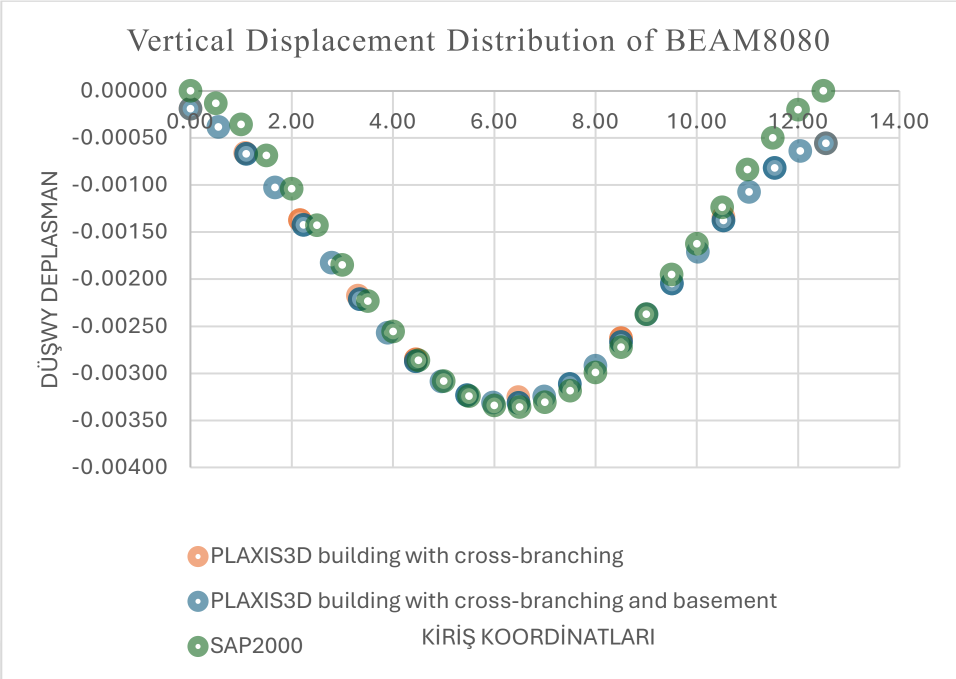

Figure 6.4. *Vertical displacement distribution along the A6–B6 beam – First floor*

An examination of the vertical displacements along the beam shows that the values obtained from the PLAXIS 3D models are very close to those from the SAP2000 results. Notably, the model that includes both diagonal reinforcement and a basement produces results that are closer to those of SAP2000.

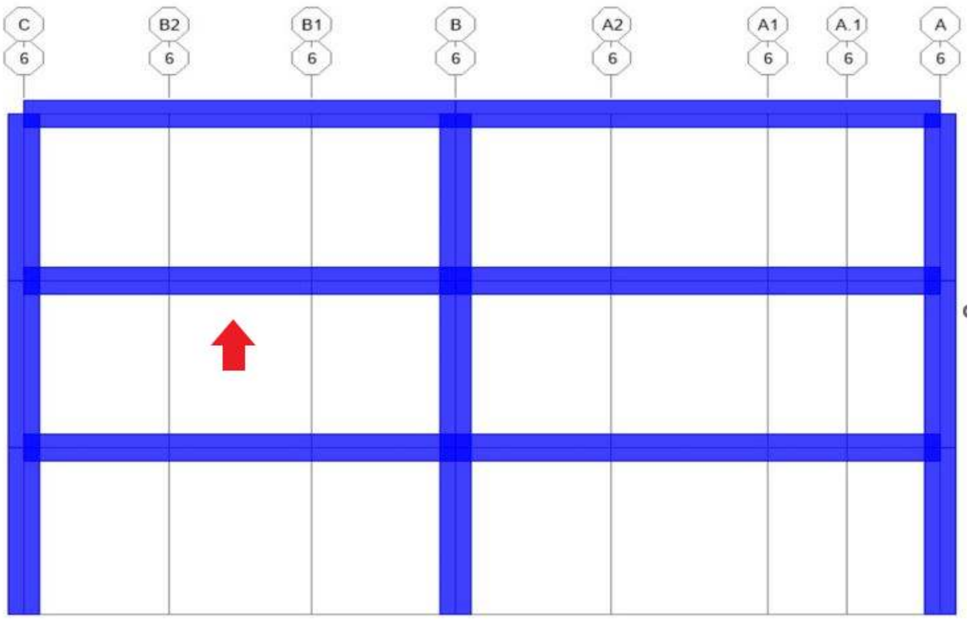

Figure 6.5. *Position of the second-floor B6–C6 beam analyzed in the PLAXIS 3D model*

In this image, the location of the B6–C6 beam on the second floor, which was analyzed for comparison, is indicated with a red arrow. The internal force and displacement values obtained along the same axial coordinates correspond to this beam.

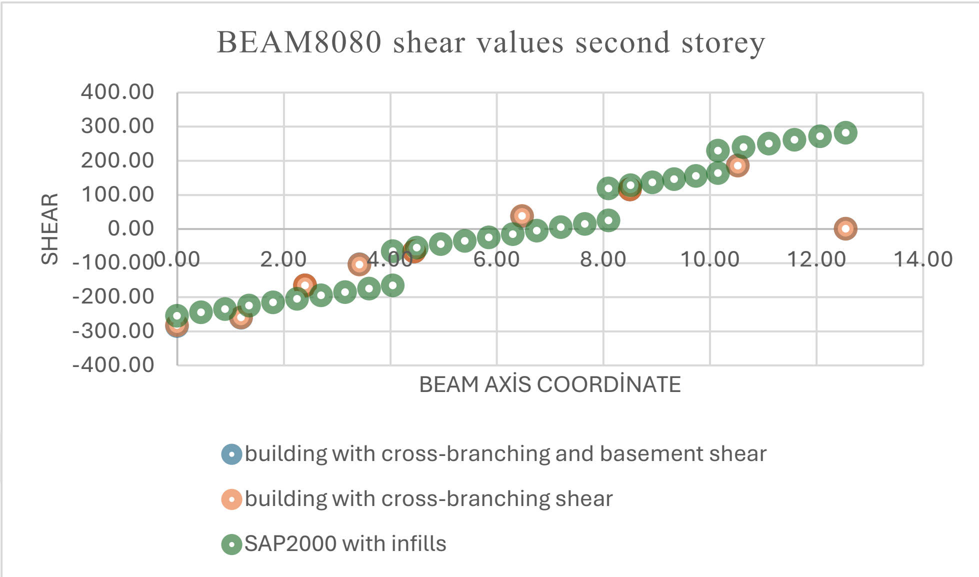

Figure 6.6. *Comparison of second-floor shear force distribution along the B6–C6 beam in SAP2000and PLAXIS 3D software*

In this graph for the second floor, the shear force values obtained along the same beam were analyzed in the PLAXIS 3D model both with and without the basement effect included, and compared with the data obtained from SAP2000 including the effects of infill walls. While the PLAXIS 3D models generally show good agreement with the SAP2000 results, noticeable differences are observed especially at the start and end points. These differences mainly stem from the more effective consideration of secondary beams providing indirect load transfer in the SAP2000 model.

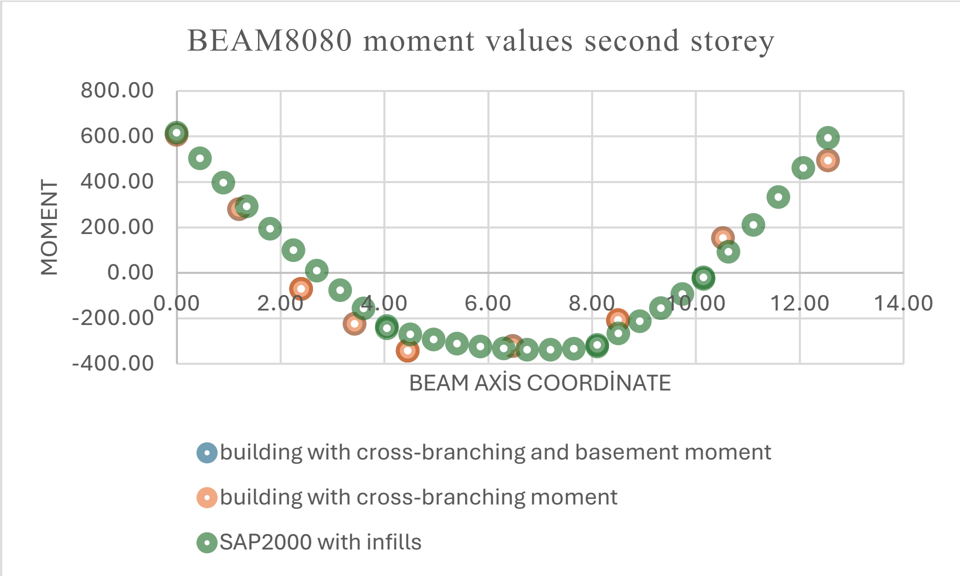

Figure 6.7. *Comparison of second-floor bending moment distribution along the B6–C6 beam in SAP2000 and PLAXIS 3D software*

Although the bending moment distributions in both models exhibit similar parabolic shapes, the moment values at the beam ends are higher in the SAP2000 model. This can be attributed to the more pronounced stiffness contribution of the infill walls in the SAP2000 model. In the PLAXIS 3D models, the moment distribution is more spread out and the values are lower. Additionally, the model with the basement effect shows a slight increase in bending moments.

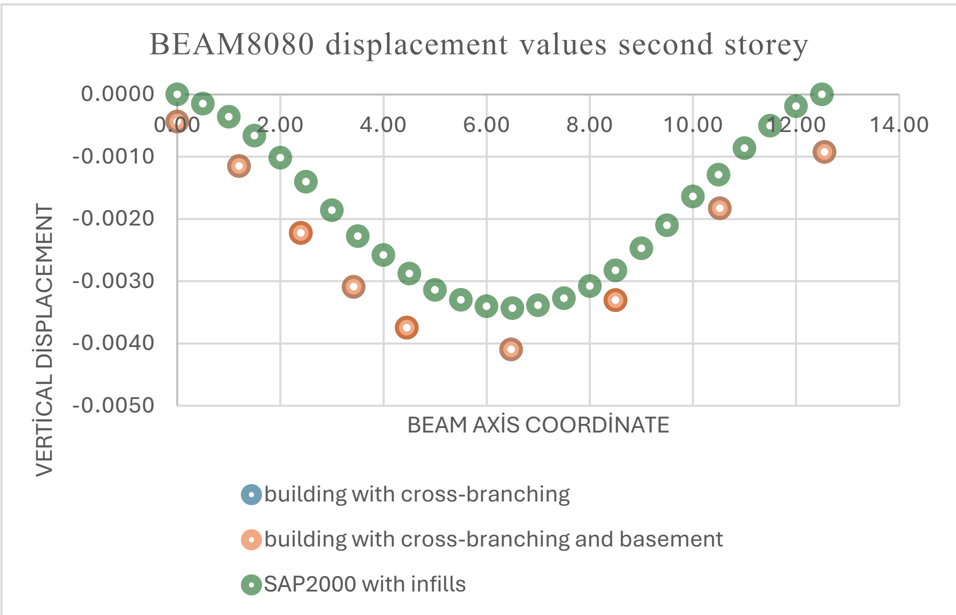

Figure 6.8. *Comparison of second-floor vertical displacement distribution along the B6–C6 beam in SAP2000 and PLAXIS 3D software*

In the displacement figures, the SAP2000 model generally exhibits lower deformations. In the buildings modeled with PLAXIS 3D, the inclusion of soil-structure interaction results in increased vertical displacements. It is observed that in the model including the basement effect, the displacements are more limited. This clearly demonstrates the contribution of foundation stiffness to the overall system behavior.

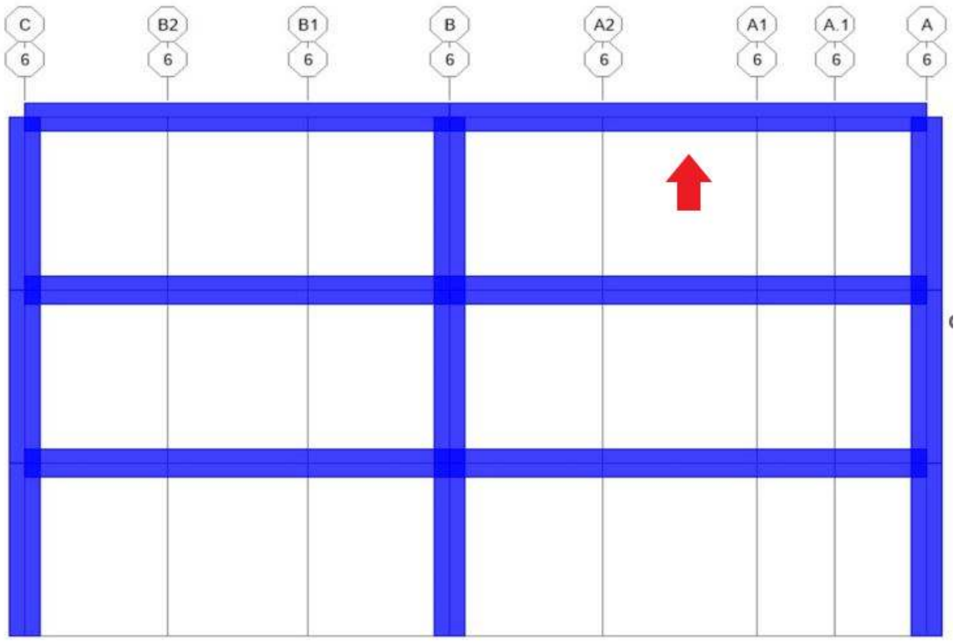

Figure 6.9. *View showing the location of the third-floor B80/80 beam between axes A6–B6*

The area indicated by the red arrow shows the location of the B80/80 section beam between axes A6–B6, which was used for comparative analyses. This section of the building model was defined in both the SAP2000 and PLAXIS 3D models.

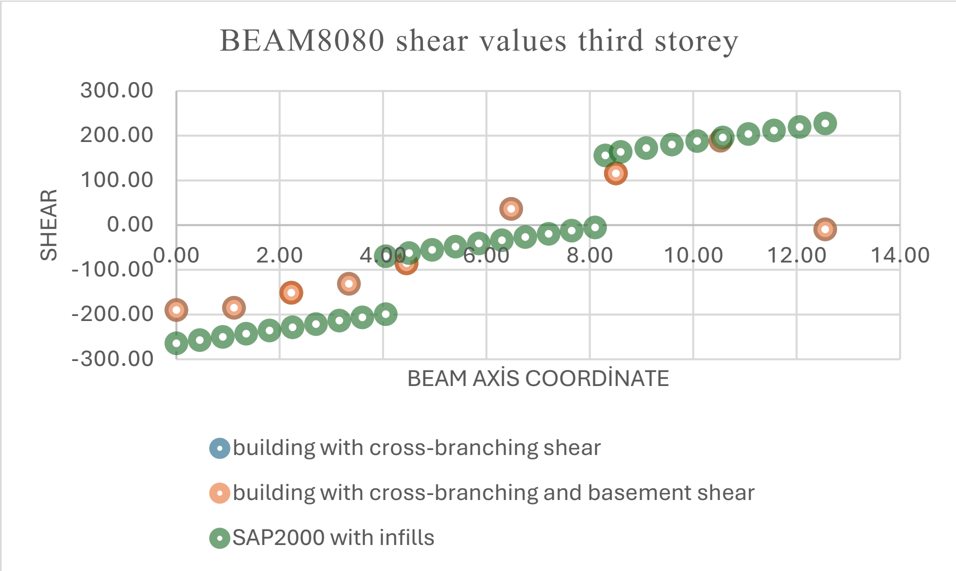

Figure 6.10. *Shear force distributions of the third-floor B80/80 beam*

This figure shows the shear force distributions for the B80/80 beam located on the third floor between axes A6–B6. For the PLAXIS 3D model, both the cross-branched structure and the variant including the basement were analyzed. In the SAP2000 model, the contribution of the infill walls was also considered.

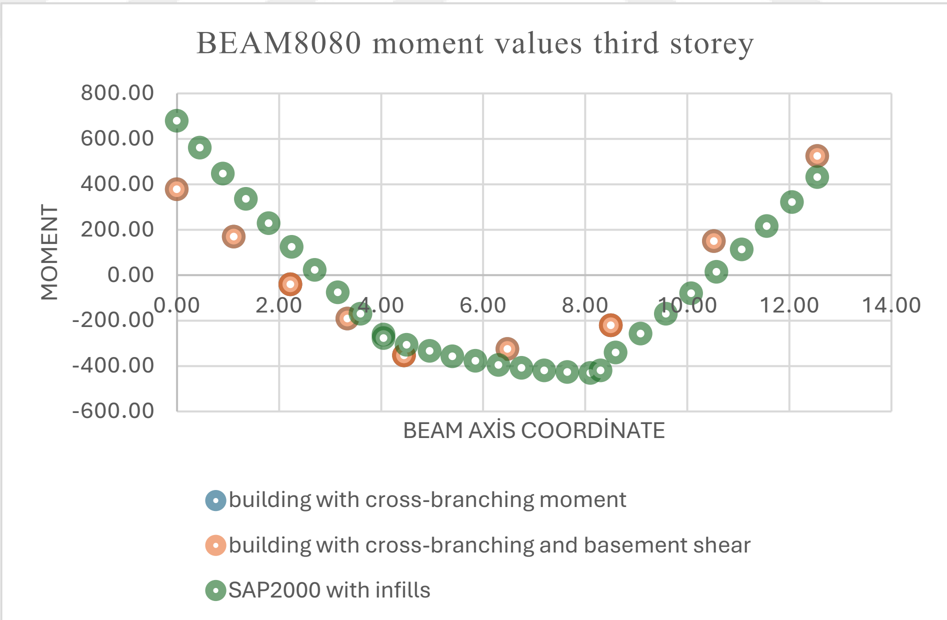

Figure 6.11. *Bending moment distributions of the third-floor B80/80 beam*

The bending moment distributions of the third-floor B80/80 section beam are presented comparatively. The difference between the PLAXIS 3D models and the SAP2000 result appears mainly due to increased moment values at the mid-span. This difference arises from variations in how the infill walls and diagonal elements were modeled.

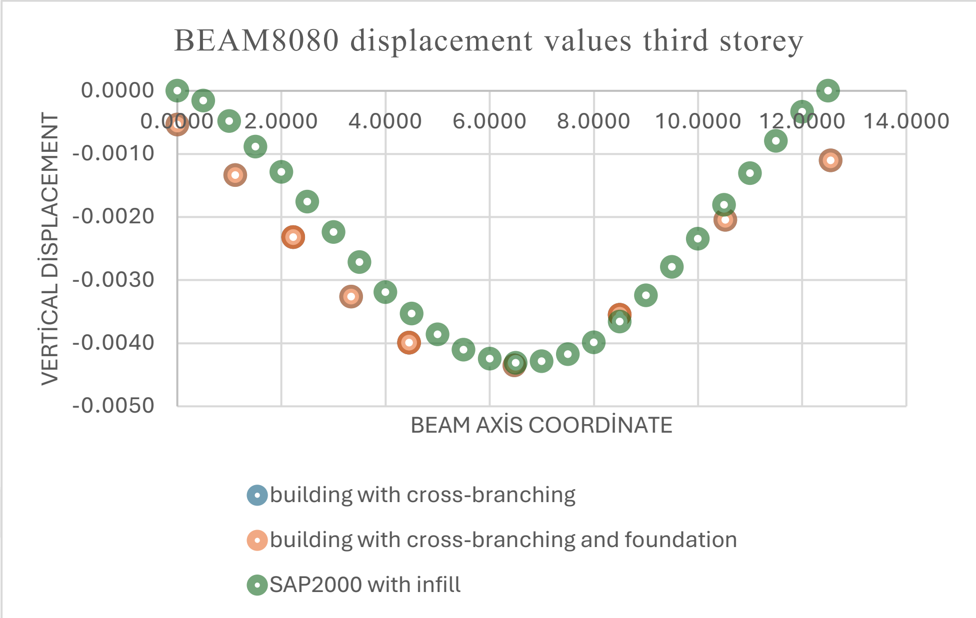

Figure 6.12. *Vertical displacement distributions of the third-floor B80/80 beam*

The vertical displacement distributions of the relevant beam are presented comparatively. In the SAP2000 model, the infill (masonry wall) effect is considered directly, whereas in the PLAXIS 3D model, it is represented indirectly using node-to-node anchor elements. The inclusion of the basement effect significantly reduces the displacements.

6.1. Analysis of Shear Force Differences and the Secondary Beam Effect

The shear force values obtained for the first-floor beam between axes A6–B6, as presented in Figure 4.1, generally exhibit a similar distribution between the PLAXIS 3D and SAP2000 models. However, certain deviations in the magnitude of the shear forces were observed, particularly near the mid-span and close to the beam ends. The primary reason for these differences can be explained by the **secondary beam effect**.

The secondary beam effect describes the situation where secondary beams connected perpendicularly to a primary beam influence the distribution of internal forces along the primary beam. Specifically, when modeling the structure:

Structural analysis software like SAP2000 directly reflects all stiffness effects at the connection points. In this case, the moments and shear force contributions generated at the points where secondary beams connect are fully incorporated into the model.

PLAXIS 3D, as a geotechnical analysis software, processes structural components in a three-dimensional environment with soil-structure interaction. However, the connection conditions of beam and slab elements (e.g., rigid, hinged) can only be defined in a limited way, and these connections are often modeled in a simplified manner. This can result in the incomplete representation of the effects of secondary beams.

In this context, because the secondary beam effect is either insufficiently or more simplistically represented in the PLAXIS 3D model, noticeable differences in shear force values can occur compared to the SAP2000 model.

Although the magnitude of these differences is small, it should be considered that PLAXIS 3D is primarily geotechnical software and may not always replicate detailed structural behaviors exactly. Nevertheless, the similarity in the overall trends demonstrates that PLAXIS 3D can provide reliable results in terms of structural accuracy.

6.2. General Behavior Comparison for Different Beam Regions

In this section, the moment and displacement behaviors at various locations of the structural system modeled using SAP2000 and PLAXIS 3D software were comparatively examined. The investigated regions include B80/80 section beams located between axes A11–A12 (2nd floor), C10–C11 (2nd floor), A8–A9 (2nd floor), and C6–C7 (1st floor). In both software models, the loading scenarios, the effects of infill walls, and foundation stiffness were defined under similar conditions. However, due to differences in finite element types, boundary conditions, and structural modeling approaches, limited discrepancies were observed in the results.

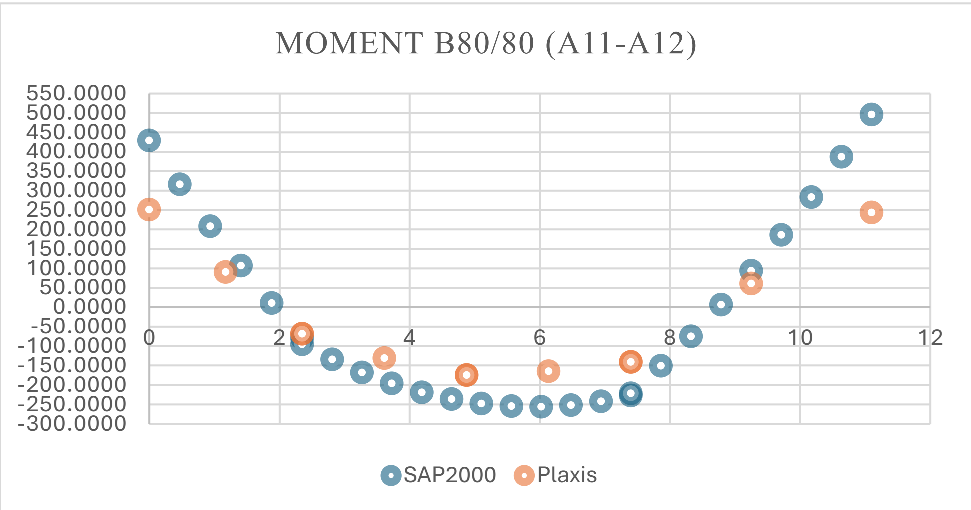

Figure 6.13. *Bending moment distributions of the A11–A12 (2nd floor)*

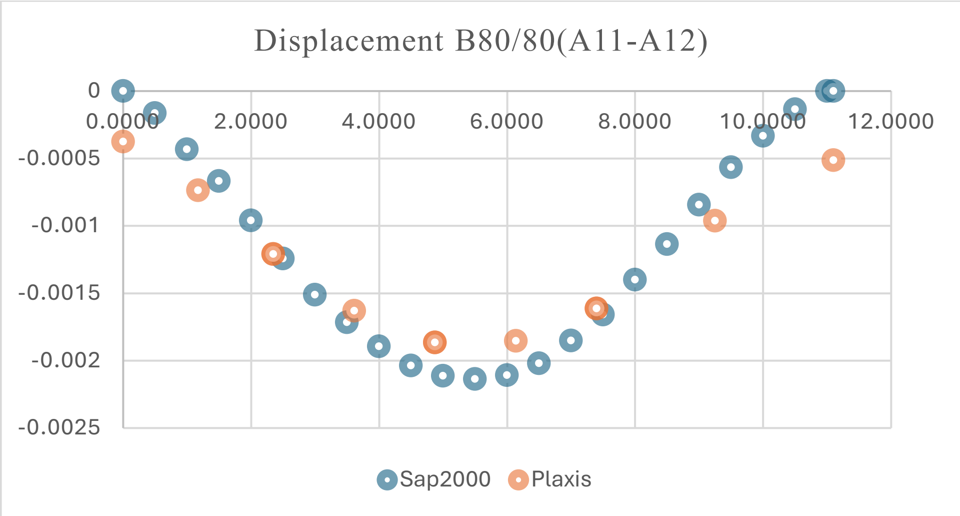

Figure 6.14. *Vertical displacement distributions of the A11–A12 (2nd floor)*

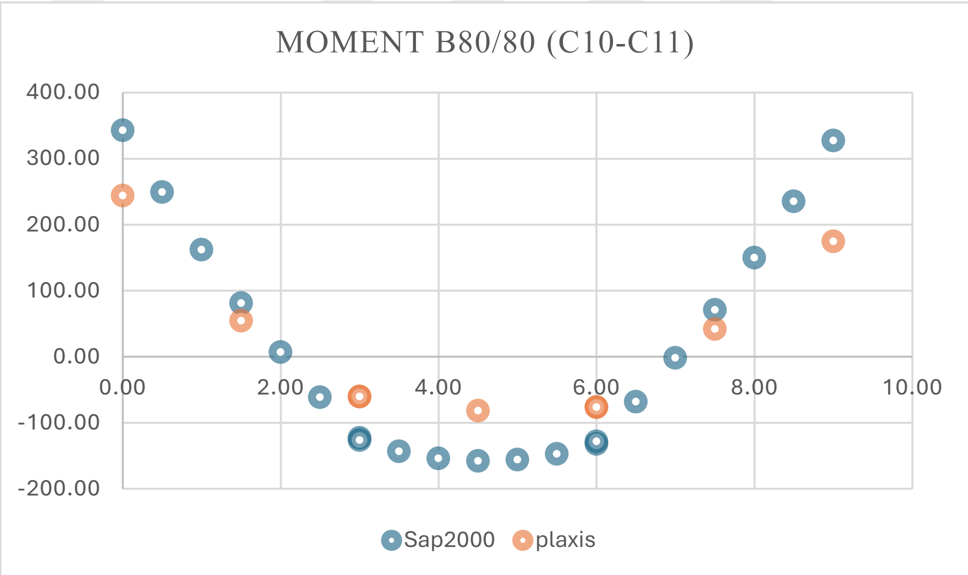

Figure 6.15. *Bending moment distributions of the C10–C11 (2nd floor)*

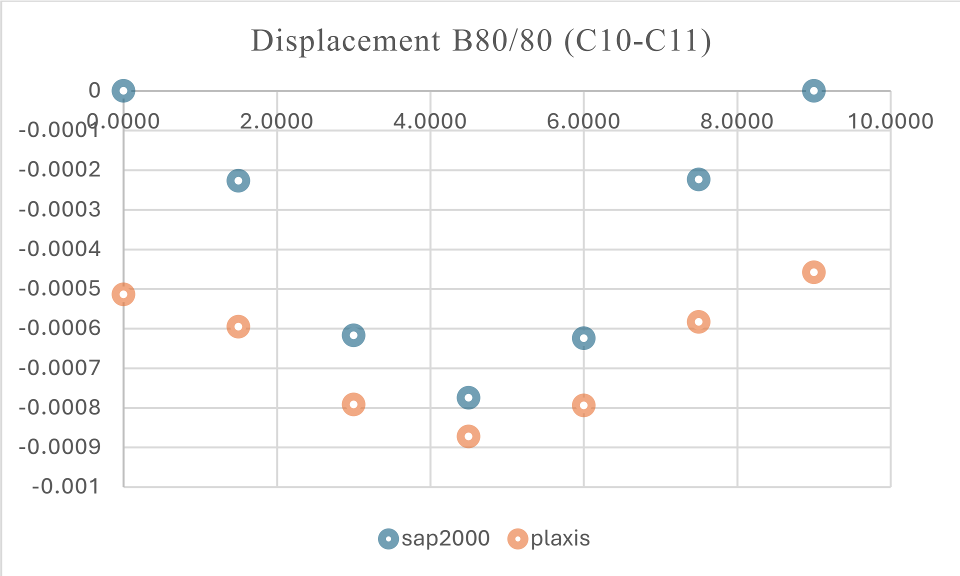

Figure 6.16. *Vertical displacement distributions of the C10–C11 (2nd floor)*

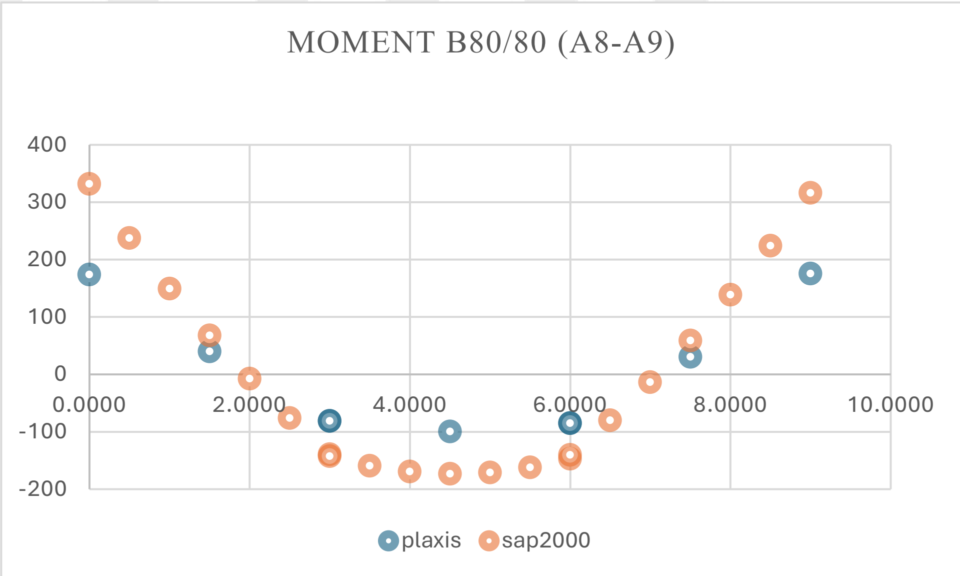

Figure 6.17. *Bending moment distributions of the A8-A9 (2nd floor)*

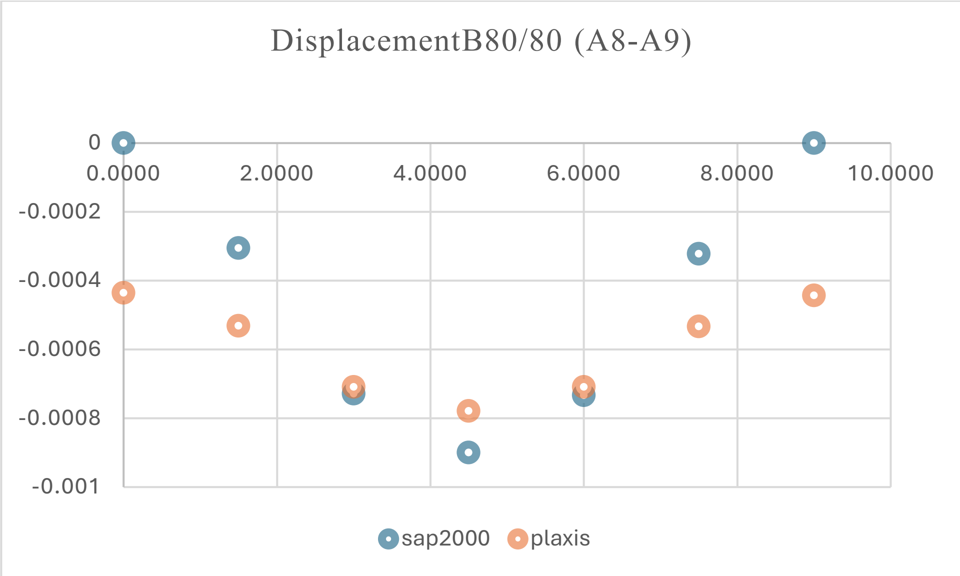

Figure 6.18. *Vertical displacement distributions of the A8-A9 (2nd floor)*

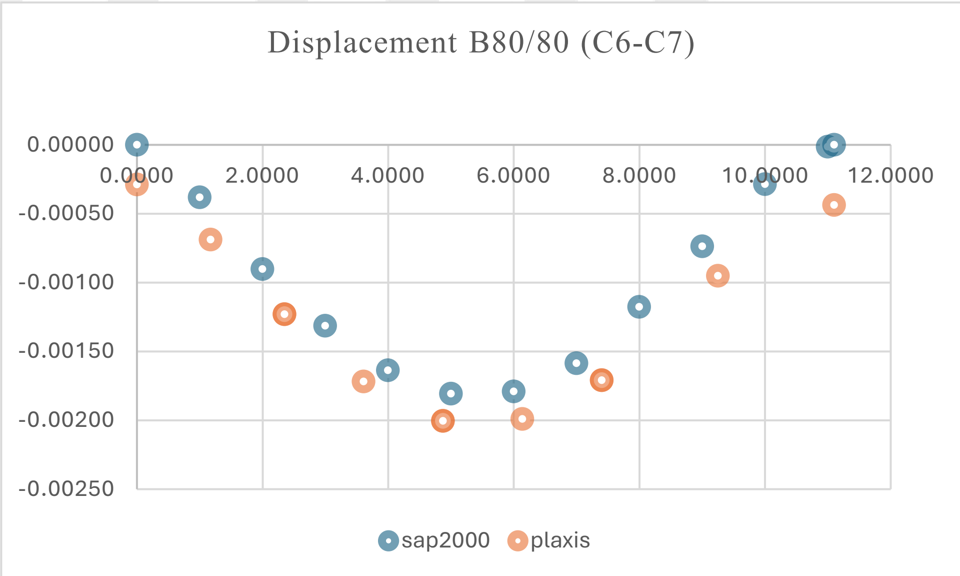

Figure 6.19. *Bending moment distributions of the C6-C7 (first floor)*

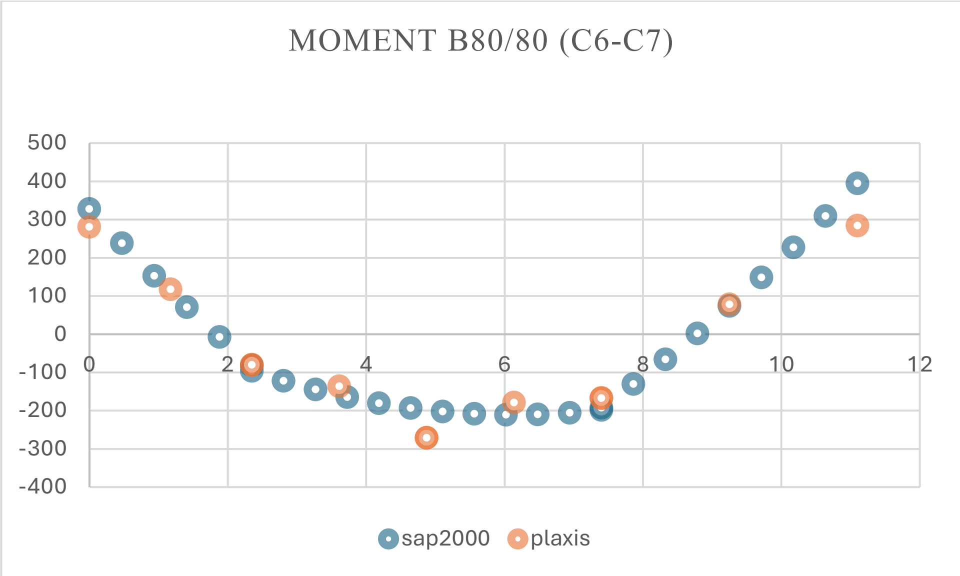

Figure 6.20. *Vertical displacement distributions of the C6-C7 (first floor)*

A11–A12 Axis (Figures 6.4 and 6.5)

Along this axis, the moment values obtained in PLAXIS 3D are generally lower than those in SAP2000, with particularly noticeable differences at the beam ends. The primary reason for this is that the soil-structure interaction system used in PLAXIS 3D has a damping effect on the moments compared to SAP2000's fixed support assumption. In the displacement graph, PLAXIS 3D shows a softer behavior.

C10–C11 Axis (Figures 6.6 and 6.7)

In the C10–C11 region, a similar trend is observed for both moment and displacement. The PLAXIS 3D model produced lower moment and displacement values compared to SAP2000. This is attributed to the more realistic reflection of soil deformations on the structure in the PLAXIS 3D model.

A8–A9 Axis (Figures 6.8 and 6.9)

Along A8–A9, the overall trend of the moment values is similar, but a decreasing tendency is observed in the mid-span in the PLAXIS 3D modeling. Compared to SAP2000, the displacement magnitudes are lower in PLAXIS 3D. This results from PLAXIS 3D producing a more stable solution by considering foundation stiffness.

C6–C7 Axis (Figures 6.10 and 6.11)

The results obtained for this region are similar in nature to the previous areas. The PLAXIS 3D model produced lower displacement and moment values compared to SAP2000. Nevertheless, the similarity in the moment distributions indicates that both software packages accurately captured the general behavioral trend.

As a general assessment in this section, the structural responses of the reinforced concrete building modeled with PLAXIS 3D were compared with the reference results obtained using SAP2000, and the model's accuracy was analyzed. Comparisons made on representative beams selected at different story levels were evaluated based on moment, shear force, and vertical displacement parameters. The findings revealed that PLAXIS 3D can realistically represent the structural system both statically and geometrically, and especially in soil-structure interaction scenarios, it provides more sensitive results compared to conventional analysis approaches.

The differences between SAP2000 and PLAXIS 3D were explained by factors such as the type of finite elements used, the way boundary conditions were defined, and the modeling of the soil. The analyses concluded that the structural system modeled in the PLAXIS 3D environment allows for reliable determination of the structural responses to ground deformations caused by future tunnel excavation.

As a result of this validation process, it was seen that the PLAXIS 3D model possesses sufficient precision and representation capability, thus establishing a solid foundation for the subsequent sections, where the effects of the Naples Metro Line 6 tunnel excavation on the building will be examined.

6.3. Effect of Tunnel Excavation on the Building: Graphical and Numerical Evaluation

In this section, the effects of the tunnel excavation on the analyzed three-story building are evaluated using both the obtained numerical data and comparative analysis with design curves recommended in the literature. This comparison aims to verify the reliability of the numerical model and the consistency of the results with theoretical approaches used in engineering practice.

In the graphs prepared according to the modification factors proposed by Franzius et al. (2004), the MDRsag (Maximum Differential Settlement Ratio – Sagging) and MDRhog (Maximum Differential Settlement Ratio – Hogging) values determined for different stiffness parameters (p*) were taken as reference. For the analyzed three-story building, the obtained p* value was determined as 2.94×10^{-3} The corresponding MDRsag value was found to be approximately 0.95. In the relevant Franzius graph (Figure 6.21), this value is seen to lie on the design curve for e/B=0 (when the tunnel axis is directly below the building center), showing excellent agreement with the theoretical model. This agreement indicates that the deformation behavior in the building's sagging zone is consistent with the literature (Franzius et al., 2004).

Additionally, the DRsag (Differential Settlement Ratio – Sagging) value calculated for the analyzed structure was 2.53×10^{-4}, while under greenfield conditions (only the ground, without the building), this value was found to be 2.66×10^{-4}. The close similarity of these values indicates that due to the building's stiffness and soil-structure interaction, the deformations caused by the tunnel excavation (particularly in the sagging zone) are largely dampened. In other words, the presence of the building does not significantly change the magnitude of settlement in the ground compared to the no-building condition; however, the deformation transferred to the building from the ground is effectively governed by the building's own stiffness.

On the other hand, the DRhog (Differential Settlement Ratio – Hogging) value for the analyzed structure was found to be nearly zero, whereas under greenfield conditions, an extremely low value of 4.17×10^{-6} was calculated. This indicates that the building's weight and stiffness effectively minimize deformations in the hogging zone. In the MDRhog graph prepared based on the design curves proposed by Potts and Addenbrooke (1997) (Figure 6.22), the data point of the analyzed three-story building ($p^*=2.94 \times 10^{-3}$) is seen to lie near zero on the theoretical curve, demonstrating that the building's behavior in the hogging zone is also consistent with theoretical approaches (Potts and Addenbrooke, 1997).

Both the Franzius and Potts and Addenbrooke graphs clearly demonstrate the decisive role of building stiffness and soil-structure interaction on surface deformations caused by tunnel excavation. The presented graphs and numerical findings offer consistent validation with both the theoretical approaches in the literature and the results obtained in this study, thereby reinforcing the reliability of the modeling and analysis outcomes.

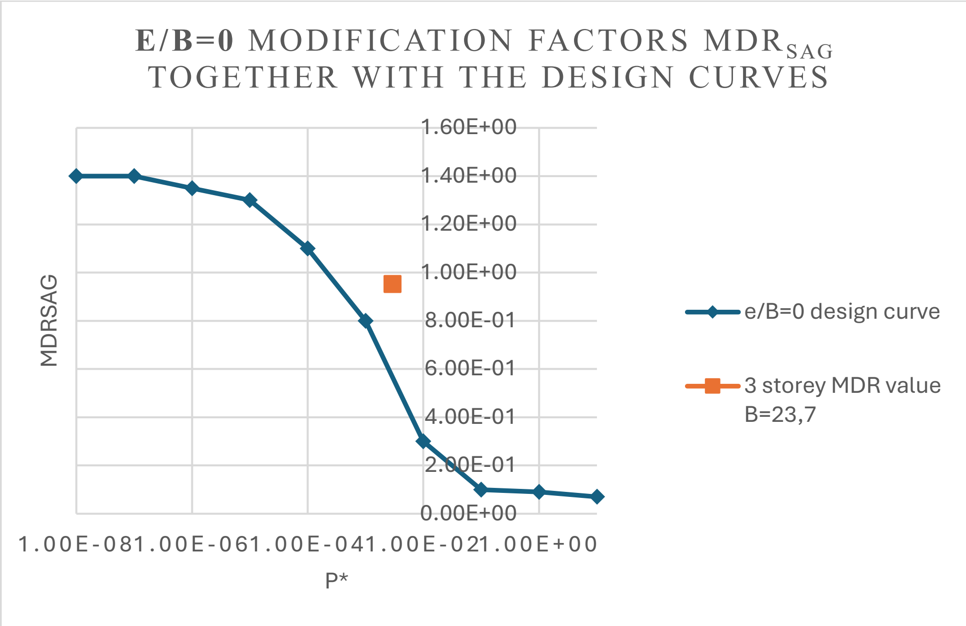

Figure 6.21. *Comparison of the design curve by Franzius et al. (2004) and the MDRsag value of the three-story building.*

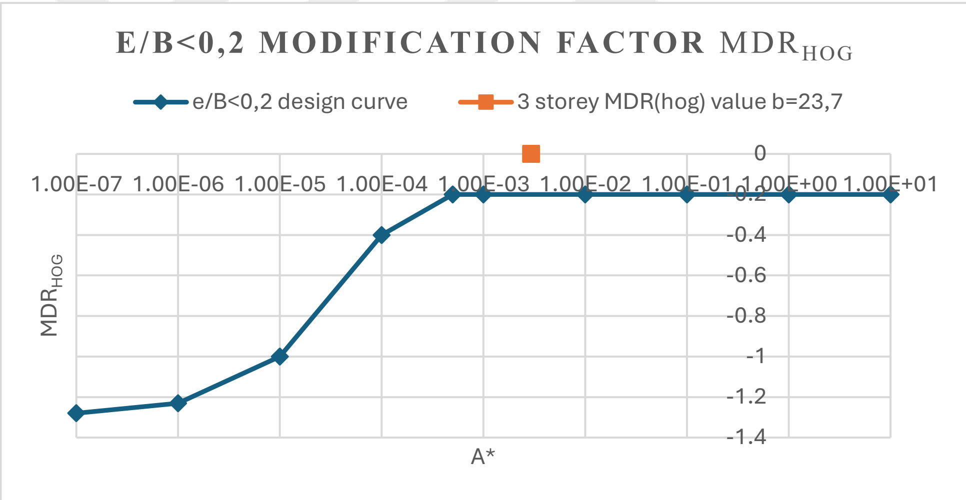

Figure 6.22. *Comparison of the design curve by Potts and Addenbrooke (1997) and the MDRhog value of the three-story building.*

7. GENERAL EVALUATION OF RESULTS

In this section, the findings obtained from the numerical modeling studies conducted for the tunnel excavation process of Naples Metro Line 6 are presented with a comprehensive approach. Analyses performed using PLAXIS 3D software, aiming to reveal the effects of tunnel-soil interaction on building behavior and surface deformations, are addressed under four main headings:

7.1. The Effect of Tunnel-Soil Interface Stiffness on Circumferential Displacements,

7.2. The Effect of Tunnel-Soil Interface Stiffness on Longitudinal Displacements,

7.3. The Effect of Tunnel-Soil Interface Stiffness on Building Behavior: ΔN and Δuz Analysis,

7.4. Changes in Internal Stresses of Column Elements During Excavation.

Under these headings, deformations in the soil and structural system, changes in internal forces, and the effects of interface stiffness occurring during tunnel advancement stages were evaluated in detail. Circumferential and longitudinal settlement profiles under different interface conditions, changes in axial forces (ΔN) and vertical displacements (Δuz) in building foundations, and internal stress distributions in column elements were analyzed. The results show that the interface stiffness parameter significantly affects both surface settlements and building performance during tunnel excavation.

These findings highlight the necessity of carefully defining interface conditions in soil-structure interaction modeling for tunnel projects and provide valuable contributions to engineering design.

7.1. The Effect of Tunnel-Soil Interface Stiffness on Circumferential Displacements

In this section, the effect of soil-structure interaction on circumferential settlement profiles during tunnel advancement was examined in detail. The study is based on analyses performed using PLAXIS 3D software with the tunnel geometry and building model of Naples Metro Line 6. The analyses present comparative circumferential settlement values at different stages of tunnel advancement (93.1 m, 98.5 m, and 119.1 m). Specifically, at the point located 87.8 meters along the y-axis where the building center lies, settlement values were analyzed when tunnel advancement reached 119.1 meters.

The settlement profiles presented in Figures 7.1-7.2-7.3 show the trends of circumferential settlement perpendicular to the tunnel axis. The graphs provide comparative settlement profiles for interface stiffness values of R=0.01, R=1, and the case without an interface, as well as a curve representing free-field (greenfield) conditions. The results indicate that the tunnel-soil interface stiffness has a significant effect on the depth and spread width of the circumferential settlement trough.

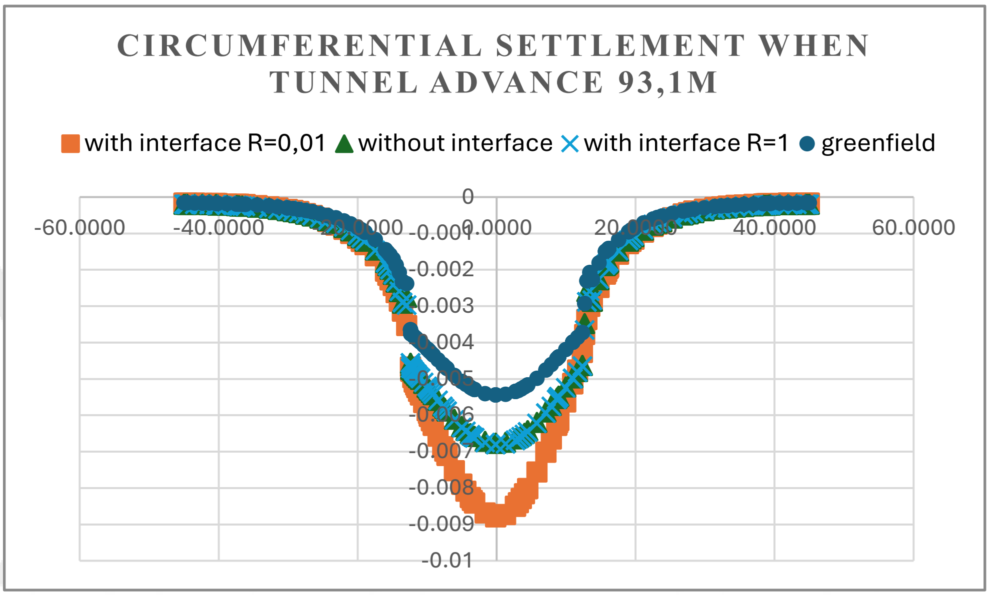

Figure 7.1. *Circumferential settlement profiles at 93.1 m of tunnel advancement.*

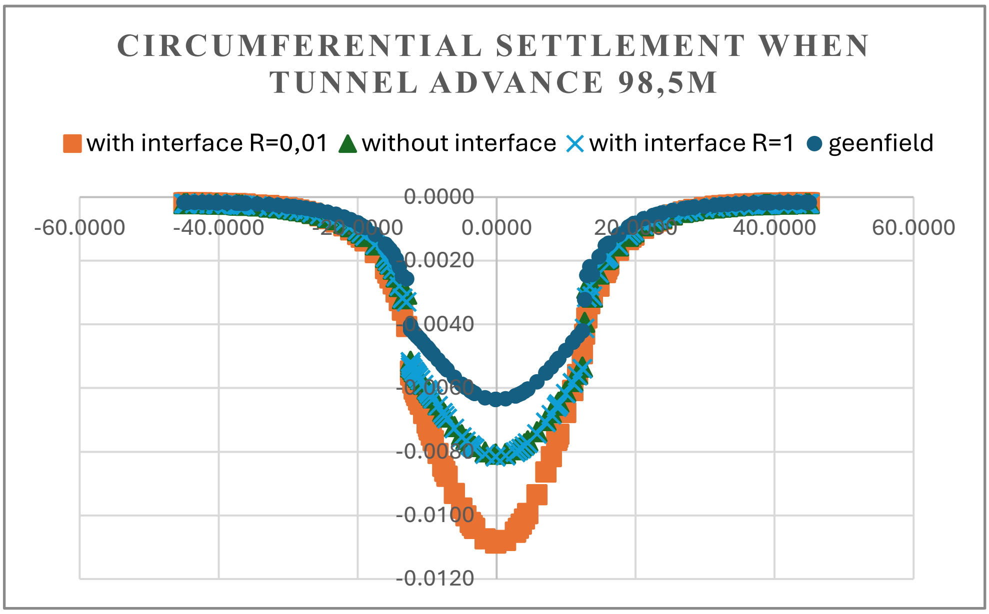

Figure 7.2. *Circumferential settlement profiles at 98.5 m of tunnel advancement.*

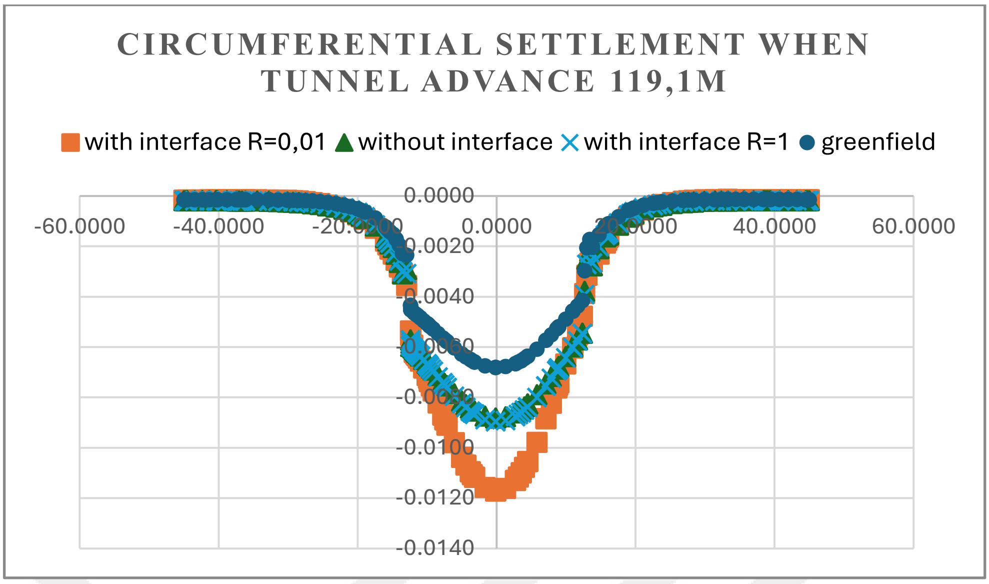

Figure 7.3. *Circumferential settlement profiles at 119.1 m of tunnel advancement.*

7.1.1. Effects of Different Interface Conditions on Settlement

Interface R=0.01 Condition (Low Stiffness Interface)

In this case, the settlement trough reaches its deepest level, and the settlement magnitude attains its highest values. The low stiffness between the soil and tunnel lining makes the soil more prone to deformation, leading to larger surface settlements.

Interface R=1 Condition (High Stiffness Interface)

In this case, the settlement trough remains shallower, and the settlement magnitude decreases significantly. High stiffness limits soil deformations, thereby reducing surface settlements.

Without Interface Condition

In this scenario, the settlement profile generally falls between the R=0.01 and R=1 conditions. This indicates that even without explicitly defined stiffness, the soil-tunnel interaction affects the settlement profile.

Greenfield Conditions (Free Field)

The greenfield curve represents the expected free-field settlement values when the effect of the building is neglected. This profile serves as a reference to understand the impact of building stiffness and interface conditions and shows the lowest settlement values.

Effect of Tunnel Advancement on Settlement Profiles

The figures show that as tunnel advancement increases (from 93.1 m to 119.1 m), the maximum settlement values generally increase under all interface conditions, and the settlement trough slightly widens. The increase in settlement is particularly more pronounced in the R=0.01 condition as advancement progresses. This indicates that as excavation advances, cumulative increases in stresses and deformations in the soil are reflected in greater surface settlements.

These analyses clearly demonstrate that the tunnel-soil interface stiffness plays a critical role in circumferential settlements occurring during tunnel excavation. Low interface stiffness leads to deeper and wider settlement troughs, while high interface stiffness limits the amount of settlement and reduces adverse effects on the surface. These findings highlight the importance of accurately modeling soil-structure interaction and carefully defining interface parameters in tunnel design and construction.

7.2. The Effect of Tunnel-Soil Interface Stiffness on Longitudinal Displacements

In this section, longitudinal settlement values occurring along the central axis of the building during tunnel excavation were examined. The analyses were conducted under four different scenarios: Greenfield condition (soil without the building), a model without an interface, a perfectly bonded model (R=1), and a weakened interface model (R=0.01). The obtained vertical displacement values were measured at certain stages of tunnel advancement (52.6 m – 98.5 m) and compared graphically (Figure 7.4–7.13.).

Interface elements are important structural components used in finite element method-based software such as PLAXIS to model interactions like relative sliding and opening/closing between structural elements and the soil. The stiffness of these interfaces is generally expressed by an interface reduction factor, R_{inter} , defined relative to the soil stiffness (Brinkgreve et al., 2023).

7.2.1. Effect of interface stiffness on displacements

- R_{inter}=1 represents a scenario of perfect bonding between the tunnel and the soil, where no relative movement occurs. In this case, soil deformations are significantly limited by the tunnel lining, resulting in lower displacement values (Addenbrooke and Potts, 2001).
- The no-interface model in PLAXIS behaves like a perfectly rigid bond by default when no connection is defined between two elements. This scenario produces results similar to the R_{inter}=1 case and represents conditions where a weak connection at the interface is not modeled (Brinkgreve et al., 2023).

• R_{inter}= 0.01 represents a very low-stiffness interface. In this scenario, shear and normal stress transfer between the tunnel and soil is minimized, allowing for nearly free deformation of the soil around the tunnel, and resulting in maximum settlements (Bobet and Einstein, 2023).

7.2.2. Numerical findings and interpretation

Analyses showed that displacement values increased in all scenarios as the excavation progressed, but the highest settlements occurred in the R_{inter} =0.01 scenario. Especially when the tunnel began to approach beneath the building (between 73 m and 98.5 m), a significant increase in deformations was observed. The main reasons for this include:

• **Weak Stress Transfer:** The low R_{inter} value hindered effective stress transfer between the soil and tunnel, causing loosening and settlements in the soil surrounding the tunnel (Brinkgreve et al., 2023; Bobet and Einstein, 2023).

• **Increased Relative Movement:** Allowing relative movement between the soil and tunnel in the R_{inter}=0.01 scenario led to larger settlement troughs around the tunnel (Potts and Zdravkovic, 2001).

• **Insufficient Support:** Due to insufficient support from the tunnel lining, deformations were concentrated especially at the tunnel crown and sidewalls (Addenbrooke and Potts, 2001).

7.2.3. Is R=0.01 realistic?

According to studies in the literature, an $\mathrm{R_{inter}}$=0.01 value represents an extremely conservative condition and is generally not considered realistic for engineering practice. The default value in PLAXIS is R_{inter} =1.0, which represents perfect bonding. In practice, some relative movement between the soil and structure is usually expected, so a value between 0.5–0.7 is often recommended for engineering calculations (Brinkgreve et al., 2023).

R=0.01 represents a frictionless, unbonded interface. This value is typically used in sensitivity analyses or worst-case scenario simulations to determine the maximum possible deformations (Bobet and Einstein, 2023). Such low-friction interface conditions are rarely encountered in actual field conditions.

The analyses conducted in this thesis show that the R_{inter} =0.01 scenario was used as an upper-bound settlement estimate. This allowed for a detailed investigation of the effect of interface stiffness on longitudinal displacements and provided valuable data on the model's behavior.

7.2.4. Recommendation and evaluation

These comparative analyses demonstrated that the value of interface stiffness significantly affects surface settlements in the modeled system. Particularly as excavation progresses, differences in deformations increase, and compared to the greenfield scenario, the presence of the building limits deformations.

Therefore, the R_{inter} =0.01 scenario should only be considered as a boundary condition (upper-bound). For realistic engineering calculations, the appropriate R value should be determined by considering parameters such as field data, tunnel lining properties, and construction methods (Potts and Zdravkovic, 2001).

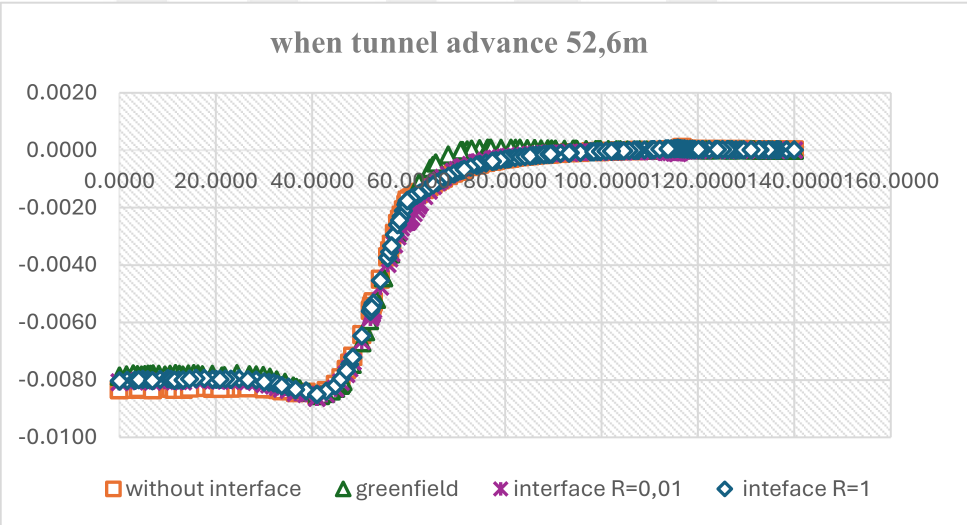

Figure 7.4. *Longitudinal settlement when tunnel advance is 52.6 m*

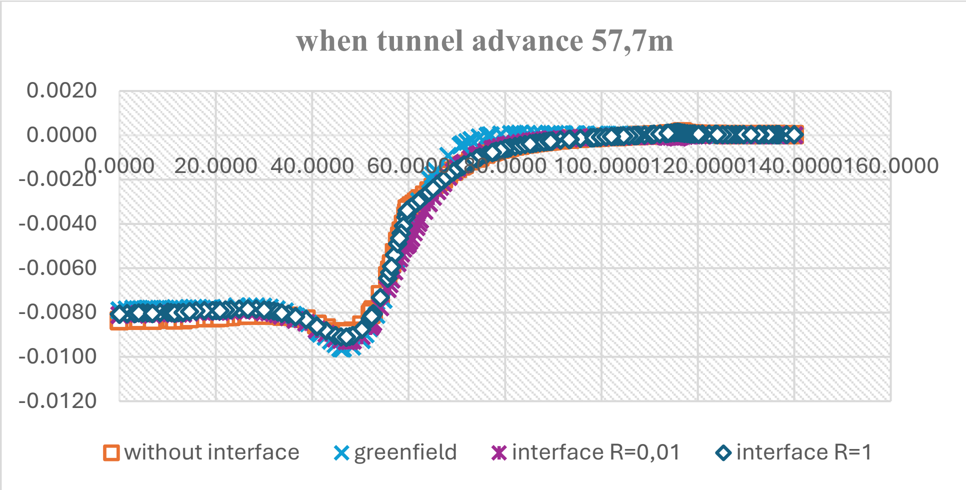

Figure 7.5. *Longitudinal settlement when tunnel advance is 57.7 m*

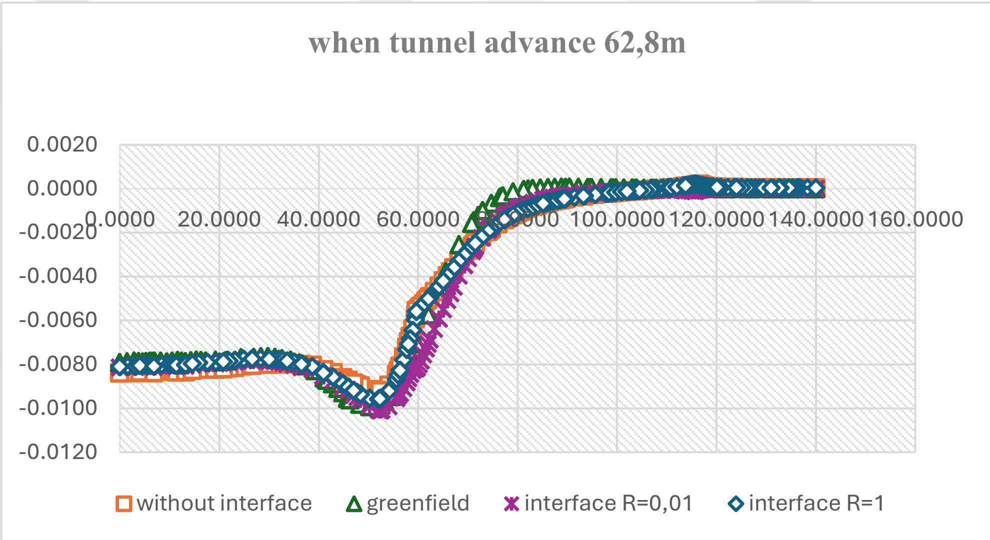

Figure 7.6. *Longitudinal settlement when tunnel advances is 62.8 m*

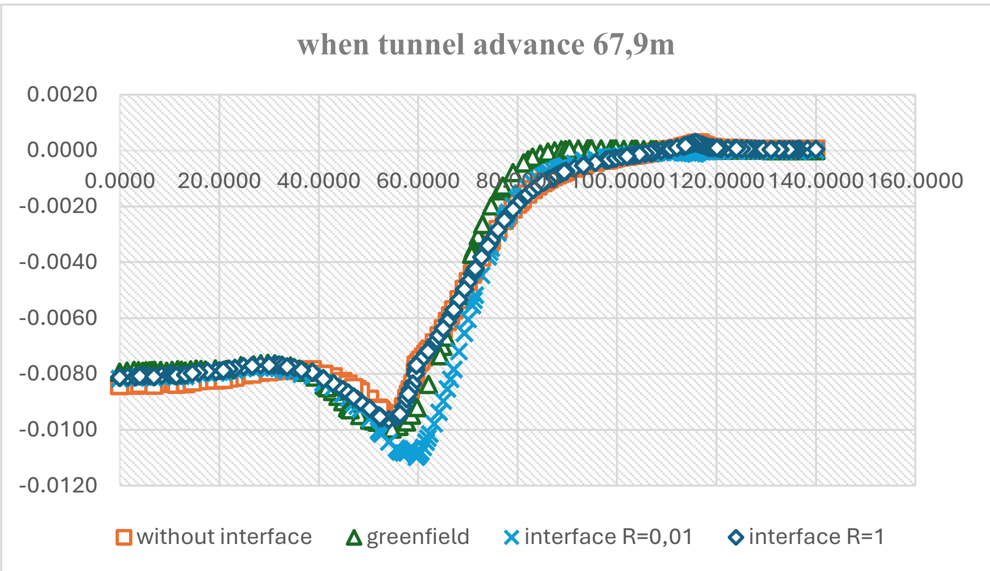

Figure 7.7. *Longitudinal settlement when tunnel advances is 67.9 m*

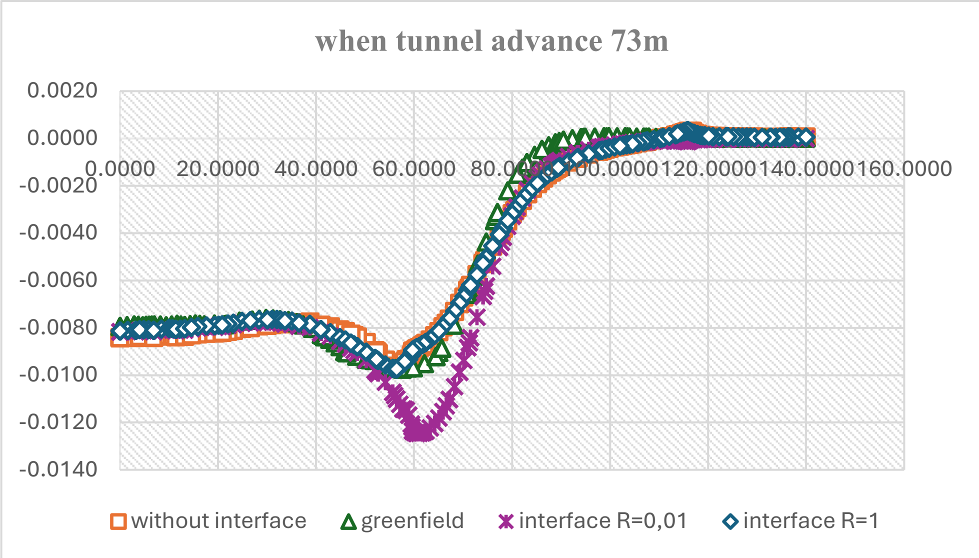

Figure 7.8. *Longitudinal settlement when tunnel advances is 73.0 m*

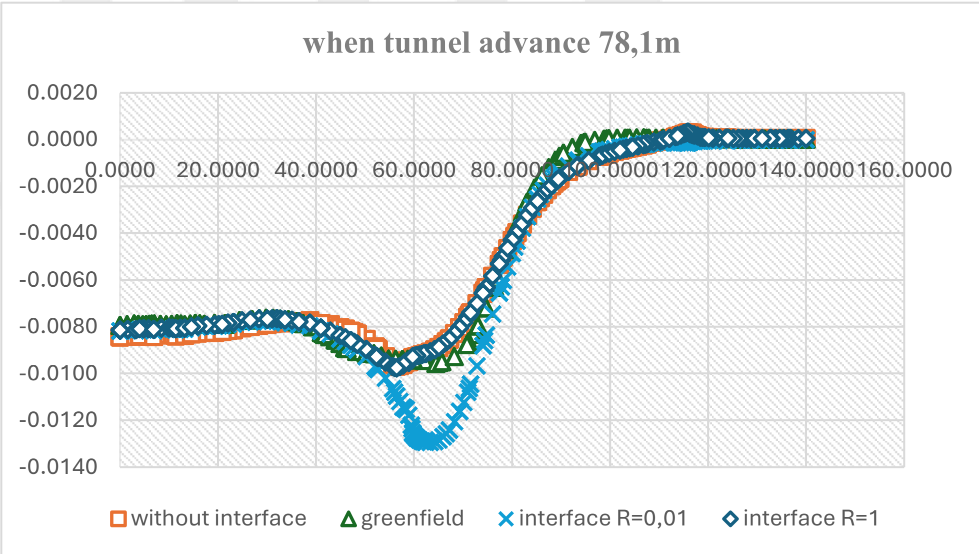

Figure 7.9. *Longitudinal settlement when tunnel advance is 78.1 m*

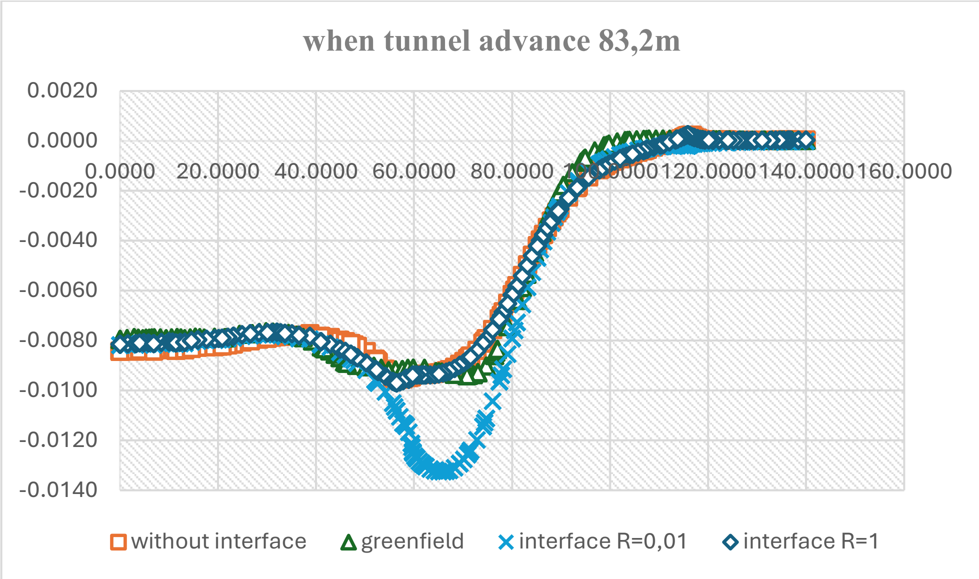

Figure 7.10. *Longitudinal settlement when tunnel advances is 83.2 m*

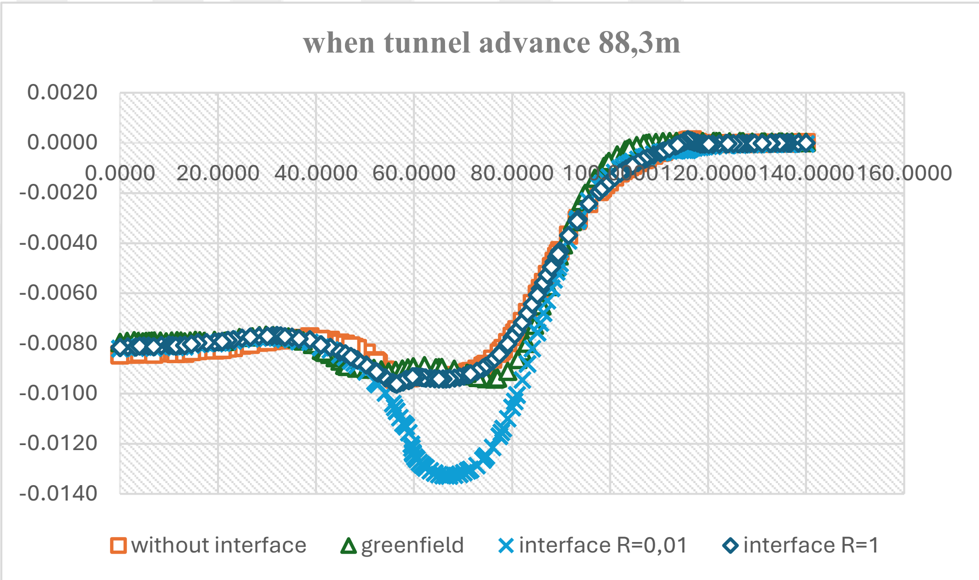

Figure 7.11. *Longitudinal settlement when tunnel advances is 88.3 m*

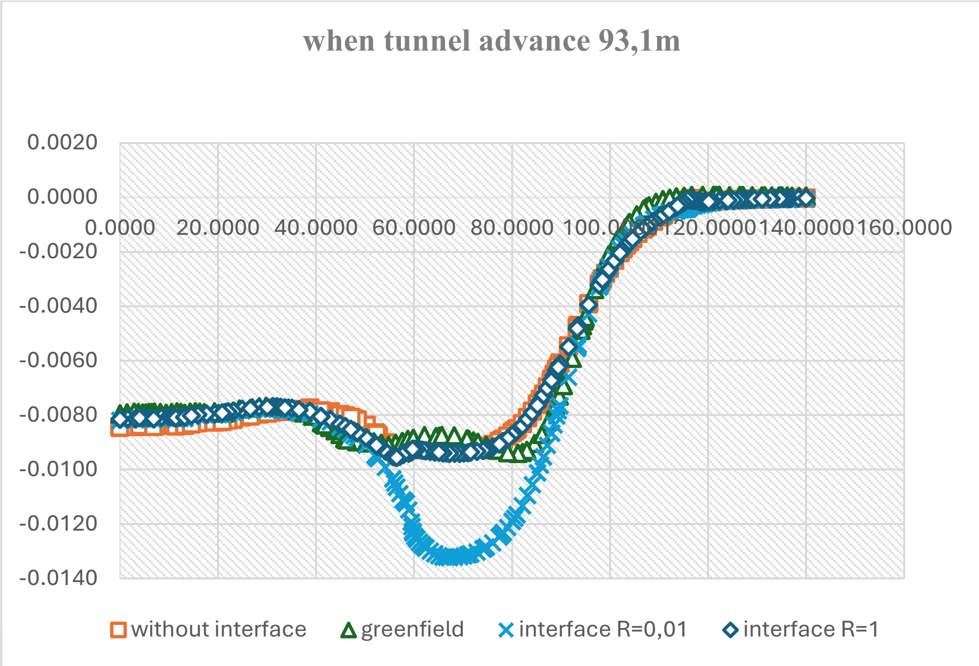

Figure 7.12. *Longitudinal settlement when tunnel advance is 93.1 m*

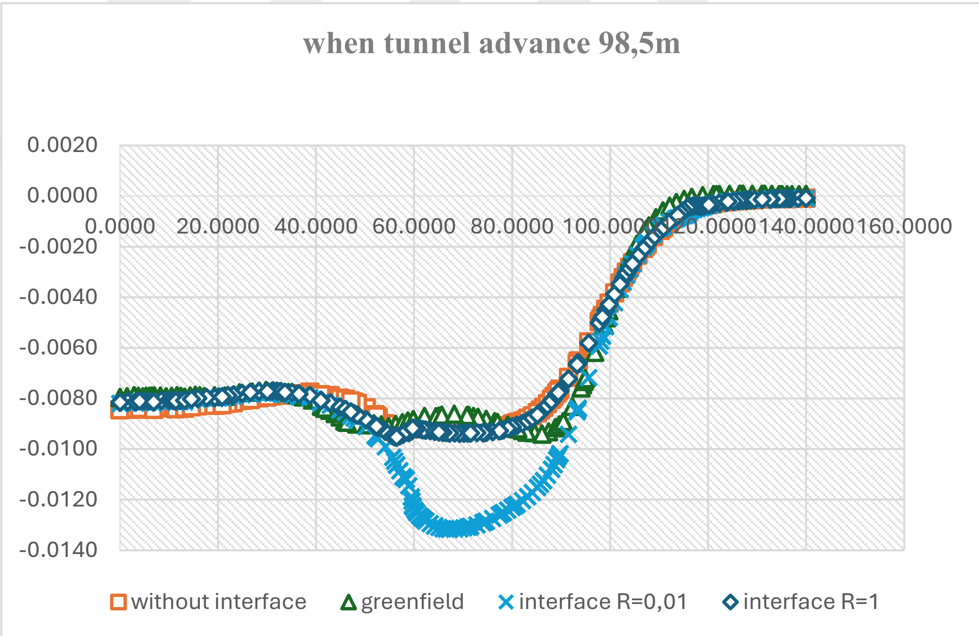

Figure 7.13. *Longitudinal settlement when tunnel advances is 98.5 m*

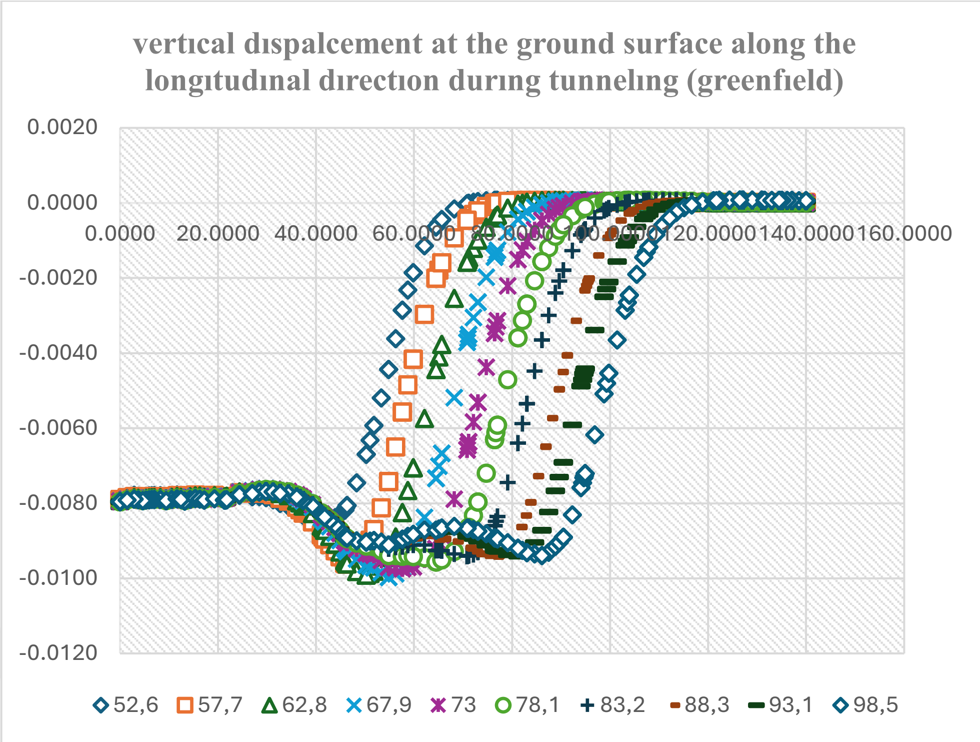

Figure 7.14. *Longitudinal vertical displacement profiles on the ground surface during tunnel excavation (Greenfield condition)*

In Figure 7.14, the vertical displacement (settlement) profiles for the "Greenfield" condition, which includes only the effect of tunnel excavation without any structural influence, are presented. The graph was created using data obtained at different stages of tunnel advancement (52.6 m – 98.5 m). The largest displacements occurred directly above the tunnel axis, with the distribution of deformations widening horizontally and gradually increasing through the near-surface soil mass as the tunnel advanced.

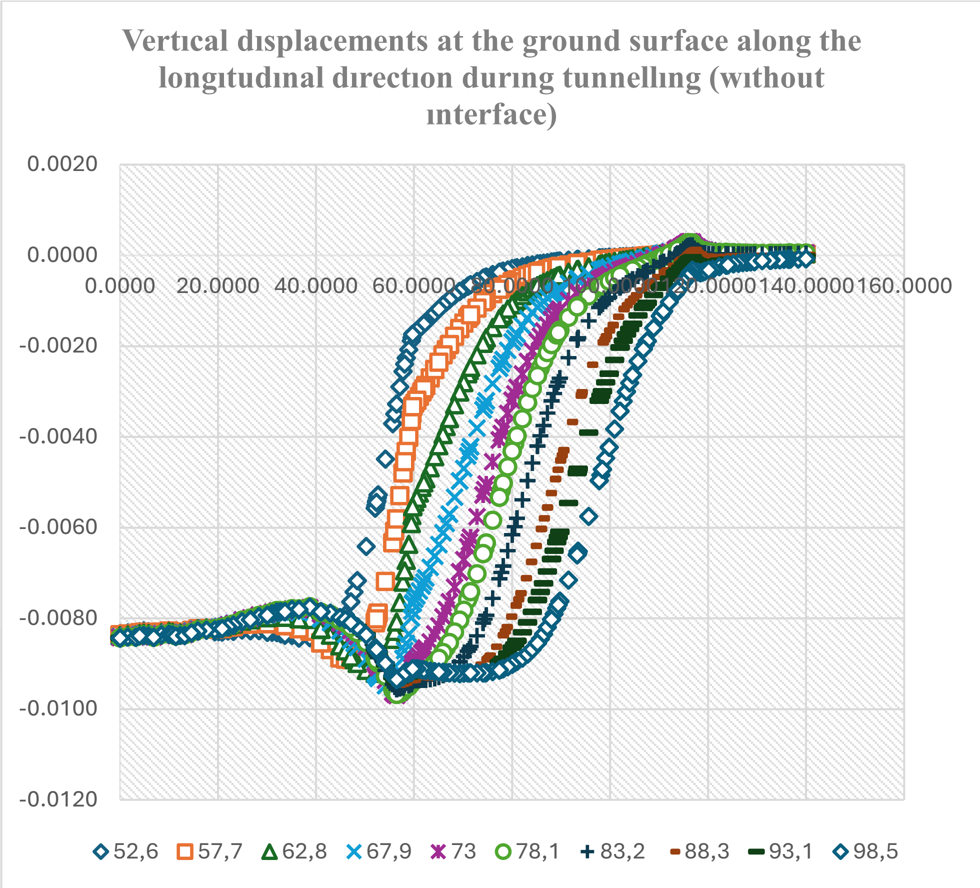

Figure 7.15. *Vertical displacement profiles on the surface during tunnel excavation in the model without an interface (No Interface)*

The figure shows the vertical displacement distributions in the model where no tunnel-soil interface was defined. Settlements occurring on the ground surface during tunnel advancement developed more freely compared to the model with an interface stiffness value of R=1. In the no-interface case, the model assumes full bonding around the tunnel with the soil, resulting in settlement profiles that exhibit similar trends and, in some excavation stages, produce results comparable to those of the R=1 model.

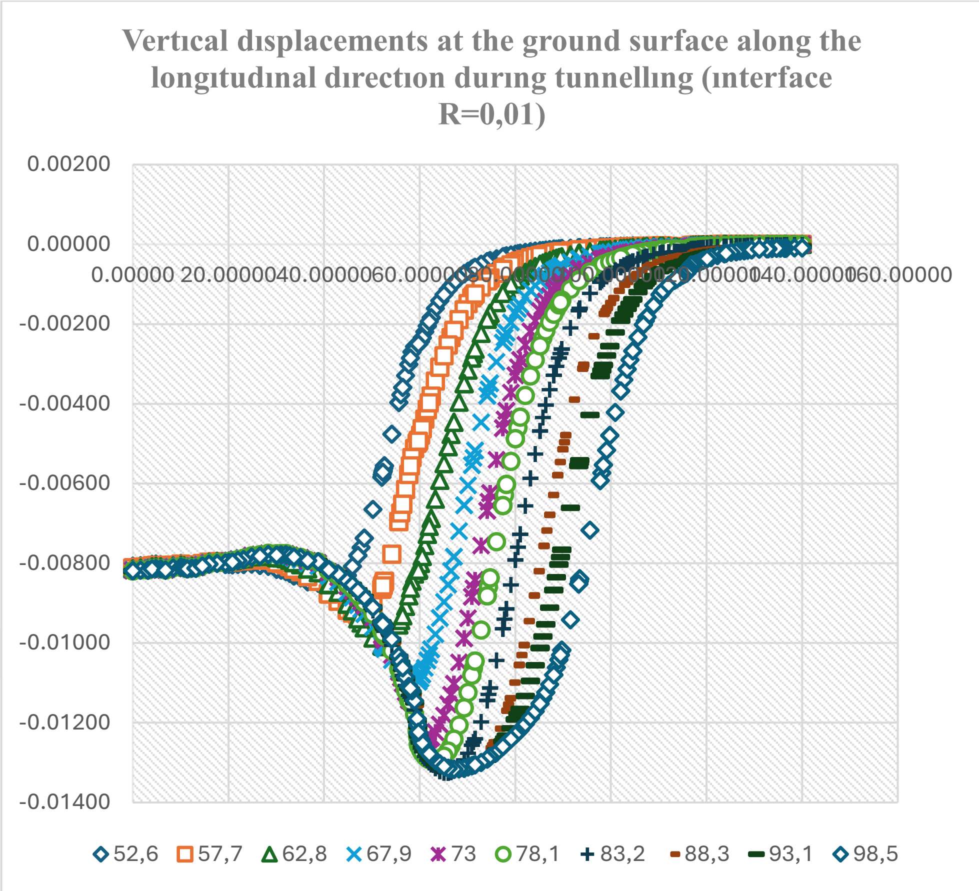

Figure 7.16. *Vertical displacement profiles on the surface during tunnel excavation in the model with interface R=0.01*

This graph shows the vertical displacements on the surface when the tunnel-soil interface stiffness factor is defined as R=0.01. Such a very low stiffness value indicates poor bonding between the tunnel structure and the surrounding soil. Consequently, the tunnel-soil interaction weakened, and displacements increased significantly compared to the Greenfield and R=1 conditions. The maximum settlement values observed, especially above the tunnel crown and beneath the building, highlight the impact of low-stiffness interfaces on deformations. This scenario represents the worst-case condition in terms of displacements.

7.3. Effect of Tunnel-Soil Interface Stiffness on Building Behavior: ΔN and Δuz Analysis

For reliably assessing the effects of tunnel excavation on buildings, it is critically important to carefully define the interaction parameters between the tunnel and the soil. In this context, the interface stiffness parameter plays a key role. In this study carried out using PLAXIS 3D software, analyses were performed on a case study of the Naples Metro Line by assigning two different values for the tunnel-soil interface stiffness: R=1 and R=0.01.

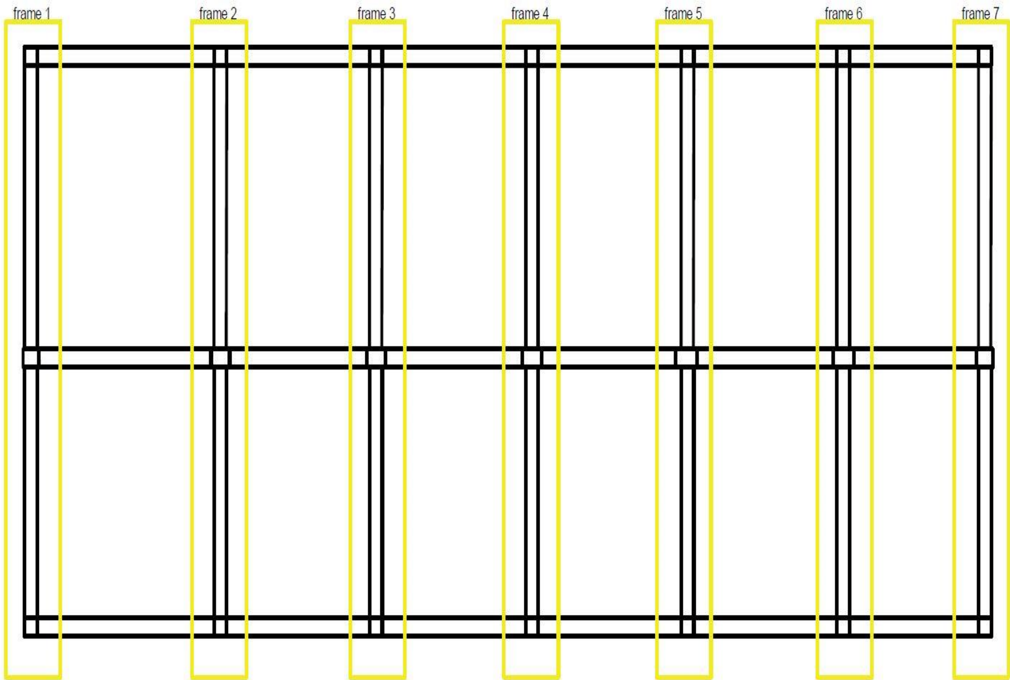

Figure 7.17. *View of the seven-frame building model analyzed under the influence of the tunnel.*

As stated in the PLAXIS user manual (PLAXIS, 2023), an R=1 value represents a fully bonded interaction between the tunnel and the soil, while an R=0.01 value simulates a weak bond condition characterized by significant friction and separation behavior between the soil and the tunnel. Each of these values was used to determine their impact on the vertical displacement (Δuz) and axial force (ΔN) changes in the building.

As part of the analyses, ΔN–Δuz relationship figures were obtained separately for each frame of the structural system consisting of seven frames (Figure 7.17.).

First, the results obtained with an interface value of R=0.01 were evaluated. In the figures obtained for each frame (Figure 7.18 – 7.24), a general trend of decreasing axial forces with increasing vertical displacement was observed. This indicates that the settlement effects occurring during tunnel excavation have a reducing effect on the axial loads of the structure. A collective presentation of the data for all frames is provided in Figure 7.24. This scenario shows that allowing the soil to deform more freely around the tunnel limits the force interaction on the building.

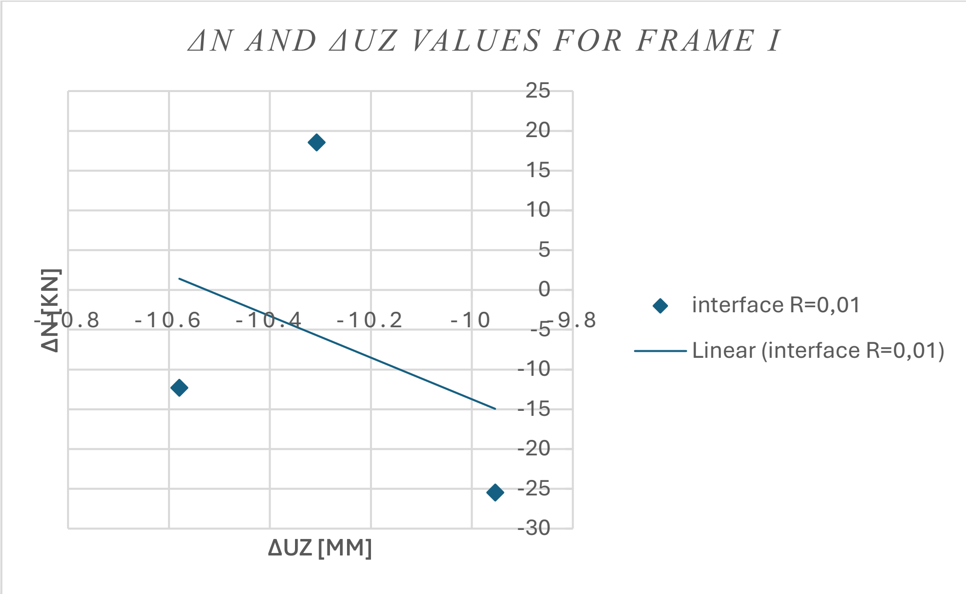

Figure 7.18. *ΔN–Δuz graphical representation for Frame 1 with interface stiffness R=0.01*

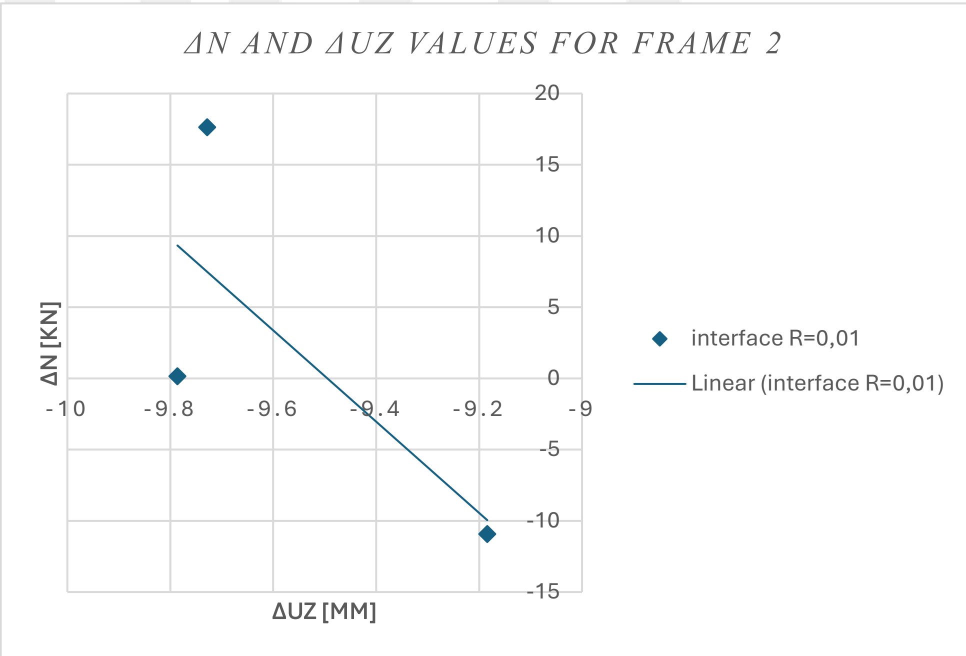

Figure 7.19. *ΔN–Δuz graphical representation for Frame 2 with interface stiffness R=0.01*

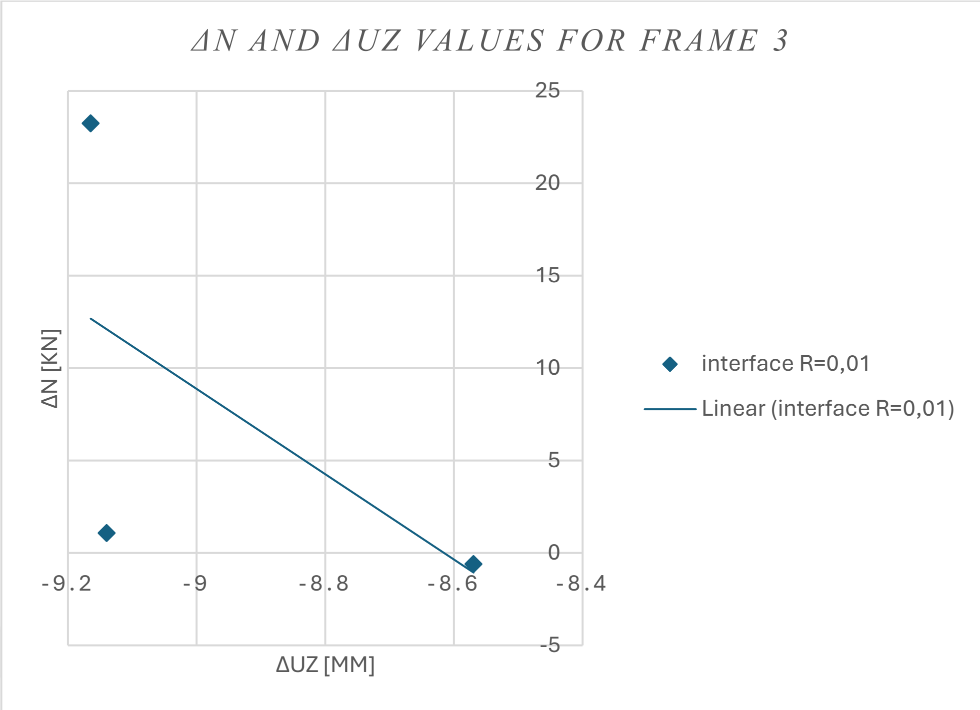

Figure 7.20. *ΔN–Δuz graphical representation for Frame 3 with interface stiffness R=0.01*

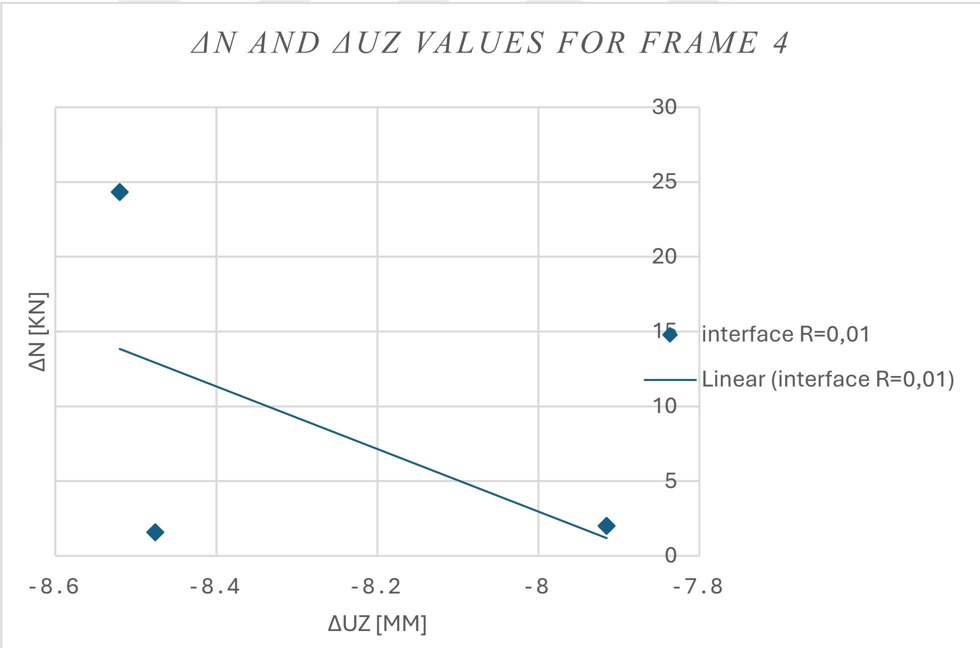

Figure 7.21. *ΔN–Δuz graphical representation for Frame 4 with interface stiffness R=0.01*

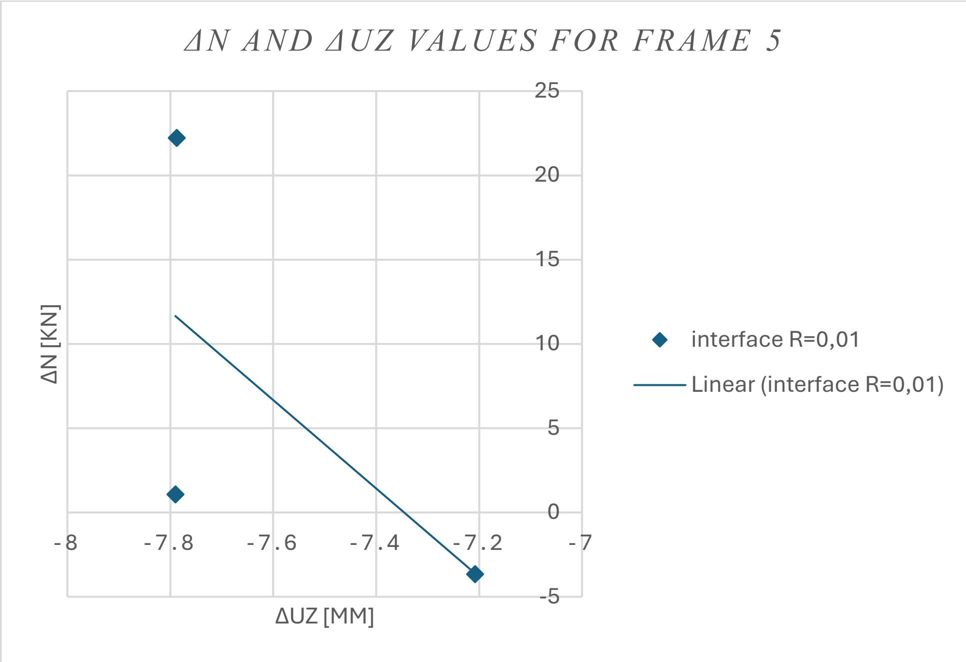

Figure 7.22. *ΔN–Δuz graphical representation for Frame 5 with interface stiffness R=0.01*

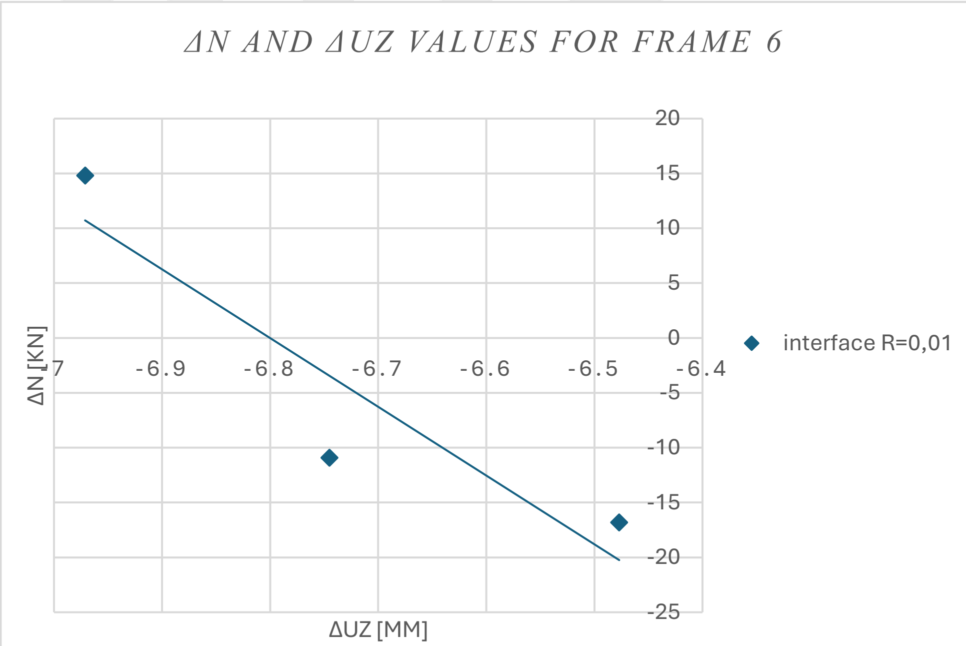

Figure 7.23. *ΔN–Δuz graphical representation for Frame 6 with interface stiffness R=0.01*

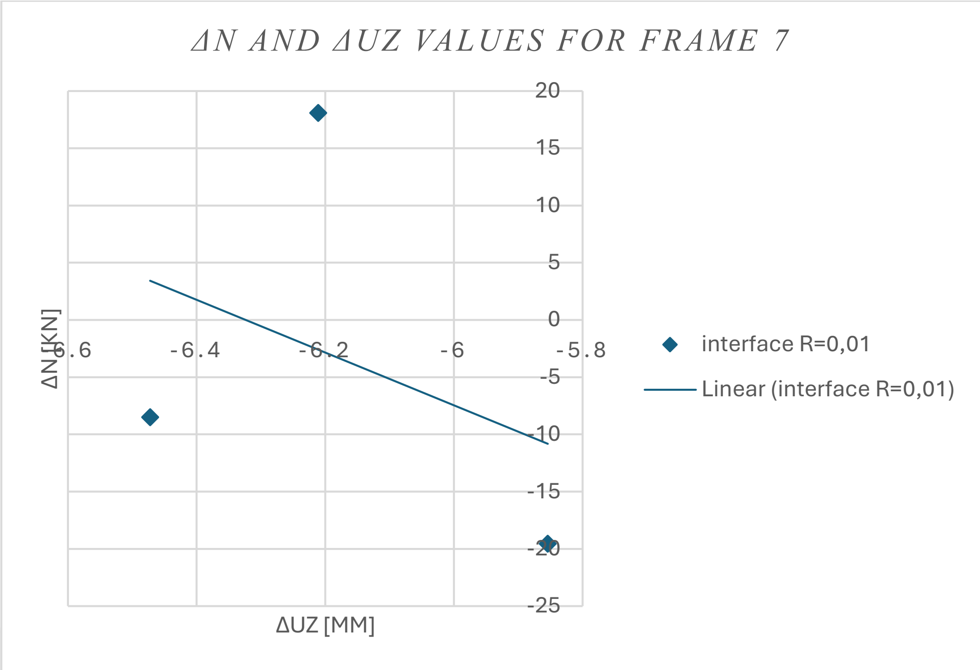

Figure 7.24. *ΔN–Δuz graphical representation for Frame 7 with interface stiffness R=0.01*

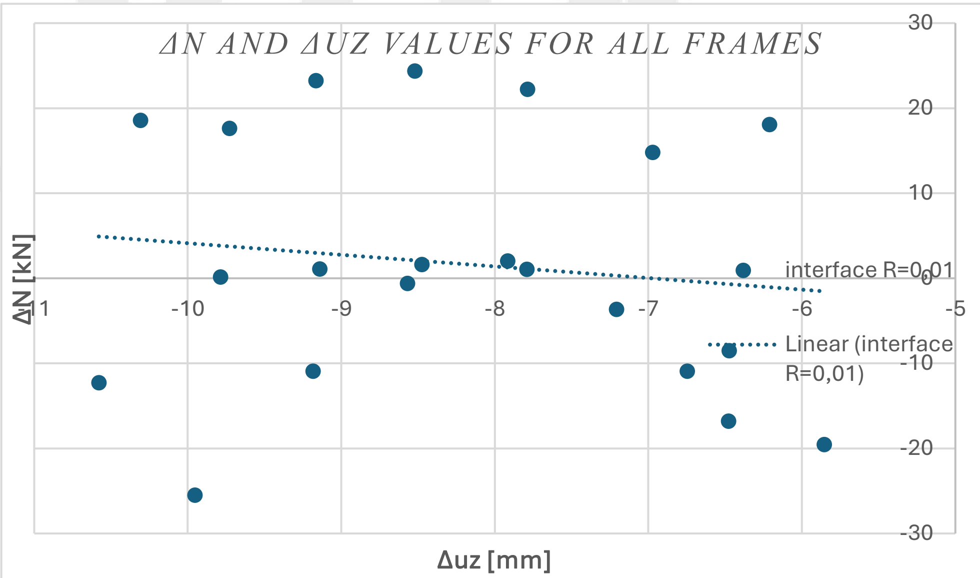

Figure 7.25. *ΔN–Δuz distribution for all frames with interface stiffness R=0.01*

For the same structural system, the analyses were repeated this time with an interface value of R=1. In the obtained Figures (Figure 7.26 – 7.32), larger axial force changes and displacement magnitudes were observed. This indicates that when the tunnel is modeled as fully bonded with the soil, the building responds more rigidly to soil movements, resulting in greater stress on the structure. It is particularly noteworthy that in the central frames (Frames 3, 4, and 5), ΔN values exceeded 200 kN (Figure 7.30. - Figure 7.31.).

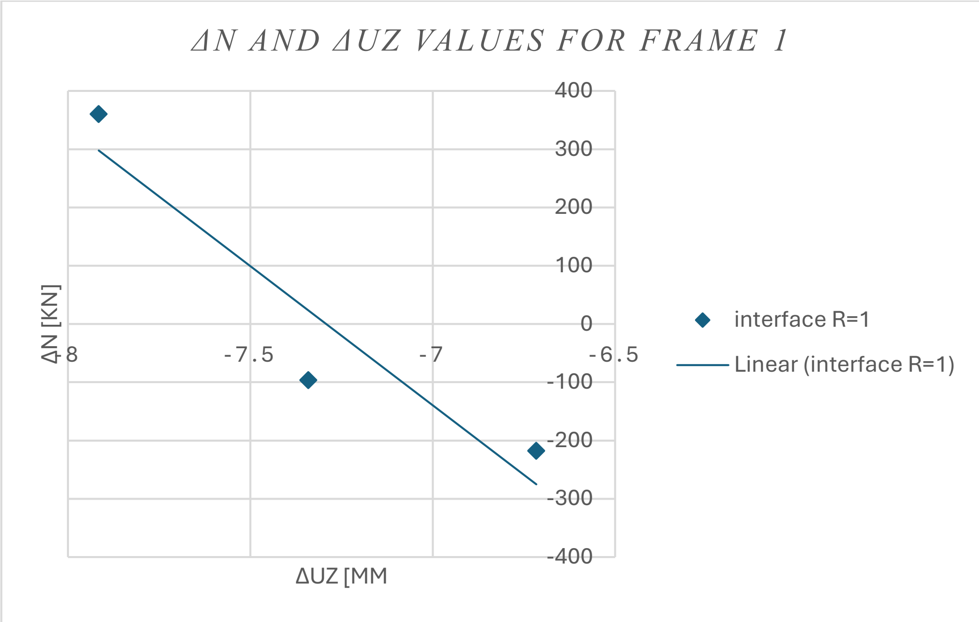

Figure 7.26. *ΔN–Δuz graphical representation for Frame 1 with interface stiffness R=1*

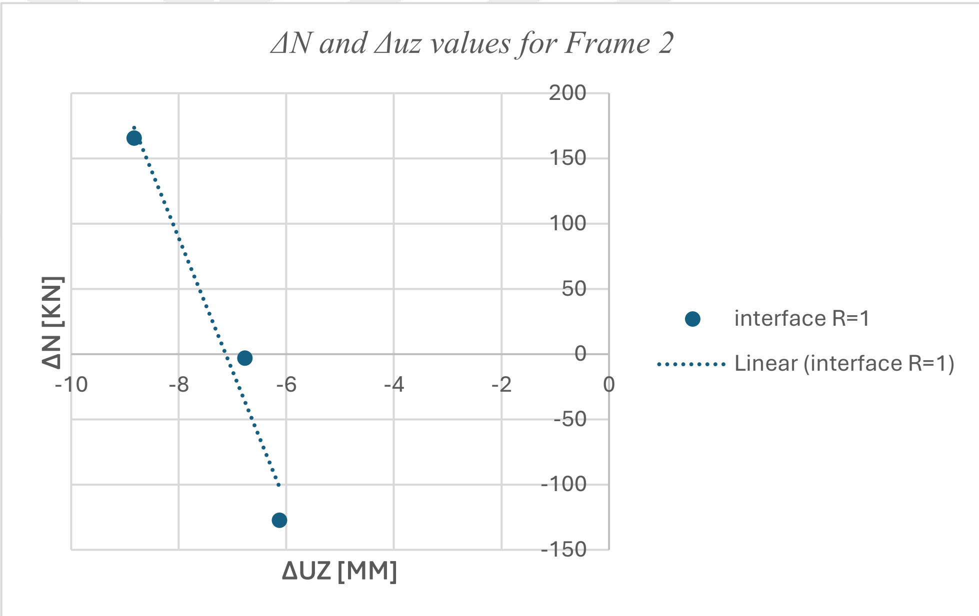

Figure 7.27. *ΔN–Δuz graphical representation for Frame 2 with interface stiffness R=1*

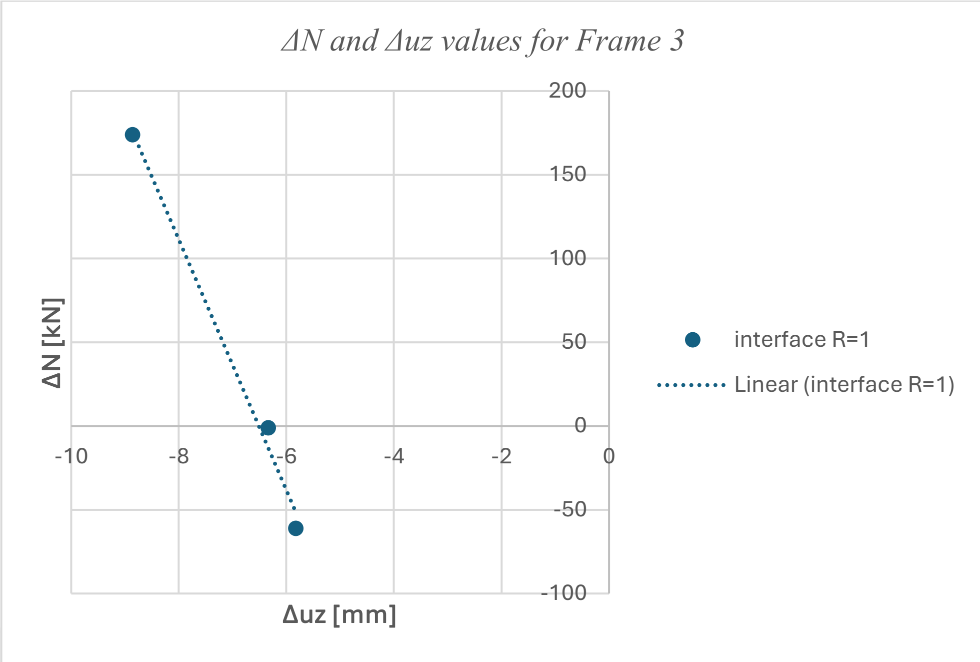

Figure 7.28. *ΔN–Δuz graphical representation for Frame 3 with interface stiffness R=1*

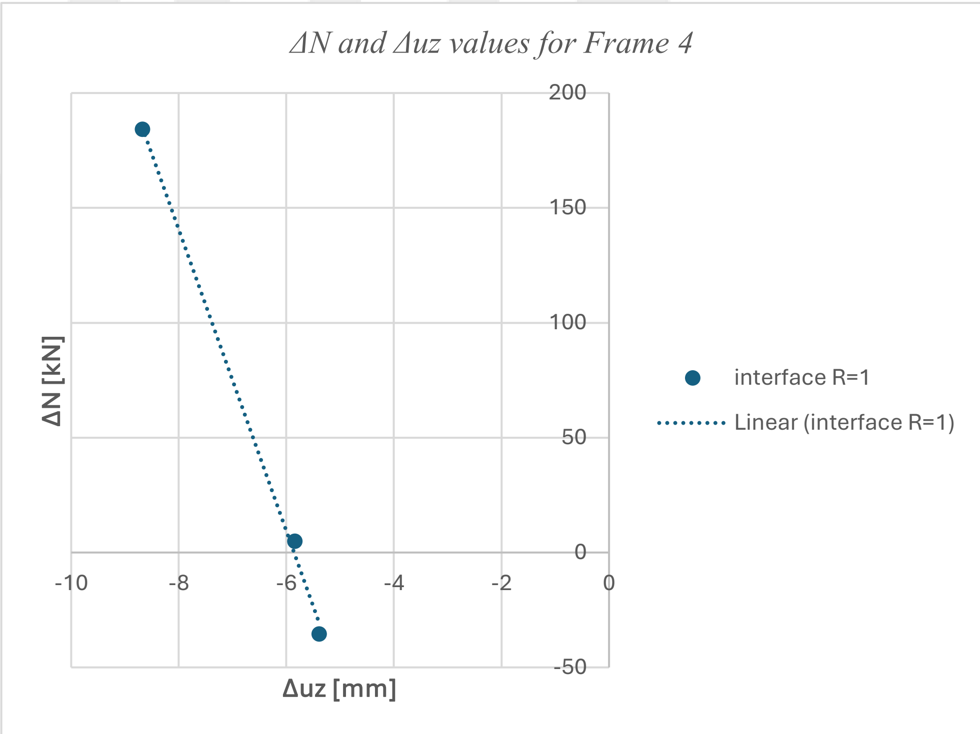

Figure 7.29. *ΔN–Δuz graphical representation for Frame 4 with interface stiffness R=1*

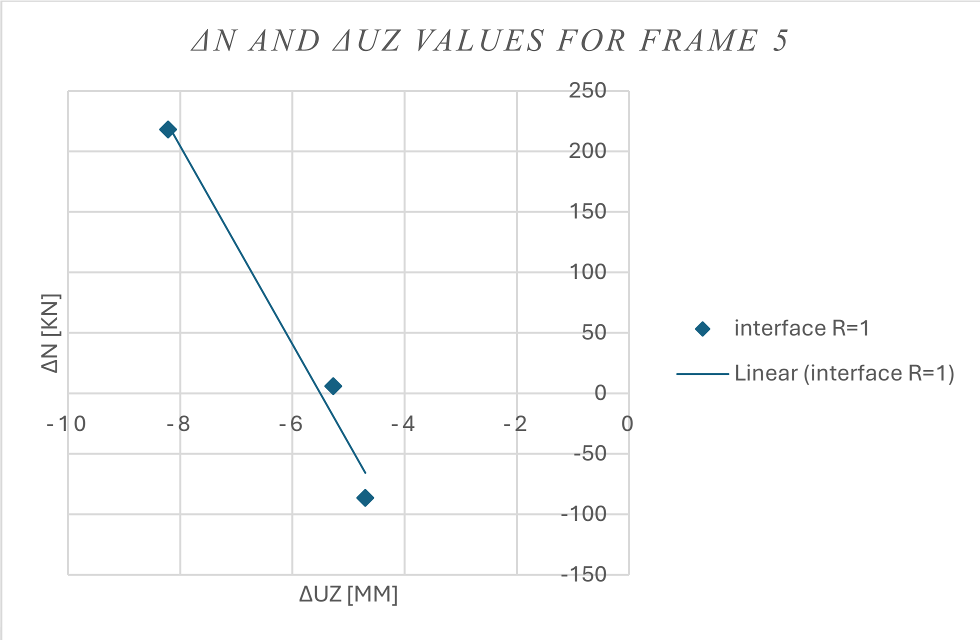

Figure 7.30. *ΔN–Δuz graphical representation for Frame 5 with interface stiffness R=1*

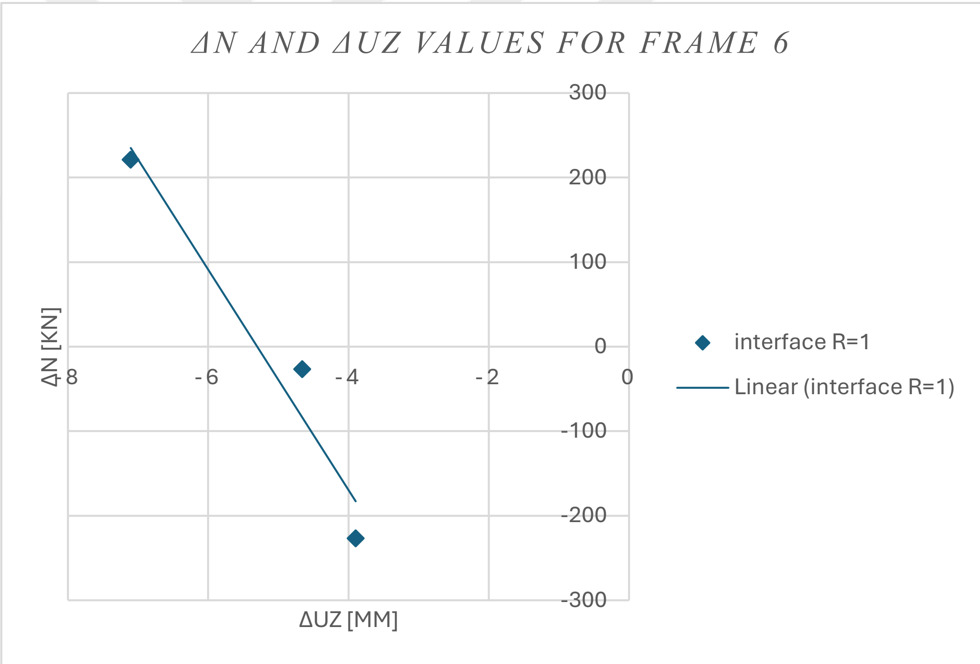

Figure 7.31. *ΔN–Δuz graphical representation for Frame 6 with interface stiffness R=1*

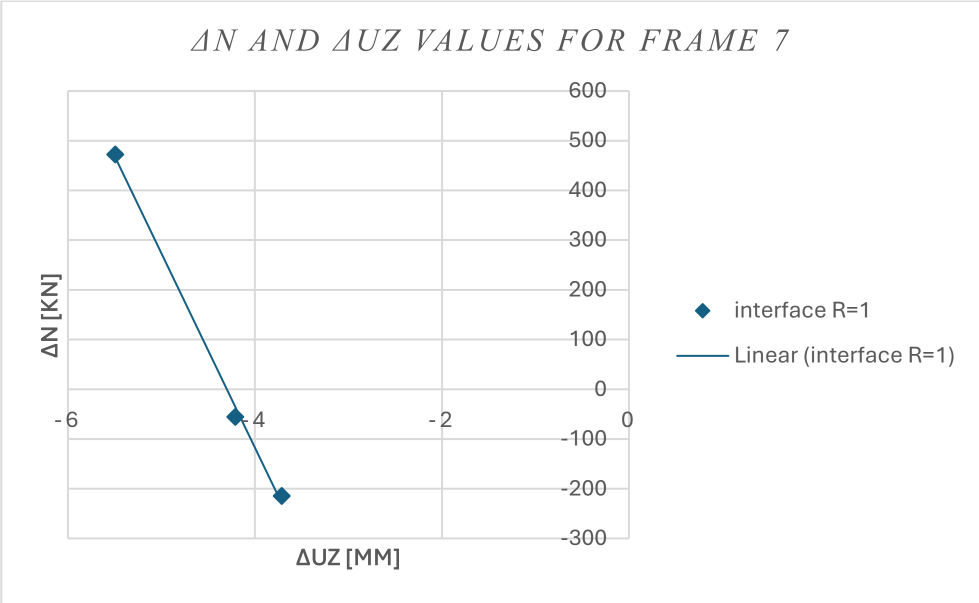

Figure 7.32. *ΔN–Δuz graphical representation for Frame 7 with interface stiffness R=1*

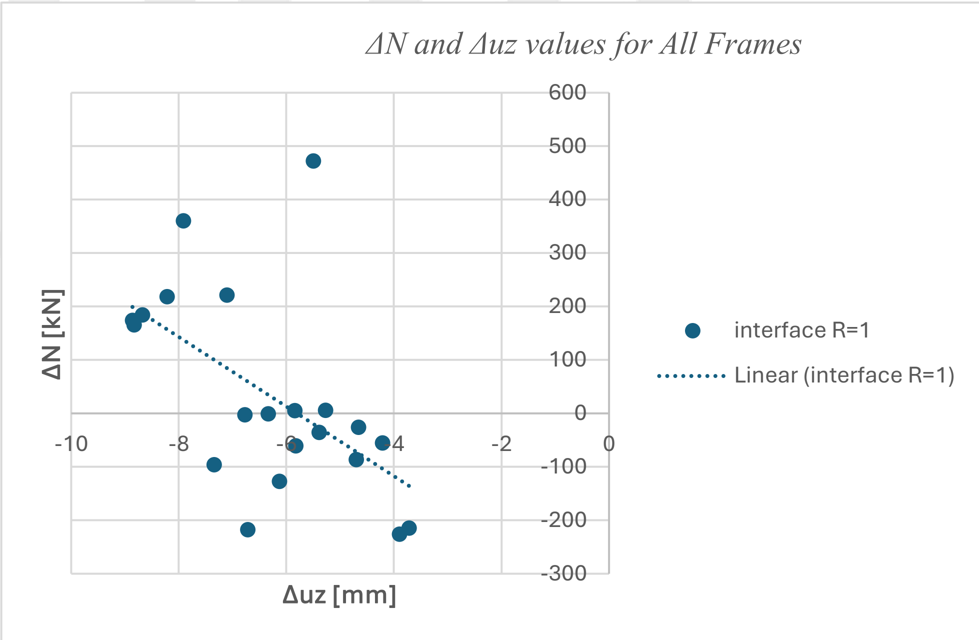

Figure 7.33. *ΔN–Δuz distribution for all frames with interface stiffness R=1*

Finally, all results obtained on a frame-by-frame basis for the two different interface stiffness values are presented comparatively in Figures 5.28 – 5.35. In these Figures, the ΔN–Δuz relationships for both cases are shown on the same plane. According to the findings, in the weak interface scenario modeled with R=0.01, lower axial force changes occur in the building, and the deformation effects remain more limited. This indicates that tunnels with low interaction with the soil (e.g., systems with gaps between the lining and soil) may lead to less force transfer to structures due to reduced stiffness transmission (Bilotta et al., 2022; Celentano, 2023). In other words, a weak interface allows the building to be partially "isolated" from ground movements, thereby reducing structural stresses.

These results clearly show that careful selection of the interface stiffness value in building-tunnel interaction analyses is critical for ensuring structural safety and prediction accuracy.

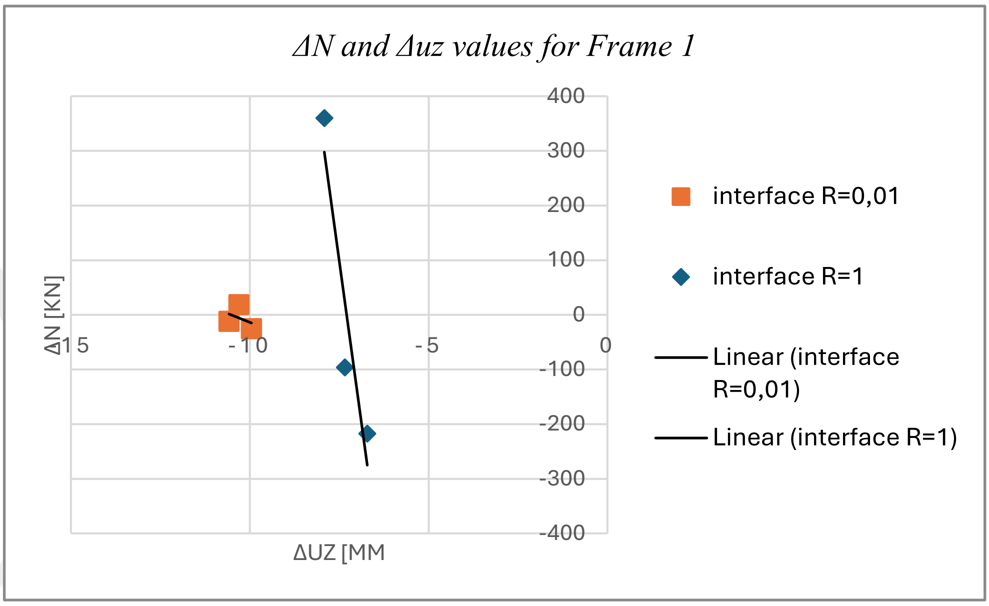

Figure 7.34. *Comparative ΔN–Δuz graphical representation for both stiffness values (Frame 1)*

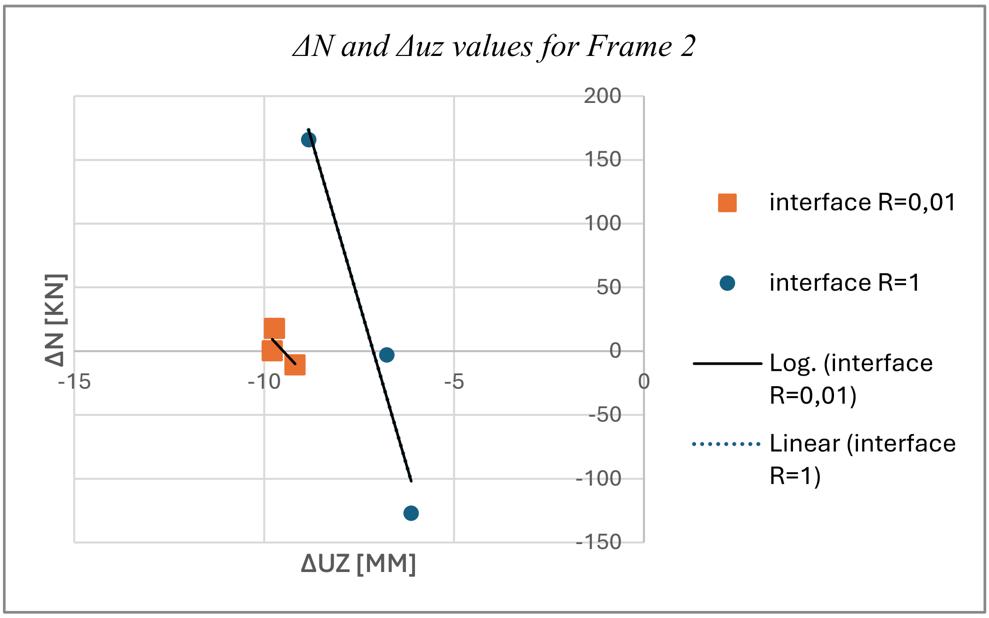

Figure 7.35. *Comparative ΔN–Δuz graphical representation for both stiffness values (Frame 2)*

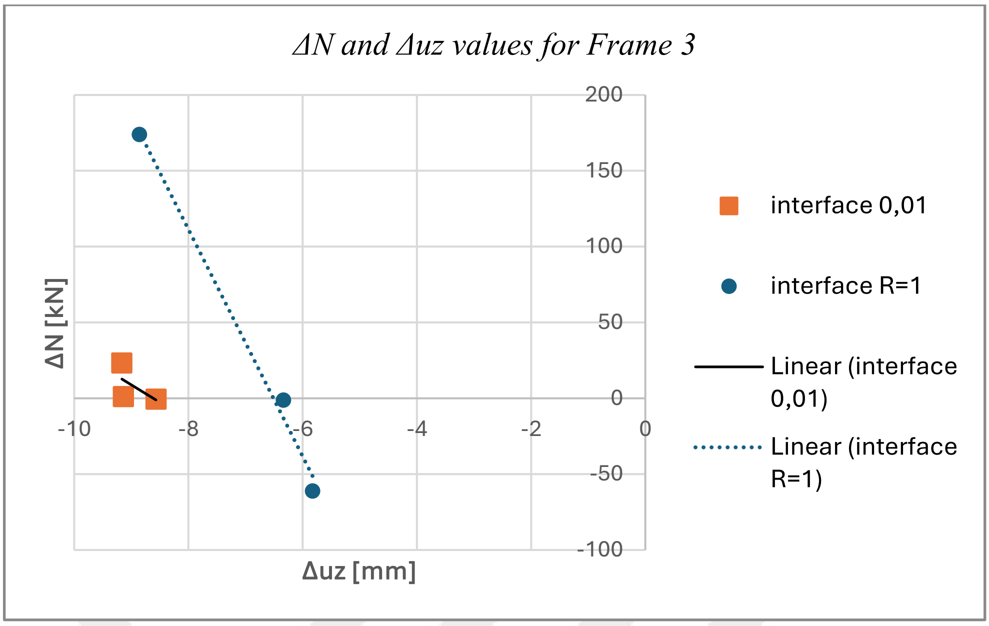

Figure 7.36. *Comparative ΔN–Δuz graphical representation for both stiffness values (Frame 3)*

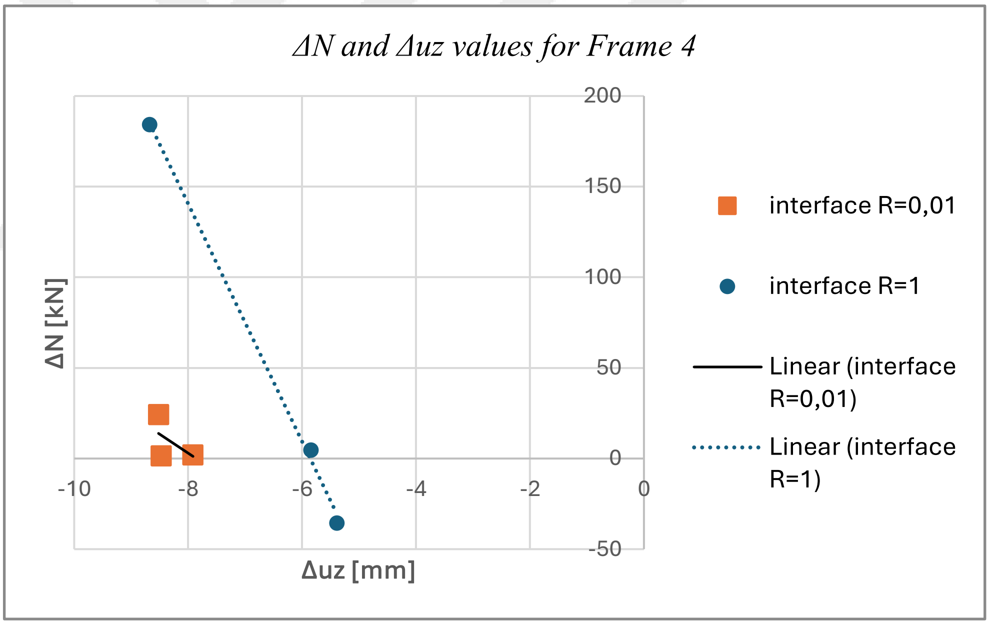

Figure 7.37. *Comparative ΔN–Δuz graphical representation for both stiffness values (Frame 4)*

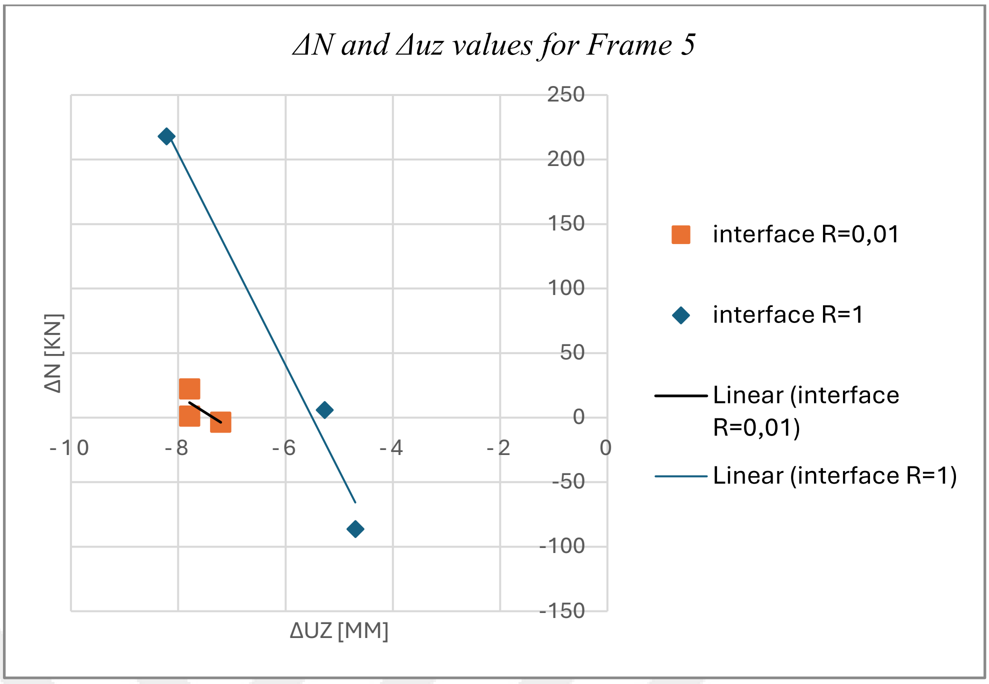

Figure 7.38. *Comparative ΔN–Δuz graphical representation for both stiffness values (Frame 5)*

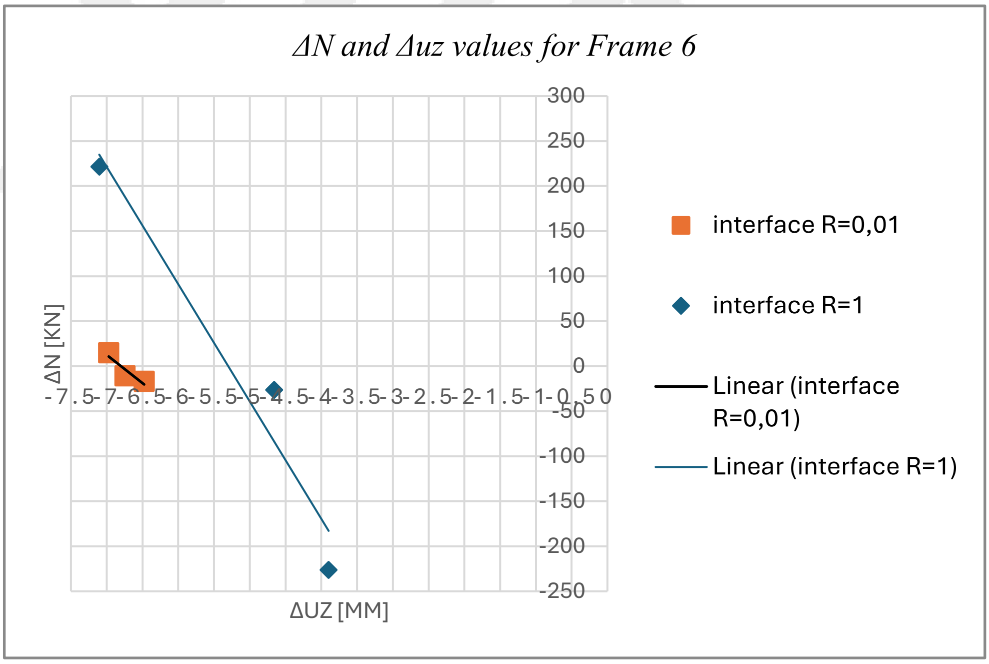

Figure 7.39. *Comparative ΔN–Δuz graphical representation for both stiffness values (Frame 6)*

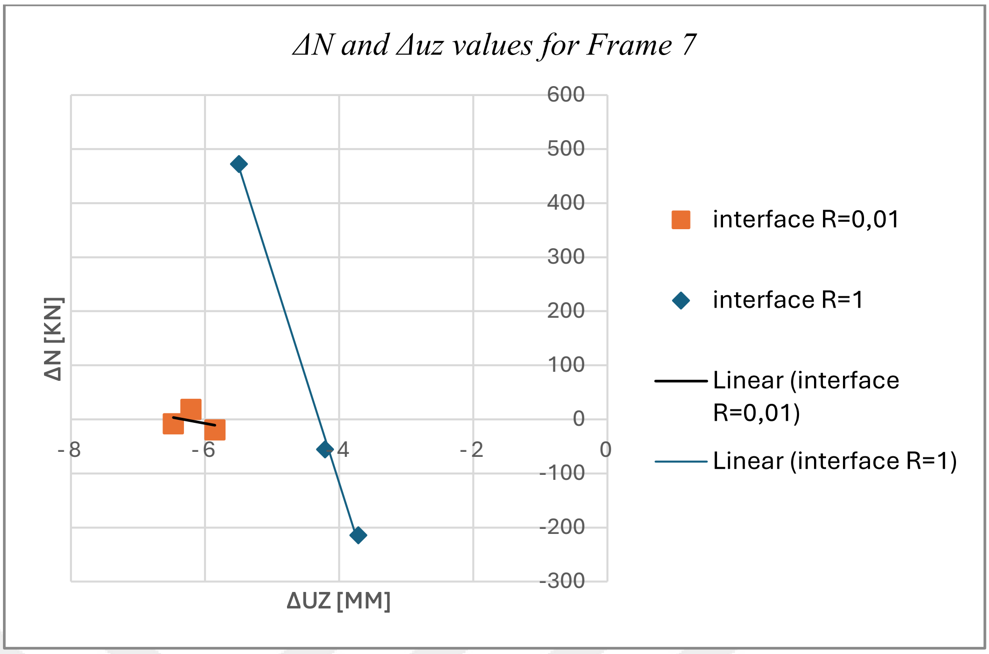

Figure 7.40. *Comparative ΔN–Δuz graphical representation for both stiffness values (Frame 7)*

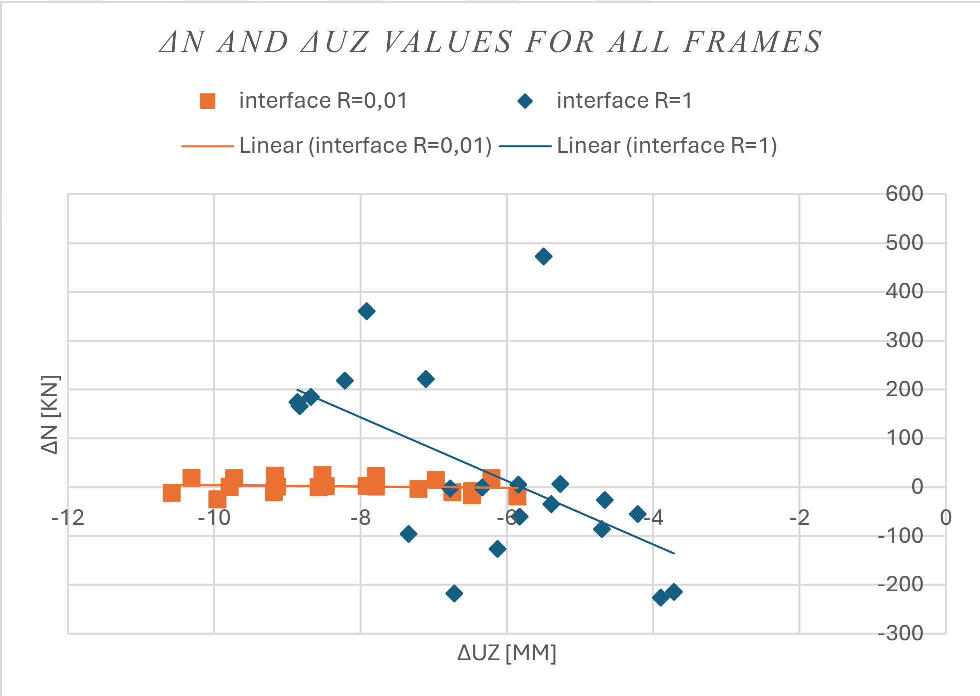

Figure 7.41. *Comparative ΔN–Δuz distribution for all frames for both interface values*

7.4. Changes in Internal Stresses of Column Elements During Excavation

In this section, the changes in bending moments (My and Mx) in the column elements of the building's structural system during tunnel advancement were examined in detail. In particular, the effect of the tunnel-soil interface stiffness reduction factor (Rinter) on these changes was comparatively evaluated through columns located at specific coordinates in the building. The local axes and internal force representations for the column elements are provided in Figure 7.42. The analyses were conducted for columns located at coordinates y=60.20, x=45.7 and y=89.30, x=45.7.

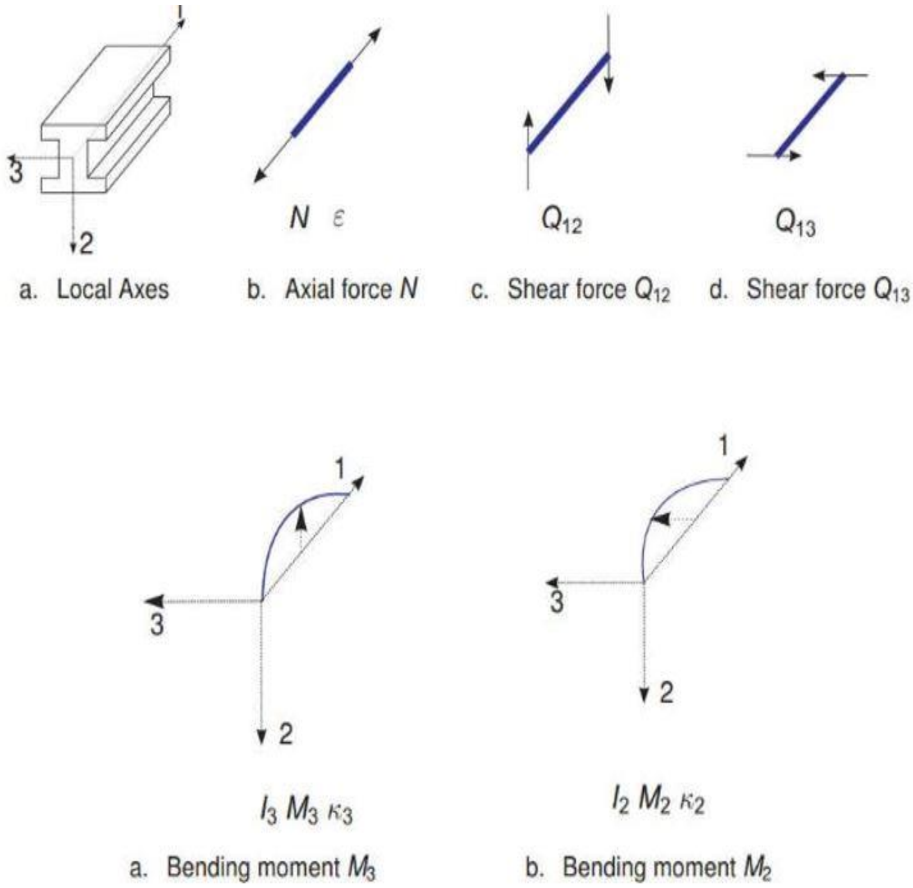

Figure 7.42. *Local axes and internal force representations for column elements. (Adapted from PLAXIS 3D Material Models Manual, 2023).*

7.4.1. Changes in internal forces for the column element at Y=60.20, X=45.7

For the column element at this location, the My (bending moment around the local 2-axis) and Mx (bending moment around the local 3-axis) values were compared for different interface stiffness values (R=1 and R=0.01) depending on the stages of tunnel excavation.

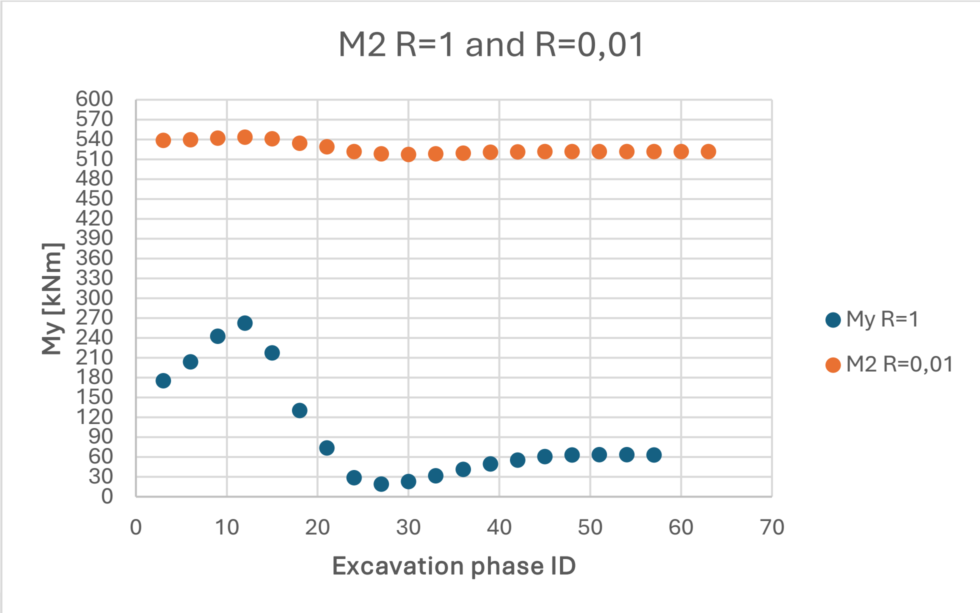

Figure 7.43. *My variation in the column element at Y=60.20, X=45.7: Comparison of R=1 and R=0.01.*

My values (Figure 7.43.): The My values obtained in the R=0.01 model were significantly higher than those in the R=1 model. In the R=1 model, My values initially increased as the excavation progressed, then showed a sharp decrease, approaching nearly zero. This drop indicates that as the tunnel excavation advanced, stress relief in the soil changed the bending behavior of the column at this point, and the deformations transferred to the soil through a stiffer interface caused a fluctuating response in the column's bending moments. In contrast, in the R=0.01 model, My values remained high and relatively stable throughout the excavation phases.

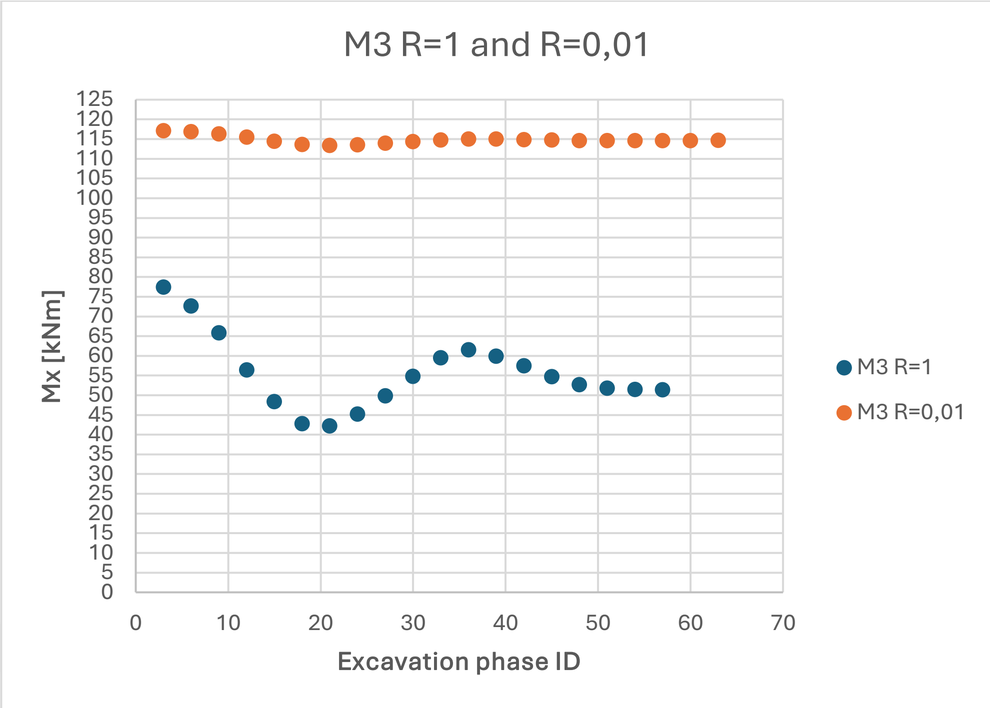

Figure 7.44. *Mx variation in the column element at Y=60.20, X=45.7: Comparison of R=1 and R=0.01.*

Mx values (Figure 7.44.): For Mx values as well, the results obtained from the R=0.01 model were larger than those from the R=1 model. In the R=1 case, Mx values showed more pronounced fluctuations and an overall decreasing trend as the excavation progressed, while in the R=0.01 case, the values remained high and followed a more stable pattern throughout the excavation phases.

These observations indicate that at the column located at Y=60.20, X=45.7, lower interface stiffness (R=0.01) generally leads to greater bending moments (My and Mx). This suggests that a weak bond between the tunnel and soil may cause the deformations in the soil to be transferred less uniformly to the building's foundation, resulting in local increases in moments within the column elements. As the building tries to redistribute internal stresses despite partially independent soil movements, such moment increases can occur.

7.4.2. Changes in internal forces for the column element at Y=89.30, X=45.7

For the column element at this location, My and Mx values were compared for different interface stiffness values (R=1 and R=0.01).

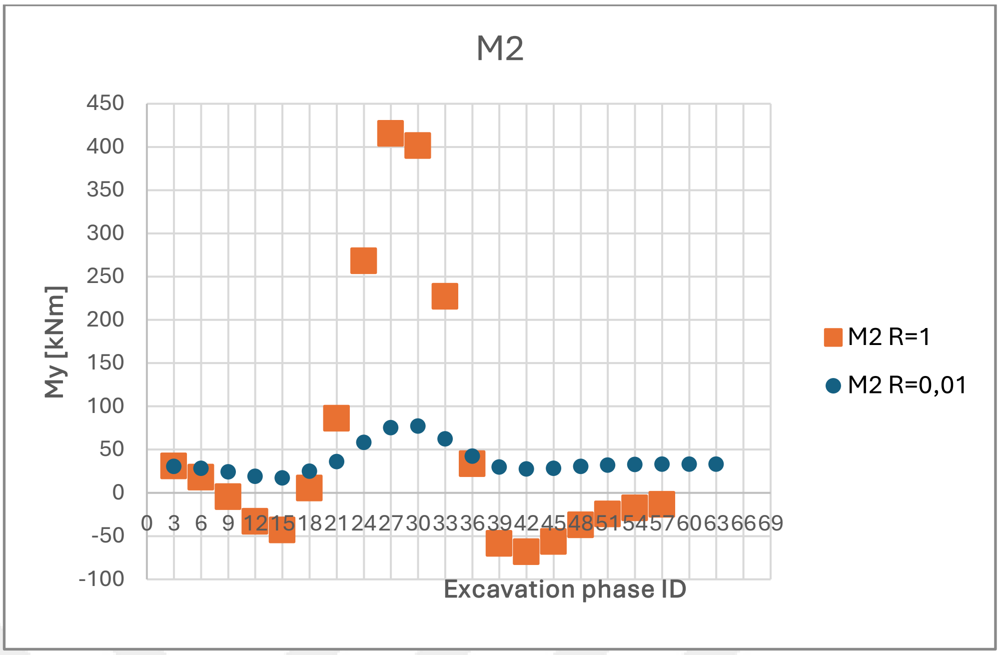

Figure 7.45. *My variation in the column element at Y=89.30, X=45.7: Comparison of R=1 and R=0.01.*

My values (Figure 7.45.): At this point, for My values, the R=1 model generally showed slightly lower values than the R=0.01 model during the early to mid and mid-to-late stages of excavation, while in the middle stages of the excavation, the R=1 model exhibited significantly higher values compared to R=0.01. Overall, the My values in the R=1 model peaked noticeably during the middle phase of excavation, surpassing those of the R=0.01 model. This indicates that under the R=1 scenario, this column experienced greater stress concentration due to tunnel effects, demonstrated a more pronounced response during critical excavation phases, and that the transfer of moments from the soil was stronger.

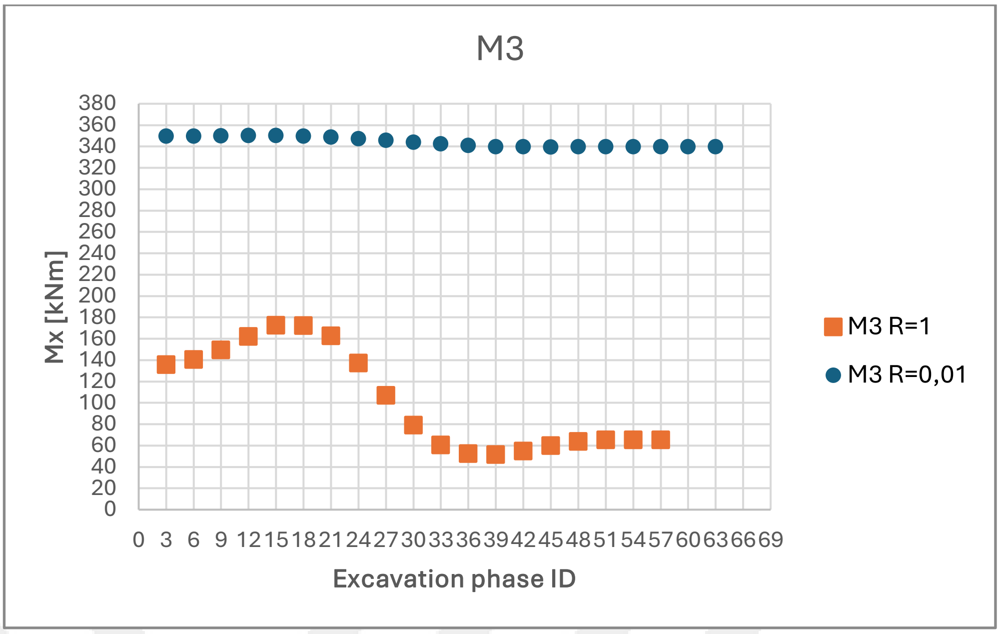

Figure 7.46. *Mx variation in the column element at Y=89.30, X=45.7: Comparison of R=1 and R=0.01.*

Mx values (Figure 7.46): For Mx values, the results obtained from the R=0.01 model were considerably higher than those from the R=1 model. In the R=1 case, Mx values remained low and followed a more stable trend, while in the R=0.01 case, they were higher and exhibited a fluctuating behavior throughout the excavation phases.

The findings at Y=89.30, X=45.7 show a similar trend to those at Y=60.20, X=45.7, especially for Mx values: generally higher Mx values were observed under the low interface stiffness scenario (R=0.01). The fluctuating relationship of My values depending on the excavation phase suggests that this location has a more complex stress state, situated at the intersection of variations in tunnel and building stiffness, and that interface stiffness significantly affects the moment distribution in this complex region.

Low interface stiffness (R=0.01): In the R=0.01 scenario, the bond between the soil and the tunnel lining weakens. This can cause tunnel-induced ground movements to be transmitted to the building foundation more "smoothly" or less sharply. However, this increases the building's internal effort to absorb differential movements, which can lead to local increases in bending moments in certain column elements (particularly in Mx and some My cases). While the building tends to move more independently of the ground, the internal stiffness variations and deformation incompatibilities within the building can trigger these moment increases.

High interface stiffness (R=1): In contrast, the R=1 scenario, representing full bonding between the tunnel and the soil, results in ground deformations being transmitted more effectively to the building. This forces the building to follow the settlement trough in the ground more closely and generally creates larger axial force changes in the structural system (see Section 7.3). In terms of bending moments, the R=1 scenario can produce higher moments at certain critical points (e.g., the middle phases of the My figure at Y=89.30, X=45.7) due to the building responding more rigidly to ground deformations. This shows that the building becomes more "locked" into the ground, leading to stress concentrations in some elements as a result of this locking.

These analyses once again emphasize the complexity and importance of interface modeling in tunnel-structure interaction. Not only global deformations and axial force changes, but also local internal force variations (such as bending moments) within structural elements must be accurately predicted by precisely defining interface properties. The analyses clearly demonstrate that different interface stiffness assumptions can have significant and sometimes unexpected effects on the distribution of internal stresses in different regions of the structure.

8. CONCLUSIONS

In this thesis, the soil deformations and building behavior induced by tunnel excavations were comprehensively analyzed through the case study of Naples Metro Line 6. Numerical modeling was performed using both Mohr-Coulomb and Hardening Soil (HS) material models, with varying soil parameters, to evaluate the impact of tunnel excavation on building response within the framework of soil-structure interaction.

Initially, settlement profiles obtained under greenfield conditions were compared with those accounting for soil-structure interaction. It was observed that the stiffness and self-weight of the building significantly influenced the shape of the settlement trough. Particularly, buildings with high stiffness reduced relative displacements in the sagging zone, whereas the settlement profile in the hogging zone closely followed the greenfield predictions. This finding is consistent with observations by Franzius et al. (2004) and Burland et al. (1977) in the literature.

In the 3D analyses conducted in PLAXIS 3D, excavation stages, face pressures, and grouting pressures were realistically simulated, enabling a detailed investigation of ground behavior during the TBM advance. Analyses of ΔN (axial force change) and Δuz (vertical displacement change) clearly revealed the differences in structural element responses for interface stiffness values of R=1 and R=0.01, highlighting the decisive role of interface stiffness in controlling deformation behavior.

The key findings of the analyses can be summarized as follows:

Settlement profiles estimated using Gaussian distribution under greenfield conditions changed significantly when building stiffness was considered. This demonstrates that stiff buildings resist ground movements and modify the settlement trough.

The longitudinal progression of TBM excavation affected the timing and magnitude of surface settlements, with most settlements occurring after shield passage in supported excavations.

Comparative analyses for interface stiffness values R=1 and R=0.01 showed that lower interface stiffness led to higher ΔN and Δuz values, implying increased deformation risk to the building.

The obtained settlement profiles and deformation values were in good agreement with pioneering works by Rankin (1988), Attewell and Woodman (1982), and Mair and Taylor (1997).

In light of these findings, it is once again emphasized that, in urban tunnel projects, considering soil-structure interaction and detailed modeling of building stiffness and foundation geometry are essential. Furthermore, advanced numerical tools such as PLAXIS 3D enable accurate prediction of settlement profiles and building deformations, which are critical for ensuring project safety and minimizing economic losses.

REFERENCES

Addenbrooke, T.I., and Potts, D.M. (2001). Structure–foundation–soil interaction: a nonlinear finite element model. *International Journal for Numerical and Analytical Methods in Geomechanics, 25*(11), 1099–1126.

Anagnostou, G., and Kovári, K. (1996). Face stability conditions with earth-pressure-balanced shields. *Tunnelling and Underground Space Technology, 11*(2), 165–173.

Attewell, P.B., and Woodman, J.P. (1982). Predicting the dynamics of ground movement from tunnelling: a review. *Ground Engineering, 15*(8).

Attewell, P.B., Yeates, J., and Selby, A.R. (1986). *Soil Movements Induced by Tunnelling and Their Effects on Pipelines and Structures*. Blackie, Glasgow.

Barla, G., and Pelizza, S. (2000). TBM tunneling in jointed rock masses. *Tunnelling and Underground Space Technology, 15*(3), 259–269.

Bilotta, E., Russo, G., and Viggiani, C. (2022). Building response to tunnelling. *Tunnelling and Underground Space Technology*.

Bobet, A., and Einstein, H.H. (2023). *Tunnel Design Methods*. Springer.

Boscardin, M.D., and Cording, E.J. (1989). Building response to excavation-induced settlement. *Journal of Geotechnical Engineering, 115*(1), 1–21.

Brinkgreve, R.B.J., Broere, W., and Waterman, D. (2004). *PLAXIS 2D Version 8: User Manual*. Delft University of Technology and PLAXIS BV.

Brinkgreve, R.B.J., Broere, W., and Waterman, D. (2011). *PLAXIS 3D Foundation – Tutorial Manual*. Delft University of Technology.

Brinkgreve, R.B.J., Kumarswamy, S., and Swolfs, W.M. (2010). *PLAXIS 3D Reference Manual*. PLAXIS BV, Delft.

Brinkgreve, R.B.J., Kumarswamy, S., and Swolfs, W.M. (2023). *PLAXIS 3D Reference Manual*. Bentley Systems.

Burland, J.B., and Wroth, C.P. (1974). Settlement of buildings and associated damage. In *Proceedings of Conference on Settlement of Structures* (pp. 611–654). Pentech Press.

Burd, H.J. (1999). The development and application of numerical analysis techniques to tunnelling in soft ground. *Géotechnique, 49*(1), 3–23.

Celentano, P. (2023). *Three-Dimensional Finite Element Analyses for the Evaluation of Building Response to Tunnelling*. Master's Thesis, University of Naples Federico II.

Chapman, D.N., Metje, N., and Stärk, A. (2010). *Introduction to Tunnel Construction*. CRC Press.

Craig, R.N., and Muir Wood, A.M. (1978). Development of settlement profile. In *Ground Engineering for Soft Ground Tunnelling*.

Dafalias, Y.F., and Manzari, M.T. (2004). Simple plasticity sand model accounting for fabric change effects. *Journal of Engineering Mechanics, 130*(6), 622–634.

De Borst, R., and Vermeer, P.A. (1984). Possibility and impossibility of finite element procedures. *International Journal for Numerical and Analytical Methods in Geomechanics, 8*(3), 239–252.

De Vivo, R. (2013). Soil characterization data from Naples Metro Line 6 investigation campaign.

Forth, R.A., Sugden, C., and Haji, M. (2006). Soil–structure interaction effects arising from tunnelling under a framed building. *Geotechnical Engineering, 159*(2), 91–101.

Franzius, J.N., Potts, D.M., and Burland, J.B. (2004). The response of surface structures to tunnel construction. *Geotechnical and Geological Engineering, 22*(1).

Frischmann, W., Wimmer, R., and Schweiger, H.F. (1994). Building response to tunnelling. In *Proceedings of the Symposium on Geotechnical Aspects of Underground Construction in Soft Ground*.

Gragnano, C.G., Fargnoli, V., Boldini, D., and Amorosi, A. (2014). Comparison of structural elements response in PLAXIS 3D and SAP2000. In *Proceedings of COMPLAS XII, Barcelona*.

ITA Working Group. (2004). *Guidelines for Tunnelling Risk Management*. International Tunnelling and Underground Space Association.

Kasper, T., and Meschke, G. (2004). A 3D finite element simulation model for TBM tunnelling in soft ground. *International Journal for Numerical and Analytical Methods in Geomechanics, 28*(14), 1441–1460.

Lee, K.M., Rowe, R.K., and Lo, K.Y. (1992). Three-dimensional analysis of ground movements due to tunneling. *Canadian Geotechnical Journal, 29*(6), 917–930.

Loganathan, N., and Poulos, H.G. (1998). Analytical prediction for tunneling-induced ground movements in clays. *Journal of Geotechnical and Geoenvironmental Engineering, 124*(9), 846–856.

Lunardi, P. (2008). *Design and Construction of Tunnels: Analysis of Controlled Deformations in Rock and Soils*. Springer.

Maidl, B., Herrenknecht, M., Maidl, U., and Wehrmeyer, G. (2013). *Mechanised Shield Tunnelling*. Ernst and Sohn.

Mair, R.J., and Taylor, R.N. (1997). Theme lecture: Bored tunnelling in the urban environment. In *Proceedings of the 14th International Conference on Soil Mechanics and Foundation Engineering*, Hamburg, Vol. 4, 2353–2385.

Mair, R.J., Taylor, R.N., and Bracegirdle, A. (1993). Subsurface settlement profiles above tunnels in clays. *Géotechnique, 43*(2), 315–320.

Manzari, M.T., and Dafalias, Y.F. (1997). A critical state two-surface plasticity model for sands. *Géotechnique, 47*(2), 255–272.

Ng, C.W.W., Cheong, H.K., and Lu, H. (2015). Three-dimensional numerical analysis of soil-structure interaction due to tunneling. *Computers and Geotechnics, 65*, 200–214.

O'Reilly, M.P., and New, B.M. (1982). Settlements above tunnels in the United Kingdom—their magnitude and prediction. In *Tunnelling '82* (pp. 173–181). London: IMM.

Peck, R.B. (1969). Deep excavations and tunnelling in soft ground. In *Proceedings of the 7th International Conference on Soil Mechanics and Foundation Engineering*, Mexico City, 225–290.

Pickhaver, J. (2006). *Modelling Masonry Facades Subjected to Tunnelling-Induced Ground Movements*. PhD Thesis, University of Cambridge.

Pinto, F., and Whittle, A.J. (2014). Ground movements due to shallow tunnels in soft ground: Analytical solutions and field comparison. *Computers and Geotechnics, 55*, 378–386.

PLAXIS. (2023). *PLAXIS 3D Reference Manual*. Bentley Systems.

Potts, D.M., and Addenbrooke, T.I. (1997). A structure's influence on tunnelling-induced ground movements. *Géotechnique, 47*(4), 741–777.

Potts, D.M., and Zdravkovic, L. (2001). *Finite Element Analysis in Geotechnical Engineering*. Thomas Telford.

Schweiger, H.F. (2002). Benchmarking of FEM codes for geotechnical applications. *International Journal for Numerical and Analytical Methods in Geomechanics, 26*(9), 917–926.

Shahsavari, H., and Ghafooripour, A. (2021). Numerical simulation of soil-structure interaction in urban tunneling using the Hardening Soil Model. *Geomechanics and Engineering, 26*(4), 393–402.

Sloan, S.W., and Randolph, M.F. (1982). Numerical prediction of collapse loads using finite element methods. *International Journal for Numerical and Analytical Methods in Geomechanics, 6*(1), 47–76.

Thewes, M. (2007). TBM tunnelling in difficult ground conditions. *Geomechanics and Tunnelling, 1*(1), 18–35.

Vermeer, P.A., and Brinkgreve, R.B.J. (1994). A new effective stress soil model for predicting settlements and pore pressure development. In *Proceedings of the European Conference on Soil Mechanics and Foundation Engineering*, 219–225

CURRICULUM VITAE

ORCID ID: 0009-0002-2727-3909

Name Surname: Bedirhan Yetkin

Foreign Language: English

Education and Professional Background:

2022 – Current, Eskişehir Technical University, Graduate School of Natural and Applied Sciences, Department of Civil Engineering, Geotechnical Engineering, Master's Degree

2015 – 2020, Eskişehir Technical University, Faculty of Civil Engineering, Department of Civil Engineering, Bachelor's Degree

11/2023 – 07/2024, Napoli Federico II University, Naples, Italy, Geotechnical Engineer Graduate Intern

05/2023 – 08/2023, Eskişehir Chamber of Civil Engineers, Eskişehir, Turkey, Civil Engineer

10/2020 – 07/2021, Liman İnşaat, Eskişehir, Turkey, Civil Engineer

02/2020 – 08/2020, Yerteknik Mühendislik İnşaat, Eskişehir, Turkey, Geotechnical Engineer Intern

02/2019 – 07/2019, Eskişehir İki Eylül Yapı Denetim, Eskişehir, Turkey, Civil Engineer Intern

Professional Union/Association/Organization Memberships:

- Member of Eskişehir Chamber of Civil Engineers, Turkey.